SPINODAL INSTABILITIES IN SYMMETRIC NUCLEAR MATTER WITHIN A NONLINEAR RELATIVISTIC MEAN-FIELD APPROACH

A THESIS SUBMITTED TO
THE GRADUATE SCHOOL OF NATURAL AND APPLIED SCIENCES
OF
MIDDLE EAST TECHNICAL UNIVERSITY

BY

FATMA ACAR

IN PARTIAL FULFILLMENT OF THE REQUIREMENTS
FOR
THE DEGREE OF MASTER OF SCIENCE
IN
PHYSICS

AUGUST 2011

Approval of the thesis:

SPINODAL INSTABILITIES IN SYMMETRIC NUCLEAR MATTER WITHIN A NONLINEAR RELATIVISTIC MEAN-FIELD APPROACH

submitted by **FATMA ACAR** in partial fulfillment of the requirements for the degree of **Master of Science in Physics Department, Middle East Technical University** by,

Prof. Dr. Canan Özgen _____
Dean, Graduate School of **Natural and Applied Sciences**

Prof. Dr. Sinan Bilikmen _____
Head of Department, **Physics**

Prof. Dr. Osman Yılmaz _____
Supervisor, **Physics Department, METU**

Prof. Dr. Şakir Ayık _____
Co-supervisor, **Physics Dept., Tennessee Tech University**

Examining Committee Members:

Prof. Dr. Ahmet Gökalp
Physics Dept., METU _____

Prof. Dr. Osman Yılmaz
Physics Dept., METU _____

Prof. Dr. Şakir Ayık
Physics Dept., Tennessee Tech University _____

Prof. Dr. Gürsevil Turan
Physics Dept., METU _____

Assoc. Prof. Dr. Hüseyin Oymak
Engineering Faculty, Atılım University _____

Date: _____

I hereby declare that all information in this document has been obtained and presented in accordance with academic rules and ethical conduct. I also declare that, as required by these rules and conduct, I have fully cited and referenced all material and results that are not original to this work.

Name, Last Name: FATMA ACAR

Signature :

ABSTRACT

SPINODAL INSTABILITIES IN SYMMETRIC NUCLEAR MATTER WITHIN A NONLINEAR RELATIVISTIC MEAN-FIELD APPROACH

Acar, Fatma
M.Sc., Department of Physics
Supervisor : Prof. Dr. Osman Yılmaz
Co-Supervisor : Prof. Dr. Şakir Ayık

August 2011, 89 pages

Spinodal instability mechanism and early development of density fluctuations for symmetric nuclear matter at finite temperature are studied. A stochastic extension of Walecka-type relativistic mean-field model including non-linear self-interactions of scalar mesons with NL3 parameter set is employed in the semi-classical approximation. The growth rates of unstable collective modes are investigated below the normal density and at low temperatures. The system exhibits most unstable behavior in longer wave lengths at baryon densities $\rho_B = 0.4\ \rho_0$, while most unstable behavior occurs in shorter wavelengths at lower baryon densities $\rho_B = 0.2\ \rho_0$. The unstable response of the system shifts towards longer wavelengths with the increasing temperature at both densities. The early growth of the density correlation functions are calculated, which provide valuable information about the initial size of the condensation and the average speed of condensing fragments. Furthermore, the relativistic results are compared with Skyrme type non-relativistic calculations. Qualitatively similar results are found in both non-relativistic and relativistic descriptions.

Keywords: Spinodal instabilities, stochastic mean-field approach, nonlinear Walecka model, Vlasov equation.

ÖZ

LİNEER OLMAYAN RELATİVİSTİK ORTALAMA ALAN YAKLAŞIMINDA SİMETRİK NÜKLEER MADDENİN SPİNODAL KARARSIZLIKLARI

Acar, Fatma
Yüksek Lisans, Fizik Bölümü
Tez Yöneticisi : Prof. Dr. Osman Yılmaz
Ortak Tez Yöneticisi : Prof. Dr. Şakir Ayık

Ağustos 2011, 89 sayfa

Sonlu sıcaklıklardaki simetrik nükleer maddenin spinodal karasızlık mekanizması ve yoğunluk dalgalanmalarının ilk anları incelendi. Relativistic stokastik ortalama alan yaklaşımı esas alınarak ve Walecka modelinin lineer olmayan scalar meson etkileşmelerini de içeren NL3 parametre seti kullanılarak yarı-klasik limitte çalışıldı. Baskın kararsız modların büyüme hızları normal yoğunluğun altındaki yoğunluklarda ve düşük sıcaklık değerlerinde incelendi. Yoğunluk değeri $\rho_B = 0.4\ \rho_0$ olduğunda baskın kararsız modlar uzun dalga boylarına doğru kayarken, daha düşük yoğunluklarda $\rho_B = 0.2\ \rho_0$ ise daha kısa dalga boylarına doğru kaydığı görüldü. Her iki yoğunluk değerinde de artan sıcaklıkla birlikte sistemin kararsız davranışı uzun dalga boylarına doğru kayar. Yoğunlaşan bölgelerin boyutu ve ortalama hızları hakkında bilgi içeren yoğunluk korelasyon fonksiyonunun erken gelişimi hesaplandı. Ayrıca, bu çalışmadaki relativistik hesaplar, Skyrme-tipi etkileşimler baz alınarak yapılan relativistik olmayan hesaplarla karşılaştırıldı. Relativistik ve relatistik olmayan yaklaşımların ikisinde de sistemin kararsızlık mekanizması için benzer sonuçlar bulundu.

Anahtar Kelimeler: Spinodal kararsızlıklar, stokastik ortalama alan yaklaşımı, Lineer olmayan Walecka modeli , Vlasov denklemi.

ACKNOWLEDGMENTS

I would like to express my deep sincere feelings to my supervisor Prof. Dr. Osman Yılmaz for his guidance, enthusiasm and endless encouragement over my entire M.Sc. program. I am deeply thankful to my co-supervisor Prof. Dr. Şakir Ayık for his stimulating scientific discussions and critics on my thesis. They provided me support in various ways. I would like to thank Assoc. Prof. Hüseyin Oymak for teaching me the computer program Fortran.

I am grateful to my family for endless support and patience throughout my education. I want to thank my friend Betül Danışman for her collaborative study during the writing of the thesis. I also thank to Mehmet Çakırca for his support and patience throughout my entire M.Sc. program.

I also express my gratitude to the committee members. I would like to acknowledge the support of TUBITAK, Turkish Scientific and Technical Research Council, through a graduate scholarship. Also, this thesis is supported in part by TUBITAK grant No. 110T274.

TABLE OF CONTENTS

ABSTRACT iv

ÖZ vi

ACKNOWLEDGMENTS viii

TABLE OF CONTENTS ix

LIST OF TABLES xi

LIST OF FIGURES xii

CHAPTERS

1 INTRODUCTION 1

2 RELATIVISTIC MEAN FIELD THEORY 6

2.1 Nonlinear Walecka Model 6

2.1.1 Introduction 6

2.1.2 Formalism 7

2.1.3 Nuclear Matter Equation of State at Zero Temperature 10

2.1.4 Nuclear Matter Equation of State at Finite Temperature 13

2.1.5 Phase Transition and Spinodal Instabilities 17

2.2 Stochastic Mean-Field Approach 20

2.3 Relativistic Vlasov Equation 22

3 EARLY GROWTH OF DENSITY FLUCTUATIONS 26

3.1 Linearization of Field Equations 26

3.2 Linearization of Vlasov Equation 28

3.3 Dispersion Relation 29

3.4 Density Correlation Functions 34

4 NUCLEAR SPINODAL INSTABILITIES 41

4.1 Growth Rates of Unstable Modes 41

4.2 Boundary of Spinodal Region 44
4.3 The Size of Primary Clusters in Spinodal Region 46
4.4 Spectral Intensity of the Density Correlation Functions 48
4.5 Early Growth of Density Correlation Functions 51
5 CONCLUSION 66
REFERENCES 69
APPENDICES
A DERIVATION OF SCALAR AND BARYON DENSITIES 71
B DERIVATION OF BARYON CORRELATION 74
C DERIVATIONS OF SCALAR AND VECTOR CORRELATIONS . . 81
D DISPERSION RELATION FOR ZERO TEMPERATURE 86

LIST OF TABLES

TABLES

Table 2.1 The parameter sets for the standard Walecka model and the NL3 model 16

Table 4.1 The average speed of initial fragments of spinodal decomposition at T=1 MeV and T=5 MeV 65

LIST OF FIGURES

FIGURES

Figure 2.1 Effective mass of nuclear matter as a function of density 17

Figure 2.2 The energy per nucleon as a function of the baryon density ρ_B, for a range of imposed temperatures, T=0,5,10,15,20 MeV. 18

Figure 2.3 Pressure as a function of the baryon density for various fixed temperatures (isotherms). 19

Figure 4.1 Growth rates of unstable modes as a function of wave numbers in the spinodal region at baryon density $\rho_B = 0.4\ \rho_0$ and at different temperature values. 42

Figure 4.2 Growth rates of unstable modes as a function of wave numbers in the spinodal region at baryon density $\rho_B = 0.2\ \rho_0$ and at different temperature values. 43

Figure 4.3 Growth rates of unstable modes as a function of wave numbers in the spinodal region at baryon densities $\rho_B = 0.2\ \rho_0$ and $\rho_B = 0.4\ \rho_0$ at $T = 5\ MeV$ for relativistic NL3 (dashed lines) and non-relativistic calculations (solid lines). 44

Figure 4.4 Growth rates of the most unstable modes as a function of baryon density in spinodal region. 45

Figure 4.5 Growth rates of the most unstable modes as a function of baryon density in spinodal region at temperature $T = 5\ MeV$ for non-relativistic calculations (solid line) and for relativistic-NL3 calculations (dashed line). 46

Figure 4.6 Boundary of spinodal region in baryon density-temperature plane of the unstable mode for the wavelengths $\lambda = 9fm$ and $\lambda = 12fm$ in relativistic-NL3 model. 47

Figure 4.7 The size of the primary clusters in the spinodal region at temperatures $T = 0, 2, 4$ and $6\ MeV$ 48

Figure 4.8 : Spectral intensity of baryon density correlation function as a function of wave number at $T = 1\ MeV$ and density $\rho_B = 0.2\ \rho_0$ 49

Figure 4.9 : Spectral intensity of baryon density correlation function as a function of wave number at $T = 1\ MeV$ and density $\rho_B = 0.4\ \rho_0$ 50

Figure 4.10 : Spectral intensity of baryon density correlation function as a function of wave number at $T = 5\ MeV$ and density $\rho_B = 0.2\ \rho_0$ 51

Figure 4.11 : Spectral intensity of baryon density correlation function as a function of wave number at $T = 5\ MeV$ and density $\rho_B = 0.4\ \rho_0$ 52

Figure 4.12 : Spectral intensity of scalar density correlation function as a function of wave number at $T = 1\ MeV$ and density $\rho_B = 0.2\ \rho_0$ 53

Figure 4.13 : Spectral intensity of scalar density correlation function as a function of wave number at $T = 1\ MeV$ and density $\rho_B = 0.4\ \rho_0$ 53

Figure 4.14 : Spectral intensity of scalar density correlation function as a function of wave number at $T = 5\ MeV$ and density $\rho_B = 0.2\ \rho_0$ 54

Figure 4.15 : Spectral intensity of scalar density correlation function as a function of wave number at $T = 5\ MeV$ and density $\rho_B = 0.4\ \rho_0$ 54

Figure 4.16 : Spectral intensity of current density correlation function as a function of wave number at $T = 1\ MeV$ and density $\rho_B = 0.2\ \rho_0$ 55

Figure 4.17 : Spectral intensity of current density correlation function as a function of wave number at $T = 1\ MeV$ and density $\rho_B = 0.4\ \rho_0$ 55

Figure 4.18 : Spectral intensity of current density correlation function as a function of wave number at $T = 5\ MeV$ and density $\rho_B = 0.2\ \rho_0$ 56

Figure 4.19 : Spectral intensity of current density correlation function as a function of wave number at $T = 5\ MeV$ and density $\rho_B = 0.4\ \rho_0$ 56

Figure 4.20 : Baryon density correlation function $\sigma_{BB}(x,t)$ as a function of distance $x = |\vec{r} - \vec{r}'|$ between two space points at temperature $T = 1\ MeV$ and density $\rho_B = 0.2\ \rho_0$. 57

Figure 4.21 : Baryon density correlation function $\sigma_{BB}(x,t)$ as a function of distance $x = |\vec{r} - \vec{r}'|$ between two space points at temperature $T = 1\ MeV$ and density $\rho_B = 0.4\ \rho_0$. 57

Figure 4.22 : Baryon density correlation function $\sigma_{BB}(x,t)$ as a function of distance $x = |\vec{r} - \vec{r}'|$ between two space points at temperature $T = 5\ MeV$ and density $\rho_B = 0.2\ \rho_0$. 58

Figure 4.23 : Baryon density correlation function $\sigma_{BB}(x,t)$ as a function of distance $x = |\vec{r} - \vec{r}'|$ between two space points at temperature $T = 5\ MeV$ and density $\rho_B = 0.4\ \rho_0$. 59

Figure 4.24 : Scalar density correlation function $\sigma_{ss}(x,t)$ as a function of distance $x = |\vec{r} - \vec{r}'|$ between two space points at temperature $T = 1\ MeV$ and density $\rho_B = 0.2\ \rho_0$. 60

Figure 4.25 : Scalar density correlation function $\sigma_{ss}(x,t)$ as a function of distance $x = |\vec{r} - \vec{r}'|$ between two space points at temperature $T = 1\ MeV$ and density $\rho_B = 0.4\ \rho_0$. 60

Figure 4.26 : Scalar density correlation function $\sigma_{ss}(x,t)$ as a function of distance $x = |\vec{r} - \vec{r}'|$ between two space points at temperature $T = 5\ MeV$ and density $\rho_B = 0.2\ \rho_0$. 61

Figure 4.27 : Scalar density correlation function $\sigma_{ss}(x,t)$ as a function of distance $x = |\vec{r} - \vec{r}'|$ between two space points at temperature $T = 5\ MeV$ and density $\rho_B = 0.4\ \rho_0$. 61

Figure 4.28 : Current density correlation function $\sigma_{\mathrm{vv}}(x,t)$ as a function of distance $x = |\vec{r} - \vec{r}'|$ between two space points at temperature $T = 1\ MeV$ and density $\rho_B = 0.2\ \rho_0$. 62

Figure 4.29 : Current density correlation function $\sigma_{\mathrm{vv}}(x,t)$ as a function of distance $x = |\vec{r} - \vec{r}'|$ between two space points at temperature $T = 1\ MeV$ and density $\rho_B = 0.4\ \rho_0$. 62

Figure 4.30 : Current density correlation function $\sigma_{\mathrm{vv}}(x,t)$ as a function of distance $x = |\vec{r} - \vec{r}'|$ between two space points at temperature $T = 5\ MeV$ and density $\rho_B = 0.2\ \rho_0$. 63

Figure 4.31 : Current density correlation function $\sigma_{\rm vv}(x,t)$ as a function of distance $x = |\vec{r} - \vec{r}'|$ between two space points at temperature $T = 5\ MeV$ and density $\rho_B = 0.4\ \rho_0$. 63

CHAPTER 1

INTRODUCTION

After the discovery of atomic nuclei in 1911 by Rutherford and the neutron was found by Chadwick in 1932, the basic problems of the nuclear physics arise to understand the structure and properties of the nuclei. In 1935, Yukawa comes up with a fundamental idea of strong interaction between the particles in nuclei. Since that time nuclear matter which is a theoretical uniform system of nucleons has become the subject of study in nuclear physics. A major interest is given to non-relativistic description of many-body system in the studies of nuclear physics. The non-relativistic many body formalism can explain the nuclear structure in terms of effective two nucleon interactions [1]. However, this approach is certainly inefficient for a full understanding of nuclei since the existing of atomic nuclei provide an inadequate explanation of the nuclear matter equation of state. Actually, most of the applications of nuclear physics depend on the behavior of nuclear matter under extreme conditions. For instance, the properties of neutron stars are related to the nuclear matter equation of state at densities of the order of magnitude higher than the densities in ordinary nuclei [1].

The extreme conditions for the nuclear matter can be produced in the laboratory through the heavy-ion collisions. With the developing technology, the new accelerators such as RHIC (Relativistic Heavy Ion Collider) and ALICE at CERN allow us to study nuclear matter at higher densities and temperatures. These experiments involve physics that cannot be explained by non-relativistic approach

such as relativistic motion of the nucleons, meson exchanges and formation of the quark-gluon plasma. However, the relativistic field theories can describe the various properties of the nuclear matter in the mean-field approximations [2].

The study of heavy-ion collisions presents the prospect of studying the properties of nuclear matter under extreme conditions. At high densities or temperatures ($\sim 150MeV$), nucleons in the nucleus changes into quark-gluon plasma and at lower temperatures, which are the results of the medium energy heavy-ion collisions (at temperatures that are tens of MeV), there is the possibility of a liquid-gas phase transition leading to the multifragmentation process [3]. This could provide information about the changes at the nuclear matter phases. However, it is not an easy task to determine such properties from these reactions since the collisions take place in order of 10^{-22} seconds and we cannot keep matter in that abnormal state to study its properties. Moreover, the detectors can measure only the products of the reaction in normal states and not the hot and dense one [4, 5].

Most of the previous investigations about nuclear matter have been carried out in non-relativistic framework. Moreover, the relativistic mean-field approaches based on covariant density functional theory have been used with great success to describe the structure and dynamics of nuclear matter in recent years [2, 6, 7, 8].

A relativistic mean-field theory (RMF) which is introduced originally by Walecka in 1974 [1] has gain a success in taking the relativistic effects [9]. However, the standard Walecka model is unable to describe the nuclear matter equation of state in a quantitative way [10]. Therefore, we use the nonlinear Walecka model which is the extension of the standard Walecka model with including the scalar meson non-linear self interaction terms [11] for a more realistic description of nuclear structure and dynamics.

In this work, the spinodal instabilities of infinite symmetric nuclear matter are studied. The symmetric infinite nuclear matter is a system that consists of infinite number of nucleons in a huge volume so the surface effects and the

Coulomb interactions between particles can be neglected. At lowest energies and normal states, the nuclear matter represents liquid-like characteristics. In the heavy-ion collisions, the temperature of the nuclear matter can be increased and the first order phase transition occurs at subnormal densities and at a few MeV temperatures. At normal density and zero temperature, nuclear matter behaves like Fermi liquids, but after the temperature increases at a few MeV, some of the nuclei start to evaporate and the liquid-gas phase transition occurs. At these conditions, nuclear matter is expected to behave like van der Waals gas, which is considered to be a classical example of liquid-gas phase transition, thermodynamically [12], since van der Waals forces are repulsive at short range and attractive at intermediate and long ranges similar to the nuclear forces. It is discussed in chapter 2 that the nuclear matter and van der Waals gas display similar properties due to phase transition.

Spinodal instability ensures a possible dynamical mechanism for fragmentation of a hot piece of nuclear matter occurring just after the heavy ion collisions [12]. The possible origin of spinodal decomposition is the growth of small amplitude density fluctuations around an equilibrium point [13]. At the reactions of intermediate energies, an intermediate system occurs at temperatures $10 - 15\ MeV$ and this hot and dense nuclear system expands with the effect of thermal pressure and then cools down. Its temperature and density start to decrease and the system enters into mechanically unstable region and it tends to breaks up into fragments. The region in which incompressibility is negative, frequencies become imaginary and the system is unstable mechanically is called spinodal instability region. The density for a nuclear matter at normal conditions is approximately $\rho_0 = 0.16 fm^{-3}$ and the nuclear matter is stable. The system of nuclear matter passes to the unstable condition at low densities. When the nuclear matter enters the spinodal region, it becomes unstable and the density fluctuations grow rapidly which leads to the break-up of the nuclear system into many fragments of different sizes known as multifragmentation. Multifragmentation is considered as a possible signature of the liquid-gas phase transformation [12].

The mean-field transport models such as the time dependent Hartree-Fock model (TDHF) [14] and the Boltzmann-Uhling-Uhlenbeck (BUU) [15] model have been used to describe the reaction dynamics in nuclear collisions at low energies and other many body systems [16]. Despite the success in explanation of mean-values of one-body observables in low energy reactions, the TDHF fails to describe fluctuation dynamics of the one-body observables [16]. Similar to the TDHF model, the BUU model cannot explain this fluctuation mechanism since only the average effect of the collisions is included in this approach [17]. Much work carried out to develop the transport approach for description of the dynamics of the density fluctuations [18]. Basically, there are two different mechanism for density fluctuations; (i) two body fluctuation mechanism and (ii) one-body mechanism or mean-field fluctuations. Since, no dissipation occurs without fluctuations [19], we need to develop a transport theory to take into account the two-body dissipation and fluctuation mechanism. Therefore, the Boltzmann-Langevin model (BL) is developed from the extension of BUU approach to include the fluctuating effect of the two-body collisions [17]. However, the BL model which is suitable for two-body dissipation and fluctuation mechanisms plays an important role in nuclear dynamics at intermediate energies but not at low energies [19]. Nuclear dynamics at low energies is studied in this work. The mean-field fluctuations at the initial state are dominant source of the density fluctuations for the low energy nuclear systems.

Stochastic Mean-Field Approach (SMF), which is proposed by S.Ayik in ref. [20], provides a suitable basis for describing dynamics of density fluctuations at low energies. The SMF approach includes the one-body dissipation and the related fluctuation mechanism in accordance with the quantal-dissipation fluctuation relation [16, 19, 21]. The SMF approach provides a useful microscopic tool to describe the dynamics of density fluctuations in nuclear processes at low energies [19].

In addition to the theoretical descriptions, there are experimental studies about spinodal decomposition in the heavy-ion collision physics. Spinodal decompo-

sition of finite nuclear matter appears as a mechanism of multifragmentation [22, 23]. The charge correlation functions are investigated experimentally in [24], and the multifragmentation event with nearly equal-sized fragments, which are possible signals of spinodal instabilities in finite nuclear systems, are observed.

In this thesis, we study the early development of density fluctuations of symmetric nuclear matter in spinodal region within the framework of the stochastic extension of the relativistic mean-field theory with the NL3 parameter set. In previous works, the spinodal dynamics are studied in the non-relativistic limit, and also in the relativistic limit with the semi-classical approximation by using the standard Walecka model [25, 26, 27]. In the standard Walecka model, the nuclear compressibility is much larger than the experimental value. Therefore, NL3 parameter set, which is the extension of the Walecka model with including nonlinear interaction terms of the scalar meson, provides a more realistic description of the nuclear dynamics.

We carry out investigations of spinodal instabilities in symmetric nuclear matter by utilizing the nonlinear Walecka model in the semi-classical approach. In chapter 2, we briefly describe the nonlinear Walecka model and then we derive the nuclear matter equation of state at zero and finite temperatures. Also, the phase transition and spinodal instabilities are determined from the pressure-baryon density variation. Furthermore, a brief description of the stochastic mean-field approach and the derivation of the relativistic Vlasov equation are given in this chapter. In chapter 3, we obtain a dispersion relation by linearization of the Vlasov equation and we investigate the early growth of density correlation functions of symmetric nuclear matter in spinodal region. In chapter 4, growth rates of unstable modes and the boundary of the spinodal region are determined numerically; and also spinodal instabilities and early growth of density fluctuations are investigated in symmetric nuclear matter. Finally, the conclusion is given in chapter 5.

CHAPTER 2

RELATIVISTIC MEAN FIELD THEORY

In this chapter, we investigate the nuclear matter equation of state based on nonlinear Walecka model. Our purpose is to develop our computer programs which will be used later in chapter 3.

2.1 Nonlinear Walecka Model

2.1.1 Introduction

Quantum hadrodynamics (QHD) is a theoretical description of nuclear many-body problem which is based on hadronic degrees of freedom and it was introduced by John Dirk Walecka in 1974 [1]. The QHD-I which is called Walecka model contains nucleons (protons and neutrons), neutral scalar σ meson and neutral vector ω meson. The effect of pions is zero since there is no pion field due to the well-defined parity and spherical symmetry in the ground state [1]. In the standard Walecka model, the scalar σ meson, which is responsible for the attractive force, and the neutral ω meson, responsible for the short range repulsion, provide the interaction between nucleons [28].

In the literature, there are many extensions of the original Walecka model and different parameter sets determined by fitting the properties of many nuclei. These models and sets are used to describe the nuclear matter properties around saturation density well. In the standard Walecka model, the coupling constants

are determined to give the saturation of nuclear matter at wavenumber $k_f = 1.30 fm^{-1}$ and the binding energy of $-15.75\ MeV$ [2, 6] . However, the standard Walecka set gives the value of nuclear matter compressibility ($K = 540\ MeV$) much higher than the experimental value. Furthermore, the effective nucleon mass is found much smaller than the value deduced from the experiments. In Ref. [29] it is stated that the Lagrangian density should involve self-interaction terms of the scalar meson field and the coupling constants are re-calculated to reach a more accurate compressibility value. The NL3 is one of the nonlinear parameter set (gives compressibility $K = 271.76\ MeV$) [11] that ensures a better description of nuclear structure properties and giant monopole excitations in medium weight and heavy nuclei. The parameters are determined by fitting the predicted values of different nuclear matter properties such as binding energy, charge radii, and neutron radii of spherical nuclei to observe the behavior of nuclear matter under extreme conditions.

2.1.2 Formalism

The effective interaction Lagrangian density for a system of nucleons of mass M in which the interaction between nucleons is provided by the exchange of a scalar meson field ϕ with mass m_s and a neutral vector meson field V_μ with mass $m_{\rm v}$ is given by [6]

$$\begin{aligned} L &= \overline{\psi}[\gamma^\mu i\hbar c\partial_\mu - Mc^2]\psi + \frac{1}{2}\partial_\mu\phi\partial^\mu\phi - U(\phi) + g_s\overline{\psi}\psi\phi \\ &\quad -\frac{1}{4}\Omega_{\mu\nu}\Omega^{\mu\nu} + \frac{1}{2}\mu_{\rm v}^2 V_\mu V^\mu - g_{\rm v}\overline{\psi}\gamma^\mu\psi V_\mu \end{aligned} \tag{2.1}$$

where the field strength tensor of the neutral vector meson is given by $\Omega_{\mu\nu} = \partial_\mu V_\nu - \partial_\nu V_\mu$ and $\mu_{\rm v} = m_{\rm v}c/\hbar$. The mass parameters, scalar coupling constant g_s, and vector coupling constant $g_{\rm v}$ are determined from experimental measurements. While the scalar meson potential is $U(\phi) = \frac{1}{2}\mu_s^2\phi^2$ in the standard Walecka model, it is given by $U(\phi) = \frac{1}{2}\mu_s^2\phi^2 + \frac{\kappa}{3!}\phi^3 + \frac{\lambda}{4!}\phi^4$ in the nonlinear Walecka model, where κ and λ are the self-coupling constants and $\mu_s \equiv (m_s c/\hbar)$.

By applying the Euler-Lagrange equations, the field equations from Eq. (2.1) can be derived as

$$
\begin{aligned}
(\partial_\mu \partial^\mu + \mu_{\rm s}^2)\phi + \frac{\kappa}{2}\phi^2 + \frac{\lambda}{6}\phi^3 &= g_{\rm s}\bar{\psi}\psi \ , && (2.2)\\
(\partial_\mu \partial^\mu + \mu_{\rm v}^2)V^\mu &= g_{\rm v}\bar{\psi}\gamma^\mu\psi, && (2.3)\\
\left[\gamma^\mu(i\hbar\partial_\mu - g_{\rm v}V_\mu) - (Mc^2 - g_{\rm s}\phi)\right]\psi &= 0 \ . && (2.4)
\end{aligned}
$$

Eq.(2.2) is a Klein-Gordon equation with a scalar source $g_{\rm s}\bar{\psi}\psi$ and Eq.(2.3) shows the Proca equation for the vector field with source term as $g_{\rm v}\bar{\psi}\gamma^\mu\psi$ [30]. The Eq.(2.4) denotes the Dirac equation of the baryon field including the interactions with scalar and vector fields.

The energy-momentum tensor $T^{\mu\nu}$ that summarizes the energy density, momentum density and the currents associated with the fields is given by [1]

$$
T^{\mu\nu} = \frac{\partial L}{\partial(\frac{\partial q_i}{\partial x^\mu})}\frac{\partial q_i}{\partial x_\nu} - g^{\mu\nu}L \ . \qquad (2.5)
$$

Since the Lagrangian density does not explicitly depend on the space-time coordinates x_μ , the energy-momentum tensor $T^{\mu\nu}$ is conserved ($\partial_\mu T^{\mu\nu} = \partial_\nu T^{\mu\nu} = 0$) and its expectation value has the form

$$
\langle T_{\mu\nu}\rangle = (\varepsilon + p)u_\mu u_\nu - p g_{\mu\nu} \qquad (2.6)
$$

where p is the pressure, ε is the energy density, and u_μ is the four velocity of the fluid [1]. The energy density and pressure are defined as

$$
\begin{aligned}
\varepsilon &= \langle T_{00}\rangle \ , \\
p &= \frac{1}{3}\langle T_{ii}\rangle \ . && (2.7)
\end{aligned}
$$

The field equations, Eq. (2.2-4), are nonlinear coupled equations so they are very difficult to solve. In addition, the coupling constants g_s and $g_{\rm v}$ are expected to be large so that the higher order terms in perturbative solutions will diverge. Thus, perturbative approaches are not useful [1]. Therefore, an approximation method, which is valid when the nuclear density increases, should be used for

solution. The relativistic mean field approximation is the method that will be used in this study. In the RMF approximation, the meson field operators are replaced by their ground state expectation values that are the classical fields in the following way [1]

$$\begin{aligned} \phi &\rightarrow \langle\phi\rangle \equiv \phi_0 \ , \\ V^\mu &\rightarrow \langle V^\mu\rangle \equiv V_0 g^{\mu 0} \ . \end{aligned} \tag{2.8}$$

The mean field approximation could be used if a system of B baryons in a large box of volume V at zero temperature is considered. As the baryon density, B/V, increases, the source terms on the right-hand sides of the equations (2.2) and (2.3) become large. If the source terms are large enough, the meson field operators can be replaced by their ground state expectation values [31]. Furthermore, for a static and uniform system, the classical fields ϕ_0 and V_0 are constants being independent of space and time (x_μ) [31] . Since the system is at rest, the baryon flux equals to zero. Thus, the space components of $\langle V^\mu\rangle$ vanish.

By the same way, the baryon operators in the meson field equations of motion are replaced by their ground state expectation values;

$$\begin{aligned} \overline{\psi}\psi &\rightarrow \langle\overline{\psi}\psi\rangle = \rho_s \ , \\ \overline{\psi}\gamma^\mu\psi &\rightarrow \langle\overline{\psi}\gamma^\mu\psi\rangle = g^{\mu 0}\rho_B \ . \end{aligned} \tag{2.9}$$

In the mean field approximation, the equations of motion for an infinite nuclear matter in the static case becomes

$$(\partial_\mu\partial^\mu + \mu_{\rm s}^2)\phi_0 + \frac{\kappa}{2}\phi_0^2 + \frac{\lambda}{6}\phi_0^3 = g_{\rm s}\rho_{\rm s}^0 \tag{2.10}$$

$$(\partial_\mu\partial^\mu + \mu_{\rm v}^2)\langle V^\mu\rangle = g_{\rm v}\langle\bar{\psi}\gamma^\mu\psi\rangle \tag{2.11}$$

where $\langle\bar{\psi}\gamma^\mu\psi\rangle \equiv \rho^\mu = (\rho_B, \vec{\rho}_{\rm v})$ and here the zero sub indices denote the equilibrium system which is uniform, static and independent of space and time. Since ϕ_0 and V_0 are constants, the final form of the equations of motions of the meson

fields at the equilibrium point is found as the following

$$\phi_0 = \frac{1}{\mu_{\rm s}^2}(g_{\rm s}\rho_{\rm s}^0 - \frac{\kappa}{2}\phi_0^2 - \frac{\lambda}{6}\phi_0^3) \tag{2.12}$$

$$V_0^0 = \frac{g_{\rm v}}{\mu_{\rm v}^2}\rho_B^0 \tag{2.13}$$

$$\vec{V_0} = 0 \tag{2.14}$$

The RMF energy-momentum tensor of QHD-I is evaluated starting from the RMF Lagrangian by using the definition of the energy momentum tensor given in Eq. (2.5) and Dirac equation which gives a simpler form as

$$T^{\mu\nu} = \overline{\psi}\gamma^\mu i\hbar\partial_\nu\psi - g^{\mu\nu}\left[-\frac{1}{2}\left(\frac{m_s c}{\hbar}\right)^2\phi_0^2 + \frac{1}{2}\left(\frac{m_{\rm v}c}{\hbar}\right)^2 V_0^2 - \frac{\kappa}{3!}\phi_0^3 - \frac{\lambda}{4!}\phi_0^4\right] . \tag{2.15}$$

From the definition in Eq.(2.7), the energy and pressure density are found as

$$\varepsilon = \langle\overline{\psi}\gamma^0 i\hbar\partial_0\psi\rangle + \frac{1}{2}\left(\frac{m_s c}{\hbar}\right)^2\phi_0^2 - \frac{1}{2}\left(\frac{m_{\rm v}c}{\hbar}\right)^2 V_0^2 + \frac{\kappa}{3!}\phi_0^3 + \frac{\lambda}{4!}\phi_0^4 , \tag{2.16}$$

$$p = \frac{1}{3}\langle\overline{\psi}\gamma^i i\hbar\partial_i\psi\rangle - \frac{1}{2}\left(\frac{m_s c}{\hbar}\right)^2\phi_0^2 + \frac{1}{2}\left(\frac{m_{\rm v}c}{\hbar}\right)^2 V_0^2 - \frac{\kappa}{3!}\phi_0^3 - \frac{\lambda}{4!}\phi_0^4 . \tag{2.17}$$

2.1.3 Nuclear Matter Equation of State at Zero Temperature

The nuclear matter equation of state (EOS) is the relation between the state variables such as temperature, pressure and density and it describes the behavior of the nuclear systems. For instance, the temperature and density values of the nuclear matter at which the liquid-gas phase transition is expected can be determined from the equation of state [32]. The energy and pressure densities are required to find the nuclear matter EOS. Therefore, the expectation values of the baryon field operators are essential to express the energy and pressure densities.

The expectation values of $\langle\overline{\psi}\gamma^0 i\hbar\partial_0\psi\rangle$ and $\langle\overline{\psi}\gamma^i i\hbar\partial_i\psi\rangle$ are evaluated by finding an explicit form of Dirac field ψ . In the RMF approximation, the assumption of uniform static system allows us to find out the field ψ in terms of the momentum eigenstates that are denoted by $\vec{k}$ with $\vec{p} = \hbar\vec{k}$. Solutions for the field are in the form like the free-particle Dirac solution, $\psi(x) = u(\vec{p}, s)e^{\frac{-ip\cdot x}{\hbar}}$ where $u(\vec{p}, s)$ is the four component Dirac spinor (s denotes the spin index) [1]. We thus have

$$\left[\varepsilon(\vec{p}) - \vec{\alpha}\cdot c\vec{p} - g_{\rm v}V_0 - \beta M^* c^2\right] u(\vec{p}, s) = 0 \tag{2.18}$$

where Dirac Hamiltonian is given by $H_D = \vec{\alpha}\cdot c\vec{p} + g_{\rm v}V_0 + \beta M^* c^2$ and M^* is the reduced baryon mass, defined as $M^*c^2 = Mc^2 - g_s\phi_0$.

The expectation value of an operator Γ in the ground state $\langle\overline{\psi}\Gamma\psi\rangle$ can be given in terms of the expectation value of the single-particle state $\left(\overline{\psi}\Gamma\psi\right)_{\vec{p},s}$ that is defined by momentum $\vec{p}$ and spin s

$$\langle\overline{\psi}\Gamma\psi\rangle = \sum_s \int \frac{d^3p}{(2\pi\hbar)^3}\left(\overline{\psi}\Gamma\psi\right)_{\vec{p},s}\Theta\left(\mu - e(\vec{p})\right) \tag{2.19}$$

where $e(\vec{p}) = g_{\rm v}V_0 + \sqrt{(\vec{p}c)^2 + (M^*c^2)^2}$ is positive single-particle energies since only the ground state is considered, μ is the chemical potential/Fermi energy and $\Theta\left(\mu - e(\vec{p})\right)$ is the step function. We first calculate the expectation values in energy density and pressure as

$$\begin{aligned}\langle\overline{\psi}H_D\psi\rangle &\equiv \langle\overline{\psi}\gamma^0 i\hbar\partial_0\psi\rangle \\ &= g_{\rm v}V_0\frac{\gamma}{(2\pi\hbar)^3}\int_0^{p_f} d^3p + \frac{\gamma}{(2\pi\hbar)^3}\int_0^{p_f} d^3p\sqrt{(c\vec{p})^2 + (M^*c^2)^2}\end{aligned} \tag{2.20}$$

and

$$\begin{aligned}\langle\overline{\psi}\vec{\gamma}\cdot\vec{\nabla}\psi\rangle &\equiv \langle\psi^\dagger\left(-i\vec{\alpha}\cdot\vec{\nabla}\right)\psi\rangle \\ &= \frac{\gamma}{(2\pi\hbar)^3}\int_0^{p_f} d^3p\frac{(c\vec{p})^2}{\sqrt{(c\vec{p})^2 + (M^*c^2)^2}}\ .\end{aligned} \tag{2.21}$$

For the scalar and baryon densities we can evaluated the expectation values are

$$\langle\overline{\psi}\psi\rangle = \frac{\gamma}{(2\pi\hbar)^3}\int_0^{p_f} d^3p \frac{M^*c^2}{\sqrt{p^2c^2+(M^*c^2)^2}} \tag{2.22}$$

and

$$\langle\overline{\psi}\gamma^0\psi\rangle = \frac{\gamma}{(2\pi\hbar)^3}\int_0^{p_f} d^3p \ . \tag{2.23}$$

By using the results of the expectation values, the scalar and the baryon densities become

$$\rho_s^0 = \frac{\gamma}{(2\pi\hbar)^3}\int_0^{p_f} d^3p \frac{M^*c^2}{\sqrt{p^2c^2+(M^*c^2)^2}} \tag{2.24}$$

$$\rho_B^0 = \frac{\gamma}{(2\pi\hbar)^3}\int_0^{p_f} d^3p = \frac{\gamma}{6\pi^2}k_F^3 \tag{2.25}$$

where the degeneracy factor γ is 4 for symmetric (N=Z) nuclear matter and 2 for pure neutron matter (Z=0). The details of the calculations are given in Appendix A. The energy and pressure density relations are obtained by substituting the above relations in the Eqs. (2.16) and (2.17) as

$$\begin{aligned}\varepsilon &= \frac{1}{2}\left(\frac{g_{\rm v}}{\mu_{\rm v}}\right)^2\left(\rho_B^0\right)+\frac{1}{2}\left(\frac{\mu_s}{g_s}\right)^2\left(Mc^2-M^*c^2\right)^2+\frac{\kappa}{6g_s^3}\left(Mc^2-M^*c^2\right)^3 \\ &\quad +\frac{\lambda}{24g_s^4}\left(Mc^2-M^*c^2\right)^4+\frac{\gamma}{(2\pi\hbar)^3}\int_0^{p_f} d^3p\sqrt{p^2c^2+(M^*c^2)^2}\ ,\end{aligned} \tag{2.26}$$

$$\begin{aligned}p &= \frac{1}{2}\left(\frac{g_{\rm v}}{\mu_{\rm v}}\right)^2\left(\rho_B^0\right)-\frac{1}{2}\left(\frac{\mu_s}{g_s}\right)^2\left(Mc^2-M^*c^2\right)^2-\frac{\kappa}{6g_s^3}\left(Mc^2-M^*c^2\right)^3 \\ &\quad -\frac{\lambda}{24g_s^4}\left(Mc^2-M^*c^2\right)^4+\frac{1}{3}\frac{\gamma}{(2\pi\hbar)^3}\int_0^{p_f} d^3p\frac{(c\vec{p})^2}{\sqrt{(c\vec{p})^2+(M^*c^2)^2}}\ .\end{aligned} \tag{2.27}$$

The first four terms of these equations come from the meson fields and the final terms are related to the relativistic gas of baryons of mass M^* [1].

Nuclear matter equation of state is given by these expressions in the parametric form $\varepsilon(\rho_B)$ and $P(\rho_B)$ at zero temperature. Besides, the pressure density expression can be found by using the relation [31]

$$P(\rho_B) = \rho_B \frac{\partial \varepsilon(\rho_B)}{\partial \rho_B} - \varepsilon(\rho_B) \ . \tag{2.28}$$

The constant V_0 can be expressed in terms of the conserved baryon density and ϕ_0 is expressed by scalar density which is the function of M^* , so to express the scalar density explicitly, M^* should be calculated self-consistently. From thermodynamics, it is calculated from the derivative of $\varepsilon(M^*)$ with respect to M^* . This produces the self-consistency condition $\frac{\partial}{\partial M^*}\varepsilon(M^*) = 0$ which gives the relation

$$M^*c^2 = Mc^2 - \left(\frac{g_s}{\mu_s}\right)^2 \rho_s^0 + \left(\frac{g_s}{\mu_s}\right)^2 \left[\frac{\kappa}{2g_s^3}\left(Mc^2 - M^*c^2\right)^2 + \frac{\lambda}{6g_s^4}\left(Mc^2 - M^*c^2\right)^3\right] , \tag{2.29}$$

where the scalar density ρ_s is given in Eq. (2.24).

2.1.4 Nuclear Matter Equation of State at Finite Temperature

In this section, the behavior of the (σ, ω) system at finite temperature is investigated by calculating the thermodynamic potential of the system within the framework of the mean-field theory. Here we use only the baryon contributions to the thermodynamic potential and we neglect the anti-baryon contributions since we use semi-classical approximation in calculations.

The thermodynamic potential Ω is calculated by using the standard expressions of the statistical mechanics:

$$\begin{aligned} \Omega(T, V, \mu) &= -k_B T \ln Z_G \\ Z_G &\equiv \sum_N \sum_j e^{-\beta(E_j - \mu N)} \\ &= \sum_N \sum_j \langle Nj | e^{-\beta(E_j - \mu N)} | Nj \rangle = Tr\left(e^{-\beta(\widehat{H} - \mu \widehat{N})}\right) \end{aligned} \tag{2.30}$$

where μ is the chemical potential and $\beta \equiv 1/k_B T$, Z_G is the grand partition function where $\widehat{H}$ and $\widehat{N}$ are the mean-field Hamiltonian and baryon number operators, respectively [1, 31]. All the thermodynamic properties of a system can be expressed in terms of $\ln Z_G$ and its partial derivatives.

The relations between the thermodynamic potential Ω, the chemical potential μ, the entropy S and other thermodynamic quantities are given as $\Omega = -pV = E - TS - \mu B$ and $d\Omega = -SdT - pdV - Bd\mu$ [1].

The mean-field Hamiltonian and baryon number operators are given by [31]

$$\begin{aligned} H_{MFT} &= V\left[-\frac{1}{2}(\mu_{\rm v})^2 V_0^2 + \frac{1}{2}(\mu_s)^2\phi_0^2\right] + g_{\rm v}V_0\widehat{B} + \sum_{k\lambda}\sqrt{\vec{p}^2c^2 + (M^*c^2)^2}A^+_{k\lambda}A_{k\lambda} \\ \widehat{B} &= \sum_{k\lambda} A^+_{k\lambda}A_{k\lambda}. \end{aligned} \tag{2.31}$$

Then the partition function and thermodynamic potential become

$$\begin{aligned} Z_G &= \sum_{n_1\ldots n_\infty}\langle n_1\ldots n_\infty|e^{-\beta(\widehat{H}-\mu\widehat{B})}|n_1\ldots n_\infty\rangle \\ &= \exp\left\{-\beta V\left[-\frac{1}{2}(\mu_v)^2V_0^2 + \frac{1}{2}(\mu_s)^2\phi_0^2\right]\right\}\prod_{i=1}^{\infty}\sum_{n=0}^{1}\left[e^{-\beta(E_i^*+g_vV_0-\mu)}\right], \end{aligned} \tag{2.32}$$

$$\begin{aligned} \Omega(T,V,\mu) &= -k_BT\ln Z_G \\ &= V\left[-\frac{1}{2}\left(\frac{g_v}{\mu_v}\right)^2\rho_B^2 + \frac{1}{2}\left(\frac{\mu_s}{g_s}\right)^2\left(Mc^2 - M^*c^2\right)^2\right] \\ &\quad -\frac{1}{\beta}\sum_i \ln\left[1 + e^{-\beta(E_i^*-\mu^*)}\right]. \end{aligned} \tag{2.33}$$

Baryon and scalar densities can be found as

$$\rho_B = -\left(\frac{\partial\Omega}{\partial\mu}\right)_{T,V} = \frac{\gamma}{(2\pi\hbar)^3}\int d^3p\frac{1}{1+e^{\beta(E_i^*-\mu^*)}}\ , \tag{2.34}$$

$$\rho_s = \frac{\gamma}{(2\pi\hbar)^3}\int_0^{p_f} d^3p\frac{M^*c^2}{\sqrt{\vec{p}^2c^2+(M^*c^2)^2}}\frac{1}{1+e^{\beta(E_i^*-\mu^*)}}\ . \tag{2.35}$$

The reduced mass as a function of temperature with Eq. (2.35) becomes

$$\begin{aligned} M^*c^2 &= Mc^2 - \left(\frac{g_s}{\mu_s}\right)^2 \frac{\gamma}{(2\pi\hbar)^3} \int_0^{p_f} d^3p \frac{M^*c^2}{\sqrt{\vec{p}^2c^2 + (M^*c^2)^2}} \frac{1}{1 + e^{\beta(E_i^* - \mu^*)}} \\ &\quad + \left(\frac{g_s}{\mu_s}\right)^2 \left[\frac{\kappa}{2g_s^3}\left(Mc^2 - M^*c^2\right)^2 + \frac{\lambda}{6g_s^4}\left(Mc^2 - M^*c^2\right)^3\right]. \end{aligned} \tag{2.36}$$

Then the energy density can be obtained from $\varepsilon = E/V = \partial\left(\beta\Omega\right)/V\partial\beta + \mu\rho_B$ as

$$\begin{aligned} \varepsilon &= \frac{1}{2}\left(\frac{g_v}{\mu_v}\right)^2 (\rho_B)^2 + \frac{1}{2}\left(\frac{\mu_s}{g_s}\right)^2 \left(Mc^2 - M^*c^2\right)^2 + \frac{\kappa}{6g_s^3}\left(Mc^2 - M^*c^2\right)^3 \\ &+ \frac{\lambda}{24g_s^4}\left(Mc^2 - M^*c^2\right)^4 + \frac{\gamma}{(2\pi\hbar)^3}\int_0^{p_f} d^3p \sqrt{p^2c^2 + (M^*c^2)^2} \frac{1}{1 + e^{\beta(E_i^* - \mu^*)}}. \end{aligned} \tag{2.37}$$

Pressure is found by using the energy density $p(\rho_B) = \rho_B \partial\varepsilon(\rho_B)/\partial\rho_B - \varepsilon(\rho_B)$

$$\begin{aligned} p &= \frac{1}{2}\left(\frac{g_v}{\mu_v}\right)^2 (\rho_B)^2 - \frac{1}{2}\left(\frac{\mu_s}{g_s}\right)^2 \left(Mc^2 - M^*c^2\right)^2 - \frac{\kappa}{6g_s^3}\left(Mc^2 - M^*c^2\right)^3 \\ &- \frac{\lambda}{24g_s^4}\left(Mc^2 - M^*c^2\right)^4 + \frac{1}{3}\frac{\gamma}{(2\pi\hbar)^3}\int_0^{p_f} d^3p \frac{(c\vec{p})^2}{\sqrt{(c\vec{p})^2 + (M^*c^2)^2}} \frac{1}{1 + e^{\beta(E_i^* - \mu^*)}}. \end{aligned} \tag{2.38}$$

For a given baryon density ρ_B and temperature T, Eq. (2.36), Eq. (2.37) and Eq. (2.38) have to be solved numerically where the reduced mass M^* and the reduced chemical potential $\mu^* = \mu - g_v V_0$ are determined self-consistently.

In the calculation, we employ two parameter sets; we use the values $C_{\rm s}^2 = g_{\rm s}^2\left(M^2/m_{\rm s}^2\right) = 357.4$ and $C_{\rm v}^2 = g_{\rm v}^2\left(M^2/m_{\rm v}^2\right) = 273.8$ in the standard Walecka model [1] and the NL3 parameter set [11] is used in the nonlinear Walecka model. These parameter sets that are given in Table 2.1 are determined by

Table 2.1: The parameter sets for the standard Walecka model and the NL3 model

	SW	NL3
$m_s(MeV)$	520.0	508.194
$m_{\mathrm{v}}(MeV)$	783.0	782.501
g_s	10.45	10.217
g_{v}	13.76	12.868
$\kappa(fm^{-1})$	0	10.431
λ	0	-28.885
Nuclear Matter Properties		
$\rho_0(fm^{-3})$	0.150	0.148
E/A (MeV)	-15.75	-16.299
K (MeV)	540	271.76
M^*/M	0.54	0.60

fitting some nuclear properties. While the large compressibility in the standard Walecka model is $K = 540MeV$, it is $K = 271.76MeV$ in the nonlinear Walecka model and it is comparable with observed value. The coupling constants in the expressions are found from the standard coupling constants given in Table 2.1 as $g_s \to g_s\sqrt{\hbar c}$, $g_{\mathrm{v}} \to g_{\mathrm{v}}\sqrt{\hbar c}$, $\kappa \to \kappa/\sqrt{\hbar c}$ and $\lambda \to \lambda/\hbar c$.

The solution of the Eq. (2.29) for M^* at zero temperature gives an effective mass as a function of baryon density as shown in Fig. 2.1. The form of the curve does not change with temperature and therefore it is not presented here. We find similar trend for standard Walecka model and NL3 model. The ratio M^*/M becomes small at high densities and it is considerably less than unity at saturation density, ρ_0, due to the large scalar field effect [1].

The resulting energy per nucleon curve is shown in Fig. 2.2. The energy per nucleon is represented as a function of the density ρ_B. The energy curves for different temperatures show that the minimum in this curve shift outwards towards to systems with higher densities as the temperature increases. Therefore, the nuclear matter becomes less bound when temperature increases.

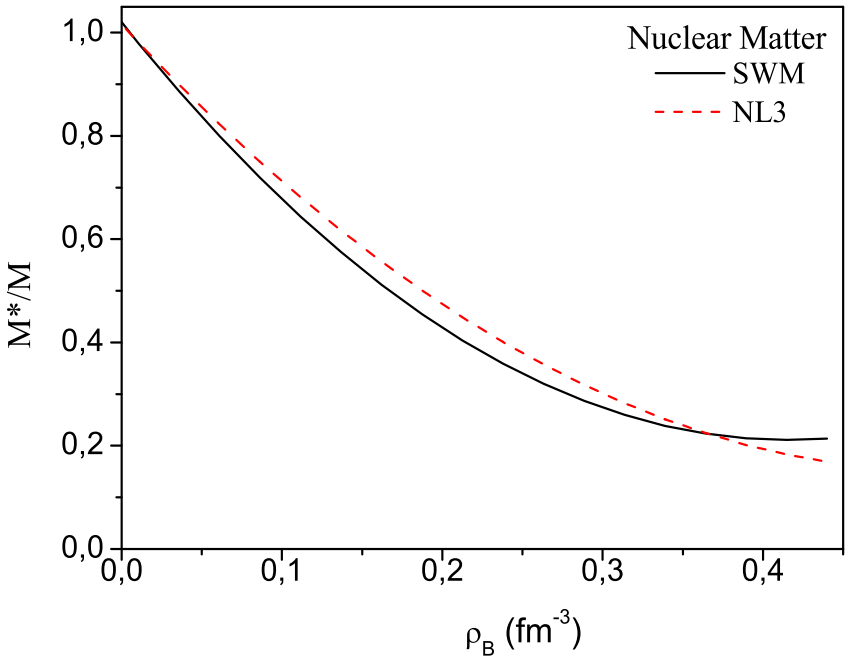

Figure 2.1: Effective mass of nuclear matter as a function of density

2.1.5 Phase Transition and Spinodal Instabilities

Compressed and hot nuclear matter occurring just after the heavy-ion collisions expands and then cools. When system enters the spinodal instability region, density fluctuations grow and nuclear matter breaks into several massive fragments. Spinodal instability is considered as a possible dynamical mechanism for multifragmentation and fragment formation, which is a signal of liquid-gas phase transformation of the nuclear matter [12].

There are two important phase transitions in heavy ion collisions related to the medium and high energies. At low temperatures $(1 - 10MeV)$, a liquid to gas phase transition occurs as van der Waals type nature. However, phase transition from hadronic matter to quark-gluon plasma is expected to occur at much higher temperatures $(\sim 150MeV)$ [4].

The most familiar way to see the qualitative behavior of a system at finite temperature is given by the equation of state, for example, the pressure as a

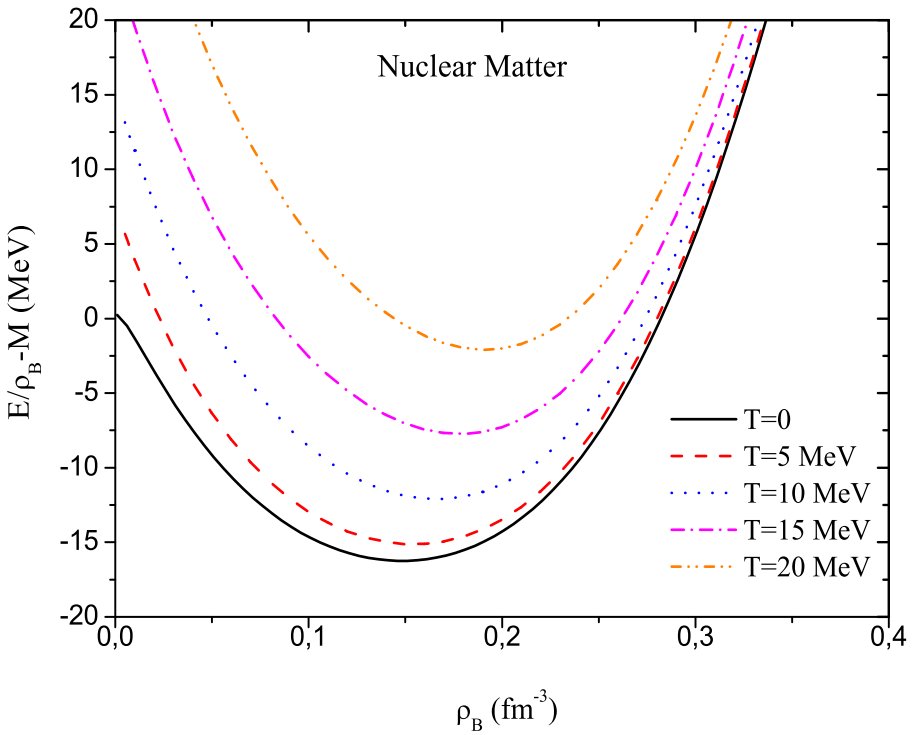

Figure 2.2: The energy per nucleon as a function of the baryon density ρ_B, for a range of imposed temperatures, T=0,5,10,15,20 MeV.

function of baryon density and temperature [32]. Fig. 2.3 is obtained by solving Eq. (2.36) and Eq. (2.38) as a function of baryon density for fixed temperatures up to 20 MeV. It exhibits a typical van der Waals behavior for a fluid gas system that includes the liquid-gas phase transition [33].

Phase equilibrium is only possible above a critical temperature T_c where pressure and its derivative with respect to baryon density are always positive at any density [33]. Nuclear matter is in gas phase above the critical temperature. As Coulomb force and the surface effects decrease T_c, it is difficult to decide critical temperature exactly because our calculation does not include Coulomb and surface effects. In our calculations, it reads about 14 MeV from Fig. 2.3.

Below the critical temperature, the pressure curves represent a region of thermodynamic instability where $\partial p/\partial \rho_B < 0$. The dashed line represents a boundary passing from the minimum and maximum points of the curves that mean the

derivative of pressure with respect to baryon density equals to zero at this points and under the region of this line the derivative is negative so the system is in the unstable region which is called the spinodal instability region [33].

Nuclear matter becomes unstable when its density decreases under a critical point and the system intends to liquid-gas phase transformation at this critical region. This region in which the nuclear matter is unstable depends on temperature and density.

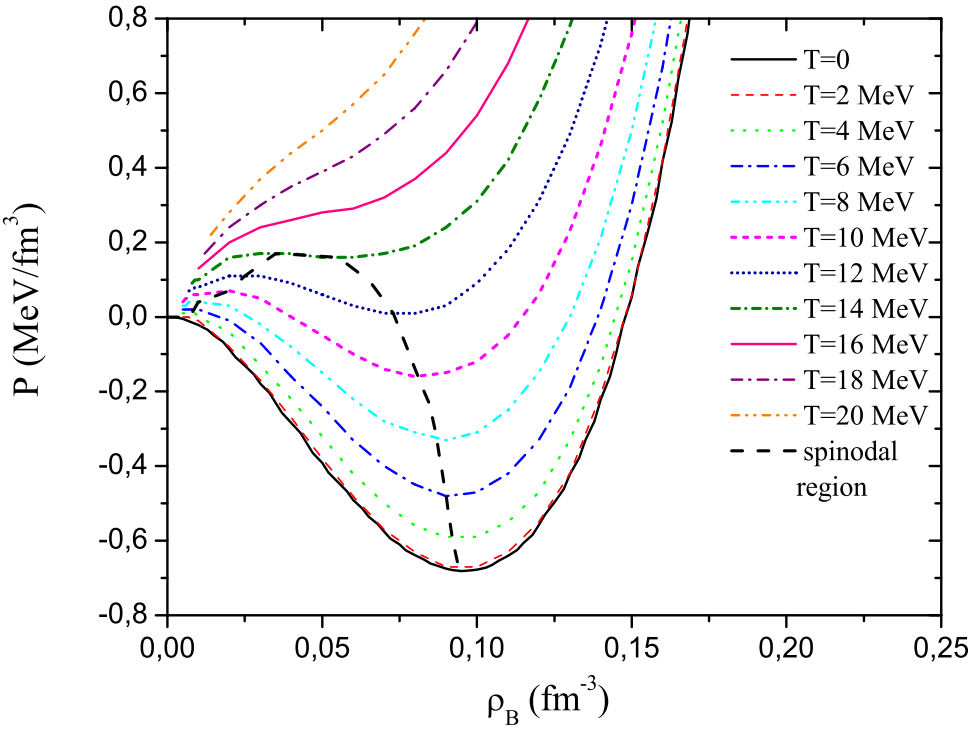

Figure 2.3: Pressure as a function of the baryon density for various fixed temperatures (isotherms).

The pressure function P has a maximum and a minimum under critical temperature $(0 < T < T_c)$. The region between the maximum and the minimum is the spinodal instability region in which the compressibility is negative and the system is mechanically unstable.

For a temperature above the critical value T_c , outside of the spinodal instability

region, there is a semi-stable region (liquid-gas mixture region) where liquid and gas phases can coexist in thermodynamic equilibrium. This coexistence region can be determined by a Maxwell construction. The matter is in the gas phase outside of the coexistence boundary below the densities corresponding to the maximum of the pressure curve, and in the liquid phase outside of the coexistence boundary above the densities corresponding to the minimum of the pressure curve [34]. These gas and liquid states have positive compressibility. At the critical point, the surface tension disappears and there is no distinction between gas and liquid phases $T \geq T_c$.

As the temperature increases, the densities corresponding to the maximum and minimum of pressure curves approach each other and they overlap at $T = T_c$. We also find that the spinodal region extends up to about $\frac{2}{3}\rho_0$, while the critical density corresponding to the critical temperature being $T_c \approx 14MeV$ is about $\frac{1}{3}\rho_0$.

2.2 Stochastic Mean-Field Approach

The standard mean field approach includes single-particle dissipation mechanism and provides a good description for the average evolution of collective motion at low energies ($\sim 10MeV$/nucleon). However, this approach strongly limits the fluctuations of collective motion [14]. Nevertheless, the stochastic mean-field approach provides a useful description for density fluctuations at low energies. In the stochastic mean-field approach, the superposition of determinantal wave functions is considered instead of a single determinantal description in order to describe fluctuations. In this description, an ensemble of single-particle density matrices related to the group of Slater determinants is generated in a stochastic framework by containing only initial correlations [20]. In this manner, the initial fluctuations are included into the calculations in a stochastic approach by generating an ensemble of events according to the initial distribution of collective modes in Walecka model [26].

Stochastic mean-field approach is developed for low energy heavy-ion collisions and fusion mechanisms. In this approach, the initial density fluctuations are simulated by considering the evolution of a set of density matrices instead of a single-particle density matrix.

Correlation gives information about the measure of a linear relationship between two variables [25]. In the stochastic mean-field approximation, the stochasticity stems from the initial correlations. In order to improve a stochastic description, it is needed to determine enough number of unoccupied single-particle states as well as occupied ones [20]. An ensemble of the phase-space distributions $\left\{f^{\lambda}(\vec{r},\vec{p},t)\right\}$ is simulated according to the initial fluctuations, where λ shows the event label. The event label is not used in calculations since the equations of motions do not change in the stochastic approach [26]. The main assumption of this approach in the semi-classical representation is stated as; in each phase-space cell, the initial-phase space distribution $f(\vec{r},\vec{p},0)$ is a Gaussian random number which is specified by a mean value $\overline{f(\vec{r},\vec{p},0)} = f_0(\vec{r},\vec{p})$ and its second moment is identified by

$$\overline{\delta f(\vec{r},\vec{p},0)\delta f(\vec{r}',\vec{p}',0)} = (2\pi\hbar^3)\delta(\vec{r}-\vec{r}')\delta(\vec{p}-\vec{p}')f_0(\vec{r},\vec{p})[1-f_0(\vec{r},\vec{p})] \qquad (2.39)$$

where the overline denotes the ensemble averaging and $f_0(\vec{r},\vec{p})$ shows the average phase-space distribution function which describes the initial state [20, 26, 27]. In the homogeneous initial state, the average phase-space distribution is given by the Fermi-Dirac distribution function $f_0(\vec{p}) = 1/[e^{\beta(\varepsilon_0^*-\mu_0^*)}+1]$. In this expression, the reduced chemical potential is given by $\mu_0^* = \mu_0 - (g_v/\mu_v)^2\rho_B^0$ where μ_0 and ρ_B^0 are the chemical potential and the baryon density in the homogeneous initial state, respectively [26].

In this thesis, the early growth of density fluctuations in the spinodal region is analyzed within the framework of linear response of this approach.

2.3 Relativistic Vlasov Equation

In the semi-classical approximation, a relativistic Vlasov equation is derived from the Walecka model [9]. Following the Walecka model, the equations of motion for the fields are obtained by using the Lagrangian density as in section 2.2. In the mean-field approximation, we considered the mesons as classical fields with the nucleons acting as their sources. If the nuclear density does not change noticeably in a time and space interval of the inverse of the meson masses, then the time and space dependence of the meson fields becomes similar to that of the nucleons [9]. In this case, the time and space derivatives in the mesonic equations of motions can be neglected. Then, we obtain the Dirac equation as

$$i\hbar\partial_t\psi = \vec{\alpha}\cdot c\vec{p}^*\psi + \left(\frac{g_{\rm v}}{\mu_{\rm v}}\right)^2 \rho_B\psi + \beta M^* c^2\psi \tag{2.40}$$

where the reduced momentum is given as $\vec{p}^* = \vec{p} - \left(\frac{g_{\rm v}}{\mu_{\rm v}}\right)^2 \vec{\rho_{\rm v}}$ ($\vec{\rho_{\rm v}}$ is the current density) and the reduced mass is written as $M^*c^2 = Mc^2 - g_s\phi$. In this expression, $\beta \equiv \gamma^0$ and $\vec{\alpha} \equiv \gamma^0\vec{\gamma}$.

By using this equation for the nucleon and expressing explicitly in terms of the large (ψ_L) and small (ψ_S) components of the nucleon field which is represent as $\psi(\vec{p},\lambda) = \begin{pmatrix} \psi_L \\ \psi_S \end{pmatrix}$, we can obtain the Dirac equation as two coupled equations [9, 25]

$$\begin{aligned} i\hbar\partial_t\psi_L &= \vec{\sigma}\cdot c\vec{p}^*\psi_S + \left[M^*c^2 + \left(g_v/\mu_v\right)^2\rho_B\right]\psi_L \\ i\hbar\partial_t\psi_S &= \vec{\sigma}\cdot c\vec{p}^*\psi_L + \left[-M^*c^2 + \left(g_v/\mu_v\right)^2\rho_B\right]\psi_S. \end{aligned} \tag{2.41}$$

Similar to the free particle, the stationary state solution for a uniform system is of the form of plane waves, $\psi = \psi(\vec{p},\lambda)e^{i(\vec{p}\cdot\vec{x}-\varepsilon(k)t)}$, where $\psi(\vec{p},\lambda)$ is a four component Dirac spinor and λ denotes the spin index. By using the free particle solution, we can write the Dirac equation as

$$\varepsilon\psi(\vec{p},\lambda) + \left[-\beta\vec{\gamma}\cdot\left(c\vec{p} - g_{\rm v}\vec{V}\right) - \beta M^*c^2\right]\psi(\vec{p},\lambda) = 0. \tag{2.42}$$

By solving this equation for the Dirac spinor of the form $\psi(\vec{p},\lambda) = \begin{pmatrix} \psi_L \\ \psi_S \end{pmatrix}$, one can obtain the following relations between its small and large components,

$$\psi_L = \frac{\vec{\sigma}\cdot c\vec{p^*}}{\varepsilon^* - M^*c^2}\psi_S \quad \text{and} \quad \psi_S = \frac{\vec{\sigma}\cdot c\vec{p^*}}{\varepsilon^* + M^*c^2}\psi_L, \tag{2.43}$$

where $\varepsilon^* = \sqrt{(c\vec{p^*})^2 + M^{*2}c^4}$. By using the above relations, the coupled equations in Eq.(2.41) reduce to a single equation,

$$i\hbar\partial_t\psi(\vec{x},t) = \sqrt{(c\vec{p^*})^2 + M^{*2}c^4}\ \psi(\vec{x},t) + \left(\frac{g_v}{\mu_v}\right)^2 \rho_B\psi(\vec{x},t) \tag{2.44}$$

and operator form of it is

$$i\hbar\partial_t\psi(\vec{x},t) = \left[E^* + \left(\frac{g_v}{\mu_v}\right)^2 \rho_B\right]\psi(\vec{x},t) \tag{2.45}$$

with the effective one-body Hamiltonian is $h = E^* + \left(\frac{g_v}{\mu_v}\right)^2\rho_B$. E^* in this expression is the operator form of the ε^* . From Eq. (2.45), we get

$$i\hbar\partial_t\left[\psi^\dagger(\vec{r}_1,t)\psi(\vec{r}_2,t)\right] = h(\vec{r}_1)\psi^\dagger(\vec{r}_1,t)\psi(\vec{r}_2,t) - \psi^\dagger(\vec{r}_1,t)\psi(\vec{r}_2,t)h(\vec{r}_2) \tag{2.46}$$

where $\psi(\vec{r},t)$ and $\psi^\dagger(\vec{r},t)$ are the single particle wave functions and the single particle density matrix is $\psi^\dagger(\vec{r}_1,t)\psi(\vec{r}_2,t) = \rho(\vec{r}_1,\vec{r}_2,t)$. By using the single-particle density matrix, Eq. (2.46) can be expressed as

$$i\hbar\partial_t\rho(\vec{r}_1,\vec{r}_2,t) = h(\vec{r}_1)\rho(\vec{r}_1,\vec{r}_2,t) - h(\vec{r}_2)\rho(\vec{r}_1,\vec{r}_2,t). \tag{2.47}$$

By using the Wigner transform, it is possible to provide a connection between the phase space distribution function and the density matrix which is given by

$$f(\vec{p},\vec{r},t) = \int \frac{d^3s}{(2\pi\hbar)^3} e^{-i\vec{p}\cdot\vec{s}/\hbar}\rho(\vec{r}+\frac{\vec{s}}{2},\vec{r}-\frac{\vec{s}}{2},t) \tag{2.48}$$

where the transformation $\vec{r} = (\vec{r}_1 + \vec{r}_2)/2$ and $\vec{s} = \vec{r}_1 - \vec{r}_2$ is used. In the momentum space, it becomes

$$f(\vec{r},\vec{p},t) = \int \frac{d^3k}{(2\pi)^3} e^{-i\vec{k}\cdot\vec{r}} \langle \vec{p} + \frac{\hbar\vec{k}}{2} | \rho(t) | \vec{p} - \frac{\hbar\vec{k}}{2} \rangle \tag{2.49}$$

and Wigner transform for $h[\rho]$ in Eq. (2.47) is given by

$$h(\vec{r},\vec{p},t) = \int \frac{d^3s}{(2\pi\hbar)^3} e^{-i\vec{p}\cdot\vec{s}/\hbar} h(\vec{r} + \frac{\vec{s}}{2}, \vec{r} - \frac{\vec{s}}{2}, t) \tag{2.50}$$

where $h(\vec{r} + \frac{\vec{s}}{2}, \vec{r} - \frac{\vec{s}}{2}, t) = \langle \vec{r} + \frac{\vec{s}}{2} | h[\rho] | \vec{r} - \frac{\vec{s}}{2} \rangle$.

As the Hamiltonian and the single particle density operator are Hermitian, the Wigner transform of both sides in Eq. (2.47) gives

$$\begin{aligned} i\hbar \frac{\partial}{\partial t} f(\vec{r},\vec{p},t) &= (h[\rho]\rho(t))_W - (\rho(t)h[\rho])_W \\ &= h(\vec{r},\vec{p}) e^{(i\hbar/2)\vec{\Lambda}} f(\vec{r},\vec{p},t) - f(\vec{r},\vec{p},t) e^{(i\hbar/2)\vec{\Lambda}} h(\vec{r},\vec{p}) \end{aligned} \tag{2.51}$$

with the operator $\vec{\Lambda} = \overleftarrow{\nabla}_r \overrightarrow{\nabla}_p - \overleftarrow{\nabla}_p \overrightarrow{\nabla}_r$. The direction of arrows represents the acting direction of the gradient operators. We can write the above equation as the following,

$$\begin{aligned} i\hbar \frac{\partial}{\partial t} f(\vec{r},\vec{p},t) &= h(\vec{r},\vec{p}) e^{(i\hbar/2)\vec{\Lambda}} f(\vec{r},\vec{p},t) - h(\vec{r},\vec{p}) e^{-(i\hbar/2)\vec{\Lambda}} f(\vec{r},\vec{p},t) \\ &= 2ih(\vec{r},\vec{p}) \sin\left(\frac{\hbar}{2}\vec{\Lambda}\right) f(\vec{r},\vec{p},t). \end{aligned} \tag{2.52}$$

By using Taylor expansion for $\sin\left(\frac{\hbar}{2}\vec{\Lambda}\right)$, we find

$$\frac{\partial}{\partial t} f(\vec{r},\vec{p},t) = 2h(\vec{r},\vec{p},t) \left[\frac{1}{2}\vec{\Lambda} + \frac{\hbar^2}{3!} \left(\frac{1}{2}\vec{\Lambda}\right)^3 + ... \right] f(\vec{r},\vec{p},t). \tag{2.53}$$

In the semi-classical limit, $\hbar \to 0$. If we use this condition into above equation, we obtain

$$\begin{aligned} \frac{\partial}{\partial t} f(\vec{r},\vec{p},t) &= 2h(\vec{r},\vec{p},t) \left[\frac{1}{2}\vec{\Lambda} \right] f(\vec{r},\vec{p},t) \\ &= h(\vec{r},\vec{p},t) \left[\overleftarrow{\nabla}_r \overrightarrow{\nabla}_p - \overleftarrow{\nabla}_p \overrightarrow{\nabla}_r \right] f(\vec{r},\vec{p},t), \end{aligned} \tag{2.54}$$

$$\frac{\partial}{\partial t} f(\vec{r}, \vec{p}, t) + \vec{\nabla}_p h(\vec{r}, \vec{p}, t) \cdot \vec{\nabla}_r f(\vec{r}, \vec{p}, t) - \vec{\nabla}_r h(\vec{r}, \vec{p}, t) \cdot \vec{\nabla}_p f(\vec{r}, \vec{p}, t) = 0. \tag{2.55}$$

This equation is called the Vlasov equation that describes the time evolution of the phase distribution function.

CHAPTER 3

EARLY GROWTH OF DENSITY FLUCTUATIONS

In this part of the thesis, we linearize the relativistic Vlasov equation around the equilibrium in order to find the early growth of density fluctuations for symmetric nuclear matter by assuming small fluctuations of the mean-field around its equilibrium value. The small fluctuations of the meson fields are necessary for linearization of the Vlasov equation. Therefore, the linearization of the fields is firstly determined in terms of density fluctuations by using their Klein-Gordon equations, and then the Vlasov equation is linearized to reach the dispersion relation.

3.1 Linearization of Field Equations

The small fluctuations of the meson fields are determined by the linearization of the field equations given in Eqs. (2.2) and (2.3). Meson fields are linearized around their initial values as $\phi = \phi_0 + \delta\phi(\vec{r},t)$ and $V^\mu = V_0^\mu + \delta V^\mu(\vec{r},t)$. The meson field fluctuations $\delta\phi(\vec{r},t)$ and $\delta V^\mu(\vec{r},t)$ depend on $(\vec{r},t)$, however, their initial values ϕ_0 and V_0^μ are constants. The vector component is $\vec{V_0} = 0$ since $\vec{\rho_{\rm v}}^{\,0} = 0$, however, its fluctuation depends on $\delta\vec{\rho_{\rm v}}(\vec{r},t)$ and therefore the fluctuation $\delta\vec{V}(\vec{r},t)$ is not zero. For the scalar meson field, we get

$$\left(\partial_\mu\partial^\mu + \mu_{\rm s}^2 + \kappa\phi_0 + \frac{\lambda}{2}\phi_0^2\right)\delta\phi = g_{\rm s}\delta\rho_{\rm s} \tag{3.1}$$

and for the vector meson field, the equations for time and space components become

$$\left(\partial_\mu \partial^\mu + \mu_{\rm v}^2\right) \delta V_0 = g_{\rm v} \delta \rho_B \ , \tag{3.2}$$

$$\left(\partial_\mu \partial^\mu + \mu_{\rm v}^2\right) \delta \vec{V} = g_{\rm v} \delta \vec{\rho_{\rm v}} \ . \tag{3.3}$$

These field equations are the covariant equations and we solve these equations by taking the Fourier transforms in space and one-sided Fourier transforms in time. Consequently, we can rewrite Fourier transforms of the fluctuations on the fields in terms of Fourier transforms of the density fluctuations $\delta\tilde{\rho}_s(\vec{k},\omega)$, $\delta\tilde{\rho}_B(\vec{k},\omega)$ and $\delta\tilde{\vec{\rho}}_v(\vec{k},\omega)$ as

$$\delta\tilde{\phi}(\vec{k},\omega) = \left[\frac{g_s}{-(w/c)^2 + k^2 + {\mu_s}^2 + \kappa\phi_0 + \frac{\lambda}{2}\phi_0^2}\right] \delta\tilde{\rho}_s(\vec{k},\omega) \ , \tag{3.4}$$

$$\delta\tilde{V}_0(\vec{k},\omega) = \frac{g_{\rm v}}{-(w/c)^2 + k^2 + {\mu_v}^2} \delta\tilde{\rho}_B(\vec{k},\omega) \ , \tag{3.5}$$

$$\delta\tilde{\vec{V}}(\vec{k},\omega) = \frac{g_{\rm v}}{-(w/c)^2 + k^2 + {\mu_v}^2} \delta\tilde{\vec{\rho}}_{\rm v}(\vec{k},\omega) \ . \tag{3.6}$$

We have also $\mu_s^2\phi_0 + \frac{\kappa}{2}\phi_0^2 + \frac{\lambda}{6}\phi_0^3 = g_s {\rho_s}^0$ and $M^*c^2 = Mc^2 - g_s\phi_0$.

In the mean-field approximation, we find the Dirac equation for the baryon field in Eq.(2.4) and in order to derive the one-body potential of the system in a general form, the Dirac equation is rewritten in the following way

$$i\hbar\frac{\partial}{\partial t}\psi = \left\{\vec{\alpha}\cdot\left[c\vec{p} - g_{\rm v}\vec{V}\right] + g_{\rm v}V_0 + \beta\left(Mc^2 - g_s\phi_0\right)\right\}\psi \ . \tag{3.7}$$

From this equation, the mean-field Hamiltonian in Vlasov equation becomes

$$h = \sqrt{\left(c\vec{p} - g_{\rm v}\vec{V}\right)^2 + \left(Mc^2 - g_s\phi_0\right)^2} + g_{\rm v}V_0 \ . \tag{3.8}$$

In the following of the thesis, we use the mean-field Hamiltonian U instead of h to avoid the confusion with the operator form of the Hamiltonian.

3.2 Linearization of Vlasov Equation

For investigating the early growth of density fluctuations in the spinodal region, we need to consider the linear response treatment of dynamical evolution. For the linearizaton of Vlasov equation given in Eq. (2.55), we linearize the phase-space distribution function around a homogeneous initial state $f_0(\vec{p})$ as $f(\vec{r},\vec{p},t) = f_0(\vec{p}) + \delta f(\vec{r},\vec{p},t)$ and the one-body potential around the equilibrium value $U_0 = \sqrt{(c\vec{p})^2 + (Mc^2 - g_s\phi_0)^2} + \frac{g_v^2}{\mu_v^2}{\rho_B}^0$ as $U = U_0 + \delta U$ where ${\rho_B}^0$ is the baryon density in the homogeneous initial state. We also use the linearization of the velocity around an initial value $\vec{\mathrm{v}_0} = c\vec{p}/{\varepsilon_0}^*$ as $\vec{\mathrm{v}} \equiv \vec{\nabla}_p h(\vec{r},\vec{p},t) = \vec{\mathrm{v}_0} + \delta\vec{\mathrm{v}}$ where ${\varepsilon_0}^* = \sqrt{(c\vec{p})^2 + (Mc^2 - g_s\phi_0)^2}$. By neglecting the second order fluctuation terms we then obtain the linearized Vlasov equation as

$$\frac{\partial}{\partial t}\delta f(\vec{r},\vec{p},t) + \vec{\mathrm{v}}_0 \cdot \vec{\nabla}_r \delta f(\vec{r},\vec{p},t) - \vec{\nabla}_r \delta U(\vec{r},\vec{p},t) \cdot \vec{\nabla}_p f_0(\vec{p}) = 0 \ , \tag{3.9}$$

where $f_0(\vec{p})$ represents the average phase-space distribution describing the initial state and it is given by the Fermi-Dirac distribution function $f_0(\vec{p}) = 1/\left[e^{\beta(\epsilon_0^* - \mu_0^*)} + 1\right]$. In this expression the chemical potential is given by $\mu_0^* = \mu_0 - (g_\mathrm{v}/\mu_\mathrm{v})^2 \rho_B^0$.

The small fluctuation on the mean-field Hamiltonian is written in terms of the meson field fluctuations as

$$\delta U = \left(\frac{\partial U}{\partial V_i}\right)_0 \delta V_i + \left(\frac{\partial U}{\partial V_0}\right)_0 \delta V_0 + \left(\frac{\partial U}{\partial \phi}\right)_0 \delta\phi \ , \tag{3.10}$$

where $(\ )_0$ denotes the corresponding values at the initial state. Using $U = \sqrt{\left(c\vec{p} - g_\mathrm{v}\vec{V}\right)^2 + (Mc^2 - g_s\phi_0)^2} + g_\mathrm{v}V_0$, these values are obtained as

$$\left(\frac{\partial U}{\partial V_0}\right)_0 = g_\mathrm{v} \ , \tag{3.11}$$

$$\left(\frac{\partial U}{\partial \phi}\right)_0 = -g_\mathrm{s}\frac{M_0^* c^2}{\varepsilon_0^*} \ , \tag{3.12}$$

$$\left(\frac{\partial U}{\partial V_i}\right)_0 = -g_\mathrm{v}\frac{cp_i}{\varepsilon_0^*} \ . \tag{3.13}$$

We finally find the small change in the mean-field Hamiltonian around its equi-

librium in terms of density fluctuations as

$$\delta U = -G_\omega^2 \frac{c\vec{p}}{\varepsilon_0^*} \cdot \delta\vec{\rho}_{\rm v} + G_\omega^2 \delta\rho_B - G_{\rm s}^2 \frac{M_0^* c^2}{\varepsilon_0^*} \delta\rho_{\rm s} \ . \tag{3.14}$$

The terms G_ω^2 and $G_{\rm s}^2$ are related to the meson contributions with point couplings which are given by

$$G_\omega^2 = \frac{g_{\rm v}^2}{-(w/c)^2 + k^2 + {\mu_{\rm v}}^2} \ , \tag{3.15}$$

$$G_s^2 = \frac{g_s^2}{-(w/c)^2 + k^2 + {\mu_s}^2 + \kappa\frac{1}{g_s}\left(Mc^2 - M_0^* c^2\right) + \frac{\lambda}{2}\frac{1}{g_s^2}\left(Mc^2 - M_0^* c^2\right)^2} \ . \tag{3.16}$$

In Eqs. (3.1), (3.2) and (3.3) the baryon density $\rho_B(\vec{r},t)$, the scalar density $\rho_s(\vec{r},t)$ and the current density $\vec{\rho}_{\rm v}(\vec{r},t)$ can be expressed in terms of the phase-space distribution function as

$$\rho_B(\vec{r},t) = \gamma \int \frac{d^3p}{(2\pi\hbar)^3} f(\vec{r},\vec{p},t) \tag{3.17}$$

$$\rho_{\rm s}(\vec{r},t) = \gamma \int \frac{d^3p}{(2\pi\hbar)^3} \frac{M^* c^2}{\varepsilon^*} f(\vec{r},\vec{p},t) \tag{3.18}$$

$$\vec{\rho}_{\rm v}(\vec{r},t) = \gamma \int \frac{d^3p}{(2\pi\hbar)^3} \frac{c\vec{p}^*}{\varepsilon^*} f(\vec{r},\vec{p},t) \tag{3.19}$$

where the spin-isospin element γ is 2 for neutron matter and 4 for nuclear matter. We may find the small fluctuations on these densities in terms of the small fluctuation on the phase-space distribution function that satisfies the linearized Vlasov equation.

3.3 Dispersion Relation

The dispersion relation gives information about the behavior of the system such as phase transition when it is affected dynamically. In nuclear matter, wavelengths and the growth rates of the dominant modes are determined by solving the dispersion relation.

We can solve the linear response equation by using the standard method of one-sided Fourier transformation in time [35]. And also, the Fourier transformation of the phase-space distribution in space is given as,

$$\delta\tilde{f}(\vec{k},\vec{p},\omega) = \int_0^\infty dt e^{i\omega t}\int_{-\infty}^{\infty} d^3r e^{-i\vec{k}\cdot\vec{r}}\delta f(\vec{r},\vec{p},t) \tag{3.20}$$

$$\delta\tilde{\rho}_i(\vec{k},\omega) = \int_0^\infty dt e^{i\omega t}\int_{-\infty}^{\infty} d^3r e^{-i\vec{k}\cdot\vec{r}}\delta\rho_i(\vec{r},t) \tag{3.21}$$

where i represents the current, scalar and baryon densities. The one-sided Fourier transform of the phase-space distribution function gives

$$\int_0^\infty \frac{\partial}{\partial t}\delta\tilde{f}(\vec{k},\vec{p},t)e^{i\omega t}dt = -\delta\tilde{f}(\vec{k},\vec{p},0) - i\omega\delta\tilde{f}(\vec{k},\vec{p},\omega) \tag{3.22}$$

here $\delta\tilde{f}(\vec{k},\vec{p},0)$ denotes the Fourier transform of the initial fluctuations. After one-sided Fourier transformation, we obtain the following expression for $\delta\tilde{f}(\vec{k},\vec{p},\omega)$ from the Vlasov equation

$$\begin{aligned}\delta\tilde{f}(\vec{k},\vec{p},\omega) &= \frac{\vec{\nabla}_p\tilde{f}_0\cdot\vec{k}}{\omega-\vec{\mathrm{v}}_0\cdot\vec{k}}\left\{-G_\omega^2\frac{c\vec{p}}{\varepsilon_0^*}\cdot\delta\vec{\tilde{\rho}}_{\mathrm{v}}(\vec{k},\omega)\right.\\ &\left.+G_{\mathrm{v}}^2\delta\tilde{\rho}_B(\vec{k},\omega) - G_{\mathrm{s}}^2\frac{M_0^*c^2}{\varepsilon_0^*}\delta\tilde{\rho}_{\mathrm{s}}(\vec{k},\omega)\right\} + i\frac{\delta\tilde{f}(\vec{k},\vec{p},0)}{\omega-\vec{\mathrm{v}}_0\cdot\vec{k}}.\end{aligned} \tag{3.23}$$

In this expression, the fluctuations of the meson fields are expressed in terms of Fourier transforms of the scalar density $\delta\rho_s(\vec{r},t)$, the baryon density $\delta\rho_B(\vec{r},t)$ and the current density $\delta\vec{\rho}_{\mathrm{v}}(\vec{r},t)$ fluctuations [36]. In this equation, the initial fluctuations with respect to the meson fields are ignored, thus only the initial fluctuations of the phase-space distribution function $\delta\tilde{f}(\vec{k},\vec{p},0)$ is kept.

Baryon, scalar and current densities in terms of the phase-space distribution function are given in Eqs. (3.17-19) are used to derive the equations for the density fluctuations. From Eq. (3.17) we write the baryon density fluctuation as $\delta\tilde{\rho}_{\mathrm{B}}(\vec{k},\omega) = \gamma\int\frac{d^3p}{(2\pi\hbar)^3}\delta\tilde{f}(\vec{k},\vec{p},\omega)$. If Eq. (3.23) is put into this expression we then obtain the following expression

$$
\begin{aligned}
&\delta\vec{\tilde{\rho}}_{\rm v}(\vec{k},\omega)\left\{-\gamma\int\frac{d^3p}{(2\pi\hbar)^3}G_\omega^2\frac{c\vec{p}}{\varepsilon_0^*}\frac{\vec{\nabla}_p f_0\cdot\vec{k}}{\omega-\vec{\rm v}_0\cdot\vec{k}}\right\}\\
&+\delta\tilde{\rho}_s(\vec{k},\omega)\left\{-\gamma\int\frac{d^3p}{(2\pi\hbar)^3}G_s^2\frac{M_0^*c^2}{\varepsilon_0^*}\frac{\vec{\nabla}_p f_0\cdot\vec{k}}{\omega-\vec{\rm v}_0\cdot\vec{k}}\right\}\\
&+\delta\tilde{\rho}_B(\vec{k},\omega)\left\{1+\gamma\int\frac{d^3p}{(2\pi\hbar)^3}G_\omega^2\frac{\vec{\nabla}_p f_0\cdot\vec{k}}{\omega-\vec{\rm v}_0\cdot\vec{k}}\right\}=i\gamma\int\frac{d^3p}{(2\pi\hbar)^3}\frac{\delta\tilde{f}(\vec{k},\vec{p},0)}{\omega-\vec{\rm v}_0\cdot\vec{k}}\ .
\end{aligned}
\tag{3.24}
$$

From Eq. (3.18) the fluctuation on scalar density is written as

$$
\begin{aligned}
\delta\tilde{\rho}_s(\vec{k},\omega) &= \gamma\int\frac{d^3p}{(2\pi\hbar)^3}\left\{\left(\frac{M^*c^2}{\varepsilon^*}\right)_0\delta\tilde{f}(\vec{k},\vec{p},\omega)+f_0\delta\left(\frac{M^*c^2}{\varepsilon^*}\right)\right\}\\
&= \gamma\int\frac{d^3p}{(2\pi\hbar)^3}\left\{\left(\frac{M^*c^2}{\varepsilon^*}\right)_0\delta\tilde{f}(\vec{k},\vec{p},\omega)\right.\\
&\quad\left.+f_0\left[G_s^2\left(-\frac{(cp)^2}{\varepsilon_0^{*3}}\right)\delta\tilde{\rho}_s+G_\omega^2\frac{M_0^*c^2}{\varepsilon_0^{*3}}c\vec{p}\cdot\delta\vec{\tilde{\rho}}_{\rm v}\right]\right\}.
\end{aligned}
\tag{3.25}
$$

By using Eq. (3.23) in Eq. (3.25) we obtain

$$
\begin{aligned}
&\delta\vec{\tilde{\rho}}_{\rm v}(\vec{k},\omega)\left\{-\gamma\int\frac{d^3p}{(2\pi\hbar)^3}G_\omega^2\frac{c\vec{p}}{\varepsilon_0^*}\left[f_0\left(\frac{M_0^*c^2}{\varepsilon_0^{*2}}\right)+\left(\frac{M_0^*c^2}{\epsilon_0^*}\right)\frac{\vec{\nabla}_p f_0\cdot\vec{k}}{\omega-\vec{\rm v}_0\cdot\vec{k}}\right]\right\}\\
&+\delta\tilde{\rho}_s(\vec{k},\omega)\left\{1-\gamma\int\frac{d^3p}{(2\pi\hbar)^3}G_s^2\left[-f_0\frac{(cp)^2}{\varepsilon_0^{*3}}+\left(\frac{M_0^*c^2}{\varepsilon_0^*}\right)^2\frac{\vec{\nabla}_p f_0\cdot\vec{k}}{\omega-\vec{\rm v}_0\cdot\vec{k}}\right)\right\}\\
&+\delta\tilde{\rho}_B(\vec{k},\omega)\left\{\gamma\int\frac{d^3p}{(2\pi\hbar)^3}G_\omega^2\frac{M_0^*c^2}{\varepsilon_0^*}\frac{\vec{\nabla}_p f_0\cdot\vec{k}}{\omega-\vec{\rm v}_0\cdot\vec{k}}\right\}\\
&\qquad=i\gamma\int\frac{d^3p}{(2\pi\hbar)^3}\frac{M_0^*c^2}{\varepsilon_0^*}\frac{\delta\tilde{f}(\vec{k},\vec{p},0)}{\omega-\vec{\rm v}_0\cdot\vec{k}}\ .
\end{aligned}
\tag{3.26}
$$

The fluctuation on the current density from Eq. (3.19) becomes

$$
\begin{aligned}
\delta\vec{\tilde{\rho}}_{\rm v}(\vec{k},\omega) &= \gamma\int\frac{d^3p}{(2\pi\hbar)^3}\left[f_0\delta\left(\frac{c\vec{p}^*}{\varepsilon^*}\right)+\frac{c\vec{p}}{\varepsilon_0^*}\delta\tilde{f}(\vec{k},\vec{p},\omega)\right]\\
&= \gamma\int\frac{d^3p}{(2\pi\hbar)^3}\left[G_s^2\frac{M_0^*c^2}{\varepsilon_0^{*3}}c\vec{p}\delta\tilde{\rho}_s+G_\omega^2\left(-\frac{1}{\varepsilon_0}+\frac{c\vec{p}}{\varepsilon_0^{*3}}c\vec{p}\right)\delta\vec{\tilde{\rho}}_{\rm v}\right]\\
&\quad+\gamma\int\frac{d^3p}{(2\pi\hbar)^3}\frac{c\vec{p}^*}{\epsilon_0^*}\delta\tilde{f}(\vec{k},\vec{p},\omega).
\end{aligned}
\tag{3.27}
$$

Eq. (3.23) and Eq. (3.27) give another equation between density fluctuations as

$$\delta\vec{\tilde{\rho}}_{\rm v}(\vec{k},\omega)\left\{1-\gamma\int\frac{d^3p}{(2\pi\hbar)^3}G_\omega^2\left[f_0\left(-\frac{1}{\varepsilon_0^*}+\frac{(c\vec{p})^2}{\varepsilon_0^{*3}}\right)+\frac{(c\vec{p})^2}{\varepsilon_0^{*2}}\frac{\vec{\nabla}_p f_0\cdot\vec{k}}{\omega-\vec{\rm v}_0\cdot\vec{k}}\right]\right\}$$
$$+\delta\tilde{\rho}_s(\vec{k},\omega)\left\{-\gamma\int\frac{d^3p}{(2\pi\hbar)^3}G_s^2\left[f_0\frac{c\vec{p}}{\varepsilon_0^*}\frac{M_0^*c^2}{\varepsilon_0^{*2}}+\frac{c\vec{p}}{\varepsilon_0^*}\frac{\vec{\nabla}_p f_0\cdot\vec{k}}{\omega-\vec{\rm v}_0\cdot\vec{k}}\frac{M_0^*c^2}{\varepsilon_0^*}\right]\right\}$$
$$+\delta\tilde{\rho}_B(\vec{k},\omega)\left\{\gamma\int\frac{d^3p}{(2\pi\hbar)^3}G_\omega^2\frac{c\vec{p}}{\varepsilon_0^*}\frac{\vec{\nabla}_p f_0\cdot\vec{k}}{\omega-\vec{\rm v}_0\cdot\vec{k}}\right\}=i\gamma\int\frac{d^3p}{(2\pi\hbar)^3}\frac{c\vec{p}}{\varepsilon_0^*}\frac{\delta\tilde{f}(\vec{k},\vec{p},0)}{\omega-\vec{\rm v}_0\cdot\vec{k}}\ . \tag{3.28}$$

From the explicit form of the above equations (3.24), (3.26) and (3.28) we found three coupled algebraic equations for the Fourier transform of small amplitude fluctuations of the baryon density, the scalar density and the current density.

In the relativistic mean-field approximation, non-collective single particle modes with high frequencies are not included, and we are interested only in unstable collective longitudinal modes. For longitudinal modes, the current density oscillates along the propagation axis, i.e. $\delta\vec{\tilde{\rho}}_{\rm v}(\vec{k},\omega)=\delta\tilde{\rho}_{\rm v}\hat{k}$. This requires $\vec{\nabla}_p f_0\cdot\vec{k}=(\nabla_p f_0)k\cos\theta$ and $\vec{v}_0\cdot\vec{k}=v_0k\cos\theta$. For the longitudinal modes, we can write the set of coupled equations (3.24), (3.26) and (3.28) in a matrix form

$$\begin{pmatrix}A_1&A_2&A_3\\B_1&B_2&B_3\\C_1&C_2&C_3\end{pmatrix}\begin{pmatrix}\delta\tilde{\rho}_{\rm v}(\vec{k},\omega)\\\delta\tilde{\rho}_{\rm s}(\vec{k},\omega)\\\delta\tilde{\rho}_B(\vec{k},\omega)\end{pmatrix}=i\begin{pmatrix}\tilde{S}_B(\vec{k},\omega)\\\tilde{S}_{\rm s}(\vec{k},\omega)\\\tilde{S}_{\rm v}(\vec{k},\omega)\end{pmatrix}\ , \tag{3.29}$$

where the components of the coefficient matrix are defined by the following matrix

$$\begin{pmatrix}A_1&A_2&A_3\\B_1&B_2&B_3\\C_1&C_2&C_3\end{pmatrix}=\begin{pmatrix}-G_\omega^2\chi_{\rm v}(\vec{k},\omega)&-G_{\rm s}^2\chi_{\rm s}(\vec{k},\omega)&1+G_\omega^2\chi_B(\vec{k},\omega)\\-G_\omega^2\tilde{\chi}_{\rm v}(\vec{k},\omega)&1+G_{\rm s}^2\tilde{\chi}_{\rm s}(\vec{k},\omega)&+G_\omega^2\chi_{\rm s}(\vec{k},\omega)\\1+G_\omega^2\tilde{\chi}_B(\vec{k},\omega)&-G_{\rm s}^2\chi_{\rm v}(\vec{k},\omega)&+G_\omega^2\chi_{\rm v}(\vec{k},\omega)\end{pmatrix}. \tag{3.30}$$

In the Eq.(3.30), the following definitions are used:

The stochastic source terms are given by

$$\begin{pmatrix} \tilde{S}_{\rm v}(\vec{k},\omega) \\ \tilde{S}_{\rm s}(\vec{k},\omega) \\ \tilde{S}_B(\vec{k},\omega) \end{pmatrix} = \gamma \int \frac{d^3p}{(2\pi\hbar)^3} \begin{pmatrix} c\vec{p}\cdot\vec{k}/\varepsilon_0^* \\ M_0^*c^2/\varepsilon_0^* \\ 1 \end{pmatrix} \frac{\delta\tilde{f}(\vec{k},\vec{p},0)}{\omega - \vec{\rm v}_0\cdot\vec{k}} \ . \tag{3.31}$$

In the expression of the coefficient matrix given in Eq. (3.30), $\chi_{\rm v}(\vec{k},\omega)$, $\chi_B(\vec{k},\omega)$ and $\chi_{\rm s}(\vec{k},\omega)$ represent the long wavelength limit of the Linhard functions with respect to the vector, baryon and scalar density distribution functions in the following form

$$\begin{pmatrix} \chi_{\rm v}(\vec{k},\omega) \\ \chi_{\rm s}(\vec{k},\omega) \\ \chi_B(\vec{k},\omega) \end{pmatrix} = \gamma \int \frac{d^3p}{(2\pi\hbar)^3} \begin{pmatrix} c\vec{p}\cdot\hat{k}/\varepsilon_0^* \\ M_0^*c^2/\varepsilon_0^* \\ 1 \end{pmatrix} \frac{\vec{k}\cdot\vec{\nabla}_p f_0(\vec{p})}{\omega - \vec{\rm v}_0\cdot\vec{k}} \ , \tag{3.32}$$

and the functions $\tilde{\chi}_{\rm v}(\vec{k},\omega)$, $\tilde{\chi}_B(\vec{k},\omega)$ and $\tilde{\chi}_{\rm s}(\vec{k},\omega)$ in the coefficient matrix are given by

$$\tilde{\chi}_{\rm s}(\vec{k},\omega) = \gamma \int \frac{d^3p}{(2\pi\hbar)^3} \left[\frac{(cp)^2}{\varepsilon_0^{*3}} f_0(\vec{p}) - \left(\frac{M_0^*c^2}{\varepsilon_0^*}\right)^2 \frac{\vec{k}\cdot\vec{\nabla}_p f_0(\vec{p})}{\omega - \vec{\rm v}_0\cdot\vec{k}} \right] , \tag{3.33}$$

$$\tilde{\chi}_{\rm v}(\vec{k},\omega) = \gamma \int \frac{d^3p}{(2\pi\hbar)^3} c\vec{p}\cdot\hat{k} \left[\frac{M_0^*c^2}{\varepsilon_0^{*2}} \frac{\vec{k}\cdot\vec{\nabla}_p f_0(\vec{p})}{\omega - \vec{\rm v}_0\cdot\vec{k}} \right] , \tag{3.34}$$

$$\tilde{\chi}_B(\vec{k},\omega) = \gamma \int \frac{d^3p}{(2\pi\hbar)^3} \left[\frac{\varepsilon_0^{*2} - (c\vec{p}\cdot\hat{k})^2}{\varepsilon_0^{*3}} f_0(\vec{p}) - \frac{(c\vec{p}\cdot\hat{k})^2}{\varepsilon_0^{*2}} \frac{\vec{k}\cdot\vec{\nabla}_p f_0(\vec{p})}{\omega - \vec{\rm v}_0\cdot\vec{k}} \right] . \tag{3.35}$$

The matrix equation given in Eq. (3.29) can be solved for the scalar, vector and the baryon density fluctuations and we then get the following solutions

$$\delta\tilde{\rho}_B(\vec{k},\omega) = i \frac{\tilde{S}_B(B_1C_2 - B_2C_1) + \tilde{S}_{\rm s}(A_2C_1 - A_1C_2) + \tilde{S}_{\rm v}(A_1B_2 - A_2B_1)}{\varepsilon(\vec{k},\omega)} \ , \tag{3.36}$$

$$\delta\tilde{\rho}_{\rm v}(\vec{k},\omega) = i\frac{\tilde{S}_B(B_2C_3 - B_3C_2) + \tilde{S}_{\rm s}(A_3C_2 - A_2C_3) + \tilde{S}_{\rm v}(A_2B_3 - A_3B_2)}{\varepsilon(\vec{k},\omega)} \ , \tag{3.37}$$

$$\delta\tilde{\rho}_{\rm s}(\vec{k},\omega) = i\frac{\tilde{S}_B(B_3C_1 - B_1C_3) + \tilde{S}_{\rm s}(A_1C_3 - A_3C_1) + \tilde{S}_{\rm v}(A_3B_1 - A_1B_3)}{\varepsilon(\vec{k},\omega)} \ , \tag{3.38}$$

where $\varepsilon(\vec{k},\omega)$ represents the susceptibility which is the determinant of the coefficient matrix and gives a dispersion relation of the system when $\varepsilon(\vec{k},\omega) = 0$. The susceptibility is written as

$$\varepsilon(\vec{k},\omega) = A_1(B_2C_3 - B_3C_2) - A_2(B_1C_3 - B_3C_1) + A_3(B_1C_2 - B_2C_1) \ . \tag{3.39}$$

In the infinite nuclear matter, collective modes are characterized by the wave number. There is a critical density region in which $\omega(\rho,T) = 0$ at $\rho = \rho_{critical}$. The solution of the dispersion relation gives the characteristic frequencies for every wave numbers. In the stable region ($\rho > \rho_{critical}$) frequencies are real and for unstable modes ($\rho < \rho_{critical}$) frequencies are imaginary.

3.4 Density Correlation Functions

In this part, the early growth of density correlation functions is described in symmetric nuclear matter. For this purpose, the time-dependency of density fluctuations is determined. Density fluctuations in terms of stochastic source terms $\tilde{S}_\alpha(\vec{k},\omega)$ are given in Eqs. (3.36-38).

The evolution of density fluctuations $\delta\tilde{\rho}_\alpha(\vec{k},t)$ in time is determined by taking the inverse Fourier transformation in time, $\delta\tilde{\rho}_\alpha(\vec{k},t) = \int_C \frac{d\omega}{2\pi}\delta\tilde{\rho}_\alpha(\vec{k},\omega)e^{-i\omega t}$, which can be calculated with the help of the residue theorem [35, 37]. After using the inverse Fourier transformation, we get

$$\delta\tilde{\rho}_\alpha(\vec{k},t) = \int_C \frac{d\omega}{2\pi} i\left[\frac{D_1^\alpha\tilde{S}_B(\vec{k},\omega) + D_2^\alpha\tilde{S}_{\rm s}(\vec{k},\omega) + D_3^\alpha\tilde{S}_{\rm v}(\vec{k},\omega)}{\varepsilon(\vec{k},\omega)}\right] e^{-i\omega t} \tag{3.40}$$

where $\alpha = B, \mathrm{v}, s$. In the above expression, $D_1^B = B_1C_2 - B_2C_1$, $D_2^B = C_1A_2 - C_2A_1$, $D_3^B = A_1B_2 - A_2B_1$ for baryon; $D_1^{\mathrm{s}} = C_1B_3 - B_1C_3$, $D_2^{\mathrm{s}} = A_1C_3 - C_1A_3$, $D_3^{\mathrm{s}} = B_1A_3 - A_1B_3$ for scalar; $D_1^{\mathrm{v}} = B_2C_3 - C_2B_3$, $D_2^{\mathrm{v}} = C_2A_3 - A_2C_3$, $D_3^{\mathrm{v}} = A_2B_3 - B_2A_3$ for current densities and the susceptibility is given as $\varepsilon(\vec{k}, \omega) = A_3D_1^B + B_3D_2^B + C_3D_3^B$.

We will interested only in the collective poles of $\varepsilon(\vec{k}, \omega)$. When using the Residue theorem for the evolution of the density fluctuations in time, some contributions come from the non-collective pole of susceptibility and from the poles of the stochastic source terms $\tilde{S_\alpha}(\vec{k}, \omega)$. However, these contributions are effective for the high wave numbers (above $k_c \sim 0.8fm^{-1}$) and ignored for this analysis [35]. Therefore, we take only the growing and decaying poles of susceptibility, $\omega = \pm i\Gamma$.

Cauchy-Residue theorem requires that if we consider a counter integral of the form

$$\int_C f(z)dz \equiv \int_C \frac{g(z)}{h(z)}dz \tag{3.41}$$

where $g(z_0) \neq 0, h(z_0) = 0$ and $h' = \frac{\partial h}{\partial z}|_{z=z_0} \neq 0$. It has only the poles from denominator term. Due to Cauchy-Residue theorem

$$\int_C f(z)dz \equiv \int_C \frac{g(z)}{h(z)}dz = 2\pi i \mathrm{Res}[f(z), z = z_0] = 2\pi i \sum_k A_{-1}(k) \ , \tag{3.42}$$

where the residue of the function is defined by $A_{-1}(k) = \lim_{z\to z_0} \frac{g(z)}{h'(z)}$.

With two poles at $\omega = \pm i\Gamma$, Eq. (3.40) becomes

$$\begin{aligned} \delta\rho_\alpha(\vec{k}) = \quad - \quad & \left\{ \frac{D_1^\alpha \tilde{S}_B + D_2^\alpha \tilde{S}_{\mathrm{s}} + D_3^\alpha \tilde{S}_{\mathrm{v}}}{\partial\varepsilon(\vec{k}, \omega)/\partial\omega} |_{\omega = i\Gamma_k} \ e^{\Gamma t} \right. \\ & \left. + \frac{D_1^\alpha \tilde{S}_B + D_2^\alpha \tilde{S}_{\mathrm{s}} + D_3^\alpha \tilde{S}_{\mathrm{v}}}{\partial\varepsilon(\vec{k}, \omega)/\partial\omega} |_{\omega = -i\Gamma_k} \ e^{-\Gamma t} \ . \right\} \end{aligned} \tag{3.43}$$

Consequently, time-dependent density fluctuations including growing and decaying collective poles are given by

$$\delta\tilde{\rho}_\alpha(\vec{k},t) = \delta\rho_\alpha^+(\vec{k})e^{+\Gamma_k t} + \delta\rho_\alpha^-(\vec{k})e^{-\Gamma_k t} \ . \tag{3.44}$$

The initial amplitudes of density fluctuations related to the growing and decaying modes are given by,

$$\delta\tilde{\rho}_B^{\mp}(\vec{k}) = -\left[\frac{D_1^b\tilde{S}_B(\vec{k},\omega) + D_2^b\tilde{S}_{\rm s}(\vec{k},\omega) + D_3^b\tilde{S}_{\rm v}(\vec{k},\omega)}{\partial\varepsilon(\vec{k},\omega)/\partial\omega}\right]_{\omega=\mp i\Gamma_k} \tag{3.45}$$

$$\delta\tilde{\rho}_{\rm s}^{\mp}(\vec{k}) = -\left[\frac{D_1^s\tilde{S}_B(\vec{k},\omega) + D_2^s\tilde{S}_{\rm s}(\vec{k},\omega) + D_3^s\tilde{S}_{\rm v}(\vec{k},\omega)}{\partial\varepsilon(\vec{k},\omega)/\partial\omega}\right]_{\omega=\mp i\Gamma_k} \tag{3.46}$$

$$\delta\tilde{\rho}_{\rm v}^{\mp}(\vec{k}) = -\left[\frac{D_1^v\tilde{S}_B(\vec{k},\omega) + D_2^v\tilde{S}_{\rm s}(\vec{k},\omega) + D_3^v\tilde{S}_{\rm v}(\vec{k},\omega)}{\partial\varepsilon(\vec{k},\omega)/\partial\omega}\right]_{\omega=\mp i\Gamma_k} \tag{3.47}$$

In the Eqns. (3.45), (3.46) and (3.47), the derivative of the susceptibility becomes

$$\begin{aligned}\frac{\partial\varepsilon(k,\omega)}{\partial\omega} &= \left(\frac{\partial A_3}{\partial\omega}D_1 + A_3\frac{\partial D_1}{\partial\omega}\right) + \left(\frac{\partial B_3}{\partial\omega}D_2 + B_3\frac{\partial D_2}{\partial\omega}\right) \\ &\quad + \left(\frac{\partial C_3}{\partial\omega}D_3 + C_3\frac{\partial D_3}{\partial\omega}\right)\end{aligned} \tag{3.48}$$

where

$$\begin{aligned}\frac{\partial D_1}{\partial\omega} &= \left(\frac{\partial B_1}{\partial\omega}C_2 + B_1\frac{\partial C_2}{\partial\omega} - \frac{\partial C_1}{\partial\omega}B_2 - C_1\frac{\partial B_2}{\partial\omega}\right) \ , \\ \frac{\partial D_2}{\partial\omega} &= \left(\frac{\partial C_1}{\partial\omega}A_2 + C_1\frac{\partial A_2}{\partial\omega} - \frac{\partial A_1}{\partial\omega}C_2 - A_1\frac{\partial C_2}{\partial\omega}\right) \ , \\ \frac{\partial D_3}{\partial\omega} &= \left(\frac{\partial A_1}{\partial\omega}B_2 + A_1\frac{\partial B_2}{\partial\omega} - \frac{\partial B_1}{\partial\omega}A_2 - B_1\frac{\partial A_2}{\partial\omega}\right) \ .\end{aligned} \tag{3.49}$$

In order to calculate the above derivative terms, we define the following integral

$$K_i(\vec{k},\omega) \equiv \int_{-1}^{1} dx \frac{x^i}{\omega - \alpha x} \tag{3.50}$$

and its derivative with respect to ω as

$$\frac{\partial K_i}{\partial\omega} = -\int_{-1}^{1} dx \frac{x^i}{(\omega - \alpha x)^2} \ , \tag{3.51}$$

where we use the short hand definition $\alpha \equiv ck\,(cp/\epsilon_0^*)$.

The derivatives of the terms in Eq. (3.48) and (3.49) are given as

$$\begin{pmatrix} \frac{\partial A_1}{\partial\omega}\big|_{\omega=\mp i\Gamma} \\ \frac{\partial A_2}{\partial\omega}\big|_{\omega=\mp i\Gamma} \\ \frac{\partial A_3}{\partial\omega}\big|_{\omega=\mp i\Gamma} \end{pmatrix} = \begin{pmatrix} -G_\omega^2 \\ -G_{\rm s}^2 \\ +G_\omega^2 \end{pmatrix} \frac{2\pi\gamma}{(2\pi\hbar c)^3} kc \int dp \frac{\partial f_0}{\partial\varepsilon_0^*} \begin{pmatrix} p^4 \frac{1}{\varepsilon_0^{*2}} \frac{\partial K_2}{\partial\omega}\big|_{\omega=\mp i\Gamma} \\ p^3 \frac{M_0^* c^2}{\varepsilon_0^{*2}} \frac{\partial K_1}{\partial\omega}\big|_{\omega=\mp i\Gamma} \\ p^3 \frac{1}{\varepsilon_0^*} \frac{\partial K_1}{\partial\omega}\big|_{\omega=\mp i\Gamma} \end{pmatrix}, \tag{3.52}$$

$$\begin{pmatrix} \frac{\partial B_1}{\partial\omega}\big|_{\omega=\mp i\Gamma} \\ \frac{\partial B_2}{\partial\omega}\big|_{\omega=\mp i\Gamma} \\ \frac{\partial B_3}{\partial\omega}\big|_{\omega=\mp i\Gamma} \end{pmatrix} = \begin{pmatrix} -G_\omega^2 \\ -G_{\rm s}^2 \\ +G_\omega^2 \end{pmatrix} \frac{2\pi\gamma}{(2\pi\hbar c)^3} kc \int dp \frac{\partial f_0}{\partial\varepsilon_0^*} \begin{pmatrix} p^4 \frac{M_0^* c^2}{\varepsilon_0^{*3}} \frac{\partial K_2}{\partial\omega}\big|_{\omega=\mp i\Gamma} \\ p^3 \frac{(M_0^* c^2)^2}{\varepsilon_0^{*3}} \frac{\partial K_1}{\partial\omega}\big|_{\omega=\mp i\Gamma} \\ p^3 \frac{M_0^* c^2}{\varepsilon_0^{*2}} \frac{\partial K_1}{\partial\omega}\big|_{\omega=\mp i\Gamma} \end{pmatrix}, \tag{3.53}$$

and

$$\begin{pmatrix} \frac{\partial C_1}{\partial\omega}\big|_{\omega=\mp i\Gamma} \\ \frac{\partial C_2}{\partial\omega}\big|_{\omega=\mp i\Gamma} \\ \frac{\partial C_3}{\partial\omega}\big|_{\omega=\mp i\Gamma} \end{pmatrix} = \begin{pmatrix} -G_\omega^2 \\ -G_{\rm s}^2 \\ +G_\omega^2 \end{pmatrix} \frac{2\pi\gamma}{(2\pi\hbar c)^3} kc \int dp \frac{\partial f_0}{\partial\varepsilon_0^*} \begin{pmatrix} p^5 \frac{1}{\varepsilon_0^{*3}} \frac{\partial K_3}{\partial\omega}\big|_{\omega=\mp i\Gamma} \\ p^4 \frac{M_0^* c^2}{\varepsilon_0^{*3}} \frac{\partial K_2}{\partial\omega}\big|_{\omega=\mp i\Gamma} \\ p^4 \frac{1}{\epsilon_0^{*2}} \frac{\partial K_2}{\partial\omega}\big|_{\omega=\mp i\Gamma} \end{pmatrix}. \tag{3.54}$$

For both cases, $\omega = \pm i\Gamma$, the susceptibility can be calculated numerically. The derivative $\partial\varepsilon(\vec{k},\omega)/\partial\omega$ at $\omega \to i\Gamma$ and $\omega \to -i\Gamma$ is obtained as

$$\begin{aligned} \left[\frac{\partial\varepsilon(k,\omega)}{\partial\omega}\right]_{\omega=+i\Gamma} &= \left(\frac{\partial A_3}{\partial\omega}D_1 + A_3\frac{\partial D_1}{\partial\omega}\right) + \left(\frac{\partial B_3}{\partial\omega}D_2 + B_3\frac{\partial D_2}{\partial\omega}\right) \\ &\quad + \left(\frac{\partial C_3}{\partial\omega}D_3 + C_3\frac{\partial D_3}{\partial\omega}\right) \end{aligned} \tag{3.55}$$

$$\begin{aligned} \left[\frac{\partial\varepsilon(k,\omega)}{\partial\omega}\right]_{\omega=-i\Gamma} &= \left(-\frac{\partial A_3}{\partial\omega}D_1 - A_3\frac{\partial D_1}{\partial\omega}\right) + \left(-\frac{\partial B_3}{\partial\omega}D_2 - B_3\frac{\partial D_2}{\partial\omega}\right) \\ &\quad + \left(-\frac{\partial C_3}{\partial\omega}D_3 - C_3\frac{\partial D_3}{\partial\omega}\right) \ . \end{aligned} \tag{3.56}$$

From Eq. (3.55) and Eq. (3.56) we find

$$\left(\frac{\partial\varepsilon(k,\omega)}{\partial\omega}\right)_{\omega=-i\Gamma} = -\left(\frac{\partial\varepsilon(k,\omega)}{\partial\omega}\right)_{\omega=+i\Gamma} . \tag{3.57}$$

Let us return to the spectral intensity of the density correlation functions $\tilde{\sigma}_{\alpha\alpha}(\vec{k},t)$ defined as $\overline{\delta\tilde{\rho}_\alpha(\vec{k},t)(\delta\tilde{\rho}_\alpha(\vec{k}',t))^*} = (2\pi)^3\delta^3(\vec{k}-\vec{k}')\tilde{\sigma}_{\alpha\alpha}(\vec{k},t)$ where time-dependent density functions are given by Eq. (3.44) with the amplitudes of baryon density fluctuations of the growing and decaying modes at the initial state. Spectral intensity of the baryon density function is written as [26, 27].

$$\begin{aligned}\tilde{\sigma}_{BB}(\vec{k},t)(2\pi)^3\delta^3(\vec{k}-\vec{k}') &= \overline{\delta\rho_B^+(\vec{k})(\delta\rho_B^+(\vec{k}))^*}e^{2\Gamma_k t} + \overline{\delta\rho_B^-(\vec{k})(\delta\rho_B^-(\vec{k}))^*}e^{-2\Gamma_k t} \\ &\quad +\overline{\delta\rho_B^+(\vec{k})(\delta\rho_B^-(\vec{k}))^*} + \overline{\delta\rho_B^-(\vec{k})(\delta\rho_B^+(\vec{k}))^*} \qquad (3.58)\end{aligned}$$

In order to calculate the spectral function, we use the main assumption of the stochastic mean-field approach which states that in each phase-space cell, the initial phase-space distribution $f(\vec{k},\vec{p},0)$ is a Gaussian random number and its mean value is obtained by $\overline{f(\vec{k},\vec{p},0)} = f_0(\vec{k},\vec{p})$ and its second moment is determined by [20]

$$\overline{\delta\tilde{f}(\vec{k},\vec{p},0)\delta\tilde{f}^*(\vec{k}',\vec{p}',0)} = (2\pi)^3\delta^3(\vec{k}-\vec{k}')(2\pi\hbar)^3\delta^3(\vec{p}-\vec{p}')f_0(\vec{k},\vec{p})[1-f_0(\vec{k},\vec{p})] \qquad (3.59)$$

where the overline indicates the ensemble averaging and $f_0(\vec{k},\vec{p})$ represents the average phase-space distribution at the initial state. Using this approach, we can calculate the followings:

$$\begin{aligned}&\left[\overline{\left(\delta\rho_B(\vec{k})\right)^\pm}\right]\left[\overline{\left(\delta\rho_B(\vec{k})\right)^\pm}\right]^* \\ &= (2\pi)^3\delta^3(\vec{k}-\vec{k}')\left[\frac{|D_1^B|^2K_{11}^{++}+|D_2^B|^2K_{22}^{++}+|D_3^B|^2K_{33}^{++}+2D_1^BD_2^BK_{12}^{++}}{\left|\left(\frac{\partial\varepsilon(k,\omega)}{\partial\omega}\right)_{\omega=\pm i\Gamma}\right|^2}\right] \qquad (3.60)\end{aligned}$$

and

$$\begin{aligned}&\left[\overline{\left(\delta\rho_B(\vec{k})\right)^+}\right]\left[\overline{\left(\delta\rho_B(\vec{k})\right)^-}\right]^* = \left[\overline{\left(\delta\rho_B(\vec{k})\right)^-}\right]\left[\overline{\left(\delta\rho_B(\vec{k})\right)^+}\right]^* \\ &= (2\pi)^3\delta^3(\vec{k}-\vec{k}')\left[\frac{|D_1^B|^2K_{11}^{+-}+|D_2^B|^2K_{22}^{+-}-|D_3^B|^2K_{33}^{+-}+2D_1^BD_2^BK_{12}^{+-}}{\left[\left(\frac{\partial\varepsilon(k,\omega)}{\partial\omega}\right)_{\omega=+i\Gamma}\right]\left[\left(\frac{\partial\varepsilon(k,\omega)}{\partial\omega}\right)_{\omega=-i\Gamma}\right]^*}\right] \qquad (3.61)\end{aligned}$$

with the following integrals

$$\begin{pmatrix} K_{11}^{+-} \\ K_{22}^{+-} \\ K_{33}^{+-} \\ K_{12}^{+-} \end{pmatrix} = \gamma^2 \int \frac{d^3p}{(2\pi\hbar)^3} \begin{pmatrix} 1 \\ \left(\frac{M_0^* c^2}{\varepsilon_0^*}\right)^2 \\ \left(c\frac{\vec{p}\cdot\hat{k}}{\varepsilon_0^*}\right)^2 \\ \frac{M_0^* c^2}{\varepsilon_0^*} \end{pmatrix} \frac{-\Gamma^2 + (\vec{v}_0\cdot\vec{k})^2}{\left[\Gamma^2 + (\vec{v}_0\cdot\vec{k})^2\right]^2} f_0(\vec{p})[1 - f_0(\vec{p}))] \ . \tag{3.62}$$

Finally, the spectral intensity is obtained as

$$\tilde{\sigma}_{BB}(\vec{k},t) = \frac{E_B^+(\vec{k})}{\left|\left(\frac{\partial\varepsilon(\vec{k},\omega)}{\partial\omega}\right)_{\omega=i\Gamma_k}\right|^2}(e^{2\Gamma_k t} + e^{-2\Gamma_k t}) + \frac{2E_B^-(\vec{k})}{\left|\left(\frac{\partial\varepsilon(\vec{k},\omega)}{\partial\omega}\right)_{\omega=i\Gamma_k}\right|^2} \tag{3.63}$$

where

$$\begin{aligned} E_B^+(\vec{k}) &= |D_1^B|^2 K_{11}^+ + |D_2^B|^2 K_{22}^+ + |D_3^B|^2 K_{33}^+ + 2D_1^B D_2^B K_{12}^+ \\ E_B^-(\vec{k}) &= |D_1^B|^2 K_{11}^- + |D_2^B|^2 K_{22}^- - |D_3^B|^2 K_{33}^- + 2D_1^B D_2^B K_{12}^- \end{aligned} \tag{3.64}$$

with the integrals

$$\begin{pmatrix} K_{11}^{\mp} \\ K_{22}^{\mp} \\ K_{33}^{\mp} \\ K_{12}^{\mp} \end{pmatrix} = \gamma^2 \int \frac{d^3p}{(2\pi\hbar)^3} \begin{pmatrix} 1 \\ \left(\frac{M_0^* c^2}{\varepsilon_0^*}\right)^2 \\ \left(c\frac{\vec{p}\cdot\hat{k}}{\varepsilon_0^*}\right)^2 \\ \frac{M_0^* c^2}{\varepsilon_0^*} \end{pmatrix} \frac{\Gamma^2 \mp (\vec{v}_0\cdot\vec{k})^2}{\left[\Gamma^2 + (\vec{v}_0\cdot\vec{k})^2\right]^2} f_0(\vec{p})[1 - f_0(\vec{p}))] \ . \tag{3.65}$$

The detailed calculations are given in Appendix B.

When the same derivation is applied for the scalar and vector densities, it can be seen that the spectral intensities of scalar and baryon density correlation functions have the same form, which is

$$\begin{aligned} \tilde{\sigma}_{\rm ss}(\vec{k},t) &= \frac{\left[|D_1^s|^2 K_{11}^+ + |D_2^s|^2 K_{22}^+ + |D_3^s|^2 K_{33}^+ + 2D_1^s D_2^s K_{12}^+\right]}{\left|\left(\frac{\partial\varepsilon(k,\omega)}{\partial\omega}\right)_{\omega=i\Gamma_k}\right|^2}(e^{2\Gamma_k t} + e^{-2\Gamma_k t}) \\ &+ \frac{2\left[|D_1^s|^2 K_{11}^- + |D_2^s|^2 K_{22}^- - |D_3^s|^2 K_{33}^- + 2D_1^s D_2^s K_{12}^-\right]}{\left|\left(\frac{\partial\varepsilon(k,\omega)}{\partial\omega}\right)_{\omega=i\Gamma_k}\right|^2}. \end{aligned} \tag{3.66}$$

In this expression, $D_1^{\rm s} \equiv C_1 B_3 - i^2 B_1 C_3$, $D_2^{\rm s} \equiv i^2 A_1 C_3 - C_1 A_3$, $D_3^{\rm s} \equiv i(B_1 A_3 - A_1 B_3)$ are used. However, the spectral intensity of vector density case has different form since the second term of the final result has overall minus sign. The spectral intensity function for the vector density correlation function is

$$\begin{aligned}\tilde{\sigma}_{\rm vv}(\vec{k},t) &= \frac{\left[|D_1^{\rm v}|^2 K_{11}^{+} + |D_2^{\rm v}|^2 K_{22}^{+} + |D_3^{\rm v}|^2 K_{33}^{+} + 2D_1^{\rm v} D_2^{\rm v} K_{12}^{+}\right]}{\left|\left(\frac{\partial\varepsilon(k,\omega)}{\partial\omega}\right)_{\omega=i\Gamma_k}\right|^2}\left(e^{2\Gamma_k t} + e^{-2\Gamma_k t}\right) \\ &\quad - \frac{2\left[|D_1^{\rm v}|^2 K_{11}^{-} + |D_2^{\rm v}|^2 K_{22}^{-} - |D_3^{\rm v}|^2 K_{33}^{-} + 2D_1^{\rm v} D_2^{\rm v} K_{12}^{-}\right]}{\left|\left(\frac{\partial\varepsilon(k,\omega)}{\partial\omega}\right)_{\omega=i\Gamma_k}\right|^2}\,, \qquad (3.67)\end{aligned}$$

where $D_1^{\rm v} \equiv i(B_2 C_3 - C_2 B_3)$, $D_2^{\rm v} \equiv i(C_2 A_3 - A_2 C_3)$, $D_3^{\rm v} \equiv A_2 B_3 - B_2 A_3$. The derivations for the scalar and vector case can be found in Appendix C.

Local density fluctuations depending on space $\delta\rho_\alpha(\vec{r},t)$ are obtained from the Fourier transformation of $\delta\rho_\alpha(\vec{k},t)$. Equal time correlation functions of density fluctuations as a function of distance between two space points can be represented in terms of the corresponding spectral intensity as [26, 36],

$$\sigma_{\alpha\alpha}(|\vec{r}-\vec{r}'|,t) = \overline{\delta\rho_\alpha(\vec{r},t)\delta\rho_\alpha(\vec{r}',t)} = \int \frac{d^3k}{(2\pi)^3} e^{i\vec{k}\cdot(\vec{r}-\vec{r}')}\tilde{\sigma}_{\alpha\alpha}(\vec{k},t). \qquad (3.68)$$

The density correlation functions include valuable information about the unstable behavior of the nuclear matter in the spinodal region [27, 36]. The early growth of baryon and scalar density correlation functions give information about the size of the condensation in spinodal region and the current density correlation function presents an estimation about the initial speed of condensing fragments.

CHAPTER 4

NUCLEAR SPINODAL INSTABILITIES

4.1 Growth Rates of Unstable Modes

The growth and decay rates of collective modes are determined in the spinodal region from the dispersion relation in Chapter 3 for finite temperature and for zero temperature they are determined from the dispersion relation given in Appendix D. In the standard Walecka model, the four free parameters are used; namely two coupling constants and two meson masses. In the NL3 model which includes nonlinear interactions of the scalar meson, there are two additional parameters κ and λ . In the numerical calculations, the parameter set for the NL3 model given in Table 2.1 is used. The calculations are made for different temperature values (T=0, 2, 4, 6, 8, 10 MeV) and two different initial baryon densities ($\rho_B = 0.2\ \rho_0$ and $\rho_B = 0.4\ \rho_0$).

By using the dispersion relation given in eqn. (3.39), we can find the unstable collective modes characterized by the wave number. For instance, Fig. 4.1 represents the growth rates of unstable modes as a function of wave number for the initial baryon density $\rho_B = 0.4\ \rho_0$ at various temperatures. For each temperature values, the growth rate increases from the origin linearly, and after a maximum point at a certain value of the wave number, it reduces to zero at a maximum value of the wave number since the non-local effects become important due to importance of the k^2 term in the dispersion relation [36]. The growth rate is the inverse of the time constant which describes the initial growth of the

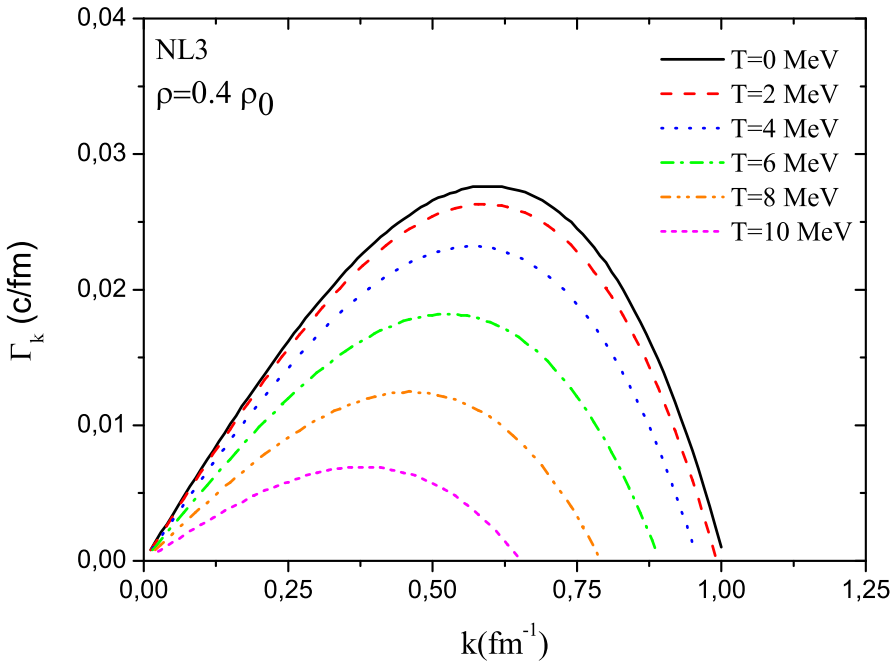

Figure 4.1: Growth rates of unstable modes as a function of wave numbers in the spinodal region at baryon density $\rho_B = 0.4\ \rho_0$ and at different temperature values.

density fluctuations. The wave number around the maximum growth rate Γ_{max} shifts from $0.4fm^{-1}$ to $0.7fm^{-1}$ when temperature decreases.

Fig. 4.2 shows the growth rates of the unstable modes for the initial baryon density $\rho_B = 0.2\ \rho_0$. The wave number around the maximum growth rate takes the values from approximately $0.5fm^{-1}$ to $0.9fm^{-1}$ according to the different temperatures. By comparing the Fig. 4.1 and Fig. 4.2, it can be said that in the nonlinear relativistic approach most unstable behavior occurs at lower densities and depends strongly on density at each temperature. For both cases, we may choose the most amplified modes occurring around the wave numbers $k \approx (0.5 - 0.7)fm^{-1}$ or the corresponding wave lengths $\lambda \approx (9 - 12)fm$ to determine the boundary of spinodal region.

In Fig. 4.3, the growth rates of the unstable modes obtained from the dispersion relation in the non-relativistic approach with an effective Skyrme force [27] and in the nonlinear Walecka model are shown. The figure is drawn at the initial baryon

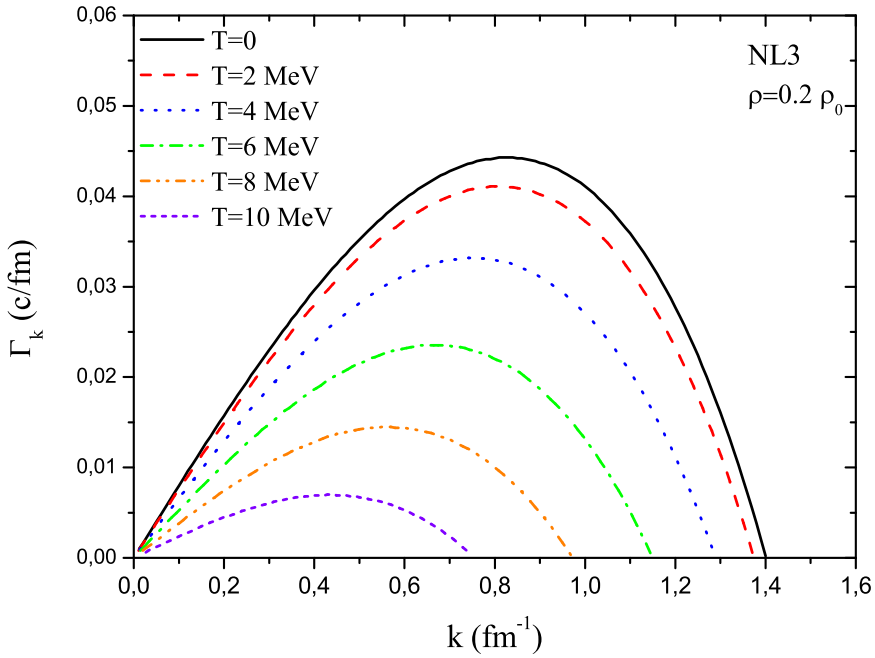

Figure 4.2: Growth rates of unstable modes as a function of wave numbers in the spinodal region at baryon density $\rho_B = 0.2\ \rho_0$ and at different temperature values.

densities $\rho_B = 0.2\ \rho_0$ and $\rho_B = 0.4\ \rho_0$ in the spinodal region at temperature $T = 5\ MeV$. For each model, the curves show similar behavior. The wave number for the maximum growth rate Γ_{max} for each model is around $0.5fm^{-1}$ for $\rho_B = 0.4\ \rho_0$ and $0.8fm^{-1}$ for $\rho_B = 0.2\ \rho_0$. The shortest growth time ($\tau \equiv 1/\Gamma_k$) that characterizes the initial growth of the density fluctuations is found approximately $50fm/c$ for NL3 and $60fm/c$ for non-relativistic model in $\rho_B = 0.4\ \rho_0$ case. It becomes about $35fm/c$ for NL3 and $30fm/c$ for non-relativistic model in $\rho_B = 0.2\ \rho_0$ case.

These results display that the dispersion relations for unstable modes obtained from the relativistic NL3 model are comparable to the dispersion relations getting from the non-relativistic calculations under similar conditions.

In Fig. 4.4, we calculate the growth rates of the most unstable modes as a function of baryon density for different temperatures. When temperature increases, the density value at which the most unstable behavior occurs shifts towards the

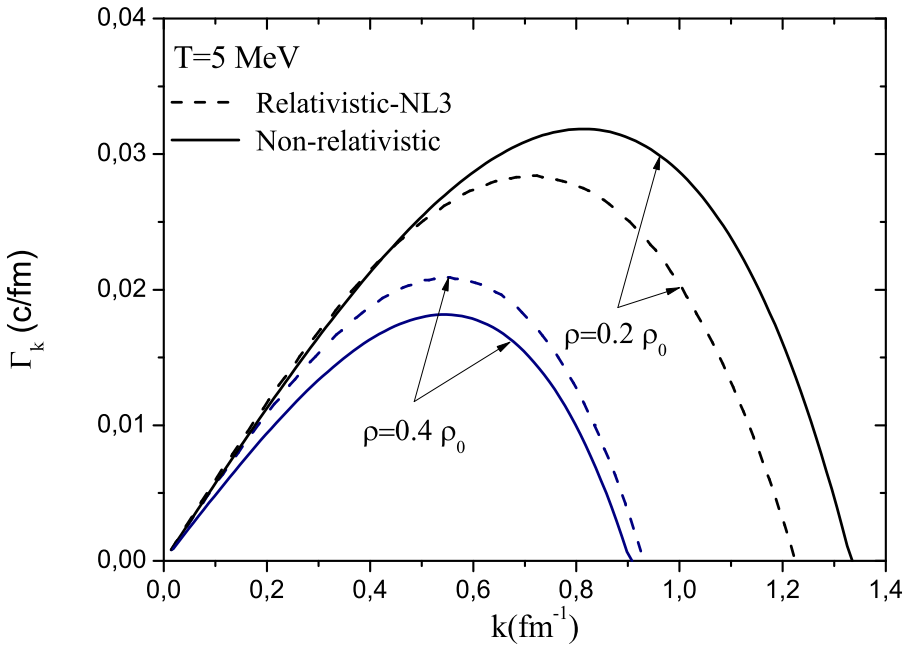

Figure 4.3: Growth rates of unstable modes as a function of wave numbers in the spinodal region at baryon densities $\rho_B = 0.2\ \rho_0$ and $\rho_B = 0.4\ \rho_0$ at $T = 5\ MeV$ for relativistic NL3 (dashed lines) and non-relativistic calculations (solid lines).

higher densities quietly. The most unstable behavior is observed in the interval $0.2\ \rho_0 < \rho_B < 0.4\ \rho_0$ depending on temperature.

Fig. 4.5 illustrates the growth rates of the most unstable modes according to the ratio of density ρ_B/ρ_0 in both relativistic-NL3 and non-relativistic approaches at T=5 MeV. In both approaches, the system exhibits most unstable behavior at lower densities around $\rho_B = 0.2\ \rho_0$. The unstable behavior of the system becomes comparable in both relativistic and non-relativistic approaches under similar conditions.

4.2 Boundary of Spinodal Region

The boundary of the spinodal instability region can be determined from the dispersion relation. As an example of the phase diagrams, Fig. 4.6 shows the boundary of the spinodal region for the unstable modes of wavelength $\lambda = 9fm$

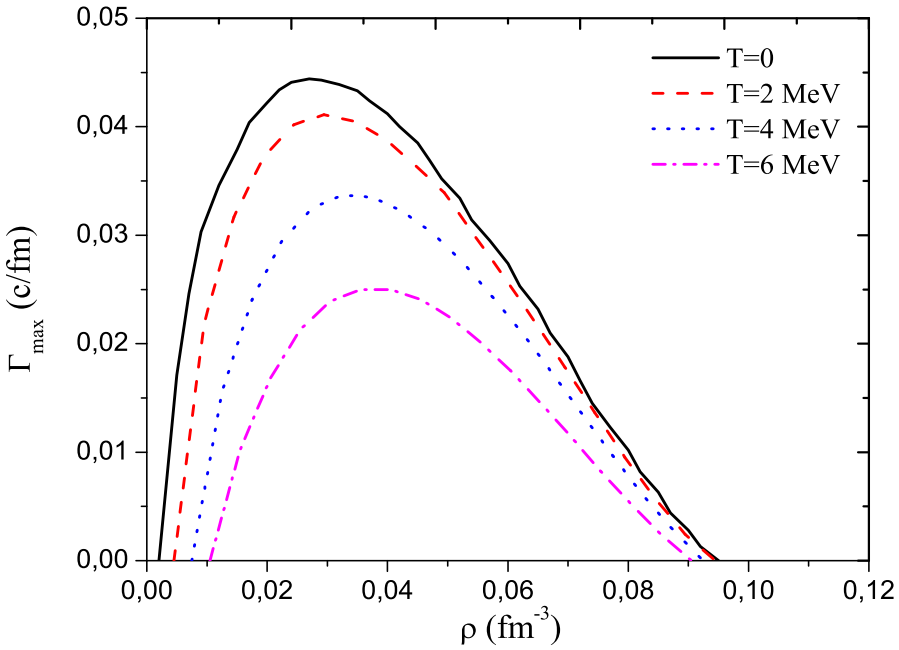

Figure 4.4: Growth rates of the most unstable modes as a function of baryon density in spinodal region.

and $\lambda = 12fm$. In the figure, as the area under the phase coexistence curve is a region for the mixture of gas and liquid, the region above the curve shows the uniform nuclear matter [38]. The curve is a parabola-like curve starting from the origin and reaching at a critical point around $\rho_c \approx 0.3\ \rho_0$ and a critical temperature $T_c \approx 12\ MeV$, then decreasing to zero about $\rho_B \approx 0.5\ \rho_0$ that corresponds to the minimum of the pressure-density curve.

At lower temperatures, there are two points (say A and B with ρ_A and ρ_B) on the boundary defined spinodal region in which the pressure is a decreasing function, $\frac{\partial P}{\partial \rho} < 0$. There are two different physical phases: a gas phase at low densities less than ρ_A and a liquid phase at densities higher than ρ_B and close to saturation density ρ_0. As temperature increases, the spinodal region narrows and these two points coincide with each other at a critical temperature T_c . At and above this temperature, the system is in a single phase. As a result, liquid and gas phases coexist at temperature lower than T_c and only gas phase can exist at or above T_c.

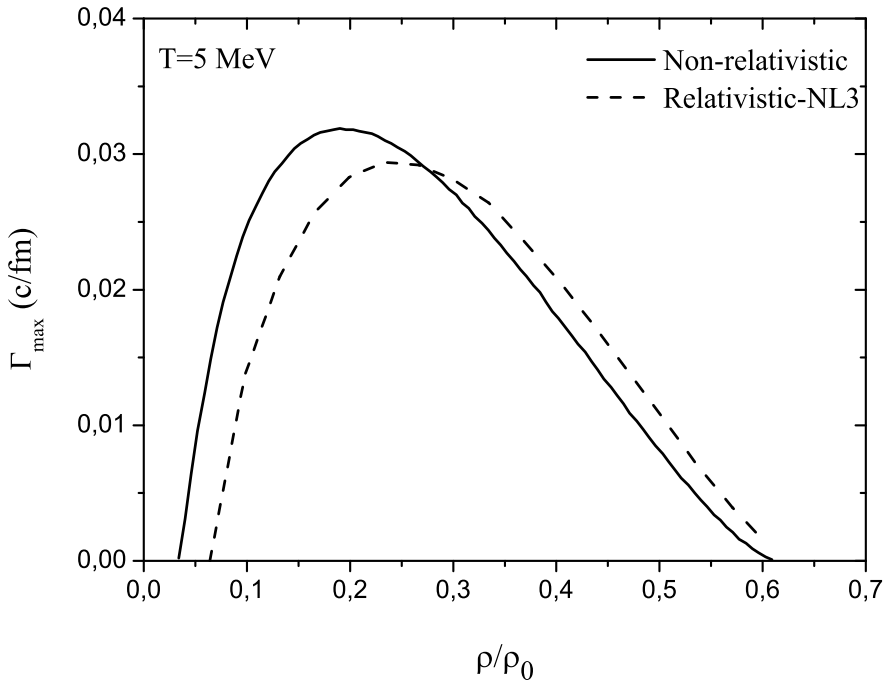

Figure 4.5: Growth rates of the most unstable modes as a function of baryon density in spinodal region at temperature $T = 5\ MeV$ for non-relativistic calculations (solid line) and for relativistic-NL3 calculations (dashed line).

In both the $\lambda = 9fm$ and $\lambda = 12fm$ case, the shortest time is about $35fm/c$ and it occurs for a density about 0.3 ρ_0 . The shortest time value is obtained from the Fig. 4.5. If we analyze the same values at non-relativistic case which is obtained from the Fig.3 in the reference-23, the shortest time is about $30fm/c$ and it occurs for the density around $0.2\rho_0$ for the $\lambda = 9fm$ case. We observe the small differences in the unstable response of the system, the system exhibits most unstable behavior around $0.2\rho_0$ in the non-relativistic case while the most unstable behavior occurs around $0.3\rho_0$ in the nonlinear relativistic case.

4.3 The Size of Primary Clusters in Spinodal Region

The wavelengths are long when compared with the inter-particle spacing and the interaction range. Therefore, the size of the initial clusters or initial condensation regions is defined as the half wavelength of the fastest amplified modes. Fig. 4.7

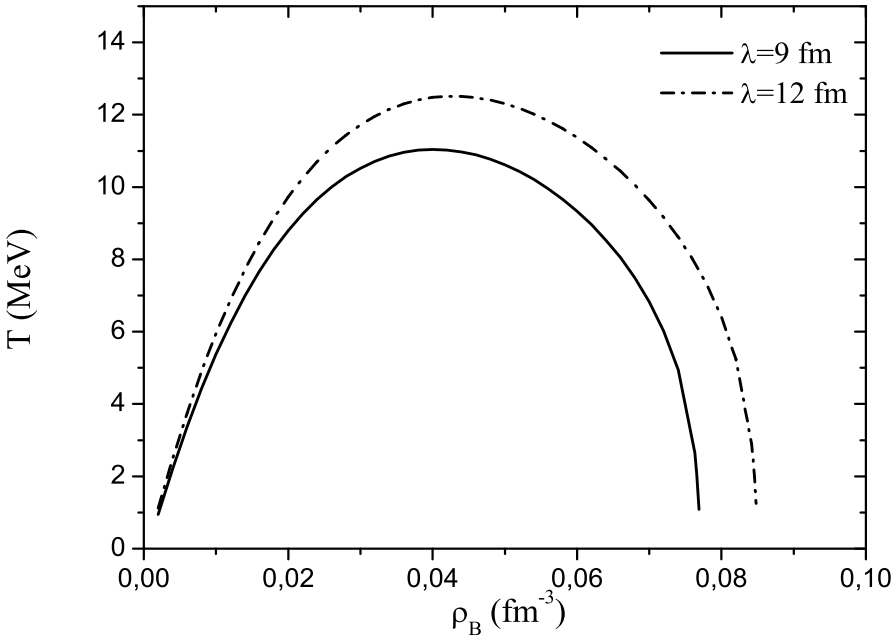

Figure 4.6: Boundary of spinodal region in baryon density-temperature plane of the unstable mode for the wavelengths $\lambda = 9fm$ and $\lambda = 12fm$ in relativistic-NL3 model.

gives the size of the primary clusters of the most unstable collective modes in spinodal region as a function of the baryon density at four different temperature values ($T = 0, 2, 4$ and $6MeV$).

The most unstable mode named as the fastest amplified mode brings to the system of the homogeneous matter changes into the non-homogeneous phase. During this formation, the primary clusters formed and half-wavelength provides a measure for typical size of these clusters [36]. We read approximately $3.5fm$ for $T = 0{-}2\ MeV$, $4fm$ for $T = 4\ MeV$ and $5fm$ for $T = 6\ MeV$ corresponding to the most unstable modes around $\rho_B \approx 0.3\ \rho_0$ and they are diameters of the initial clusters. The size of the initial clusters increases quietly with the increase of the temperature.

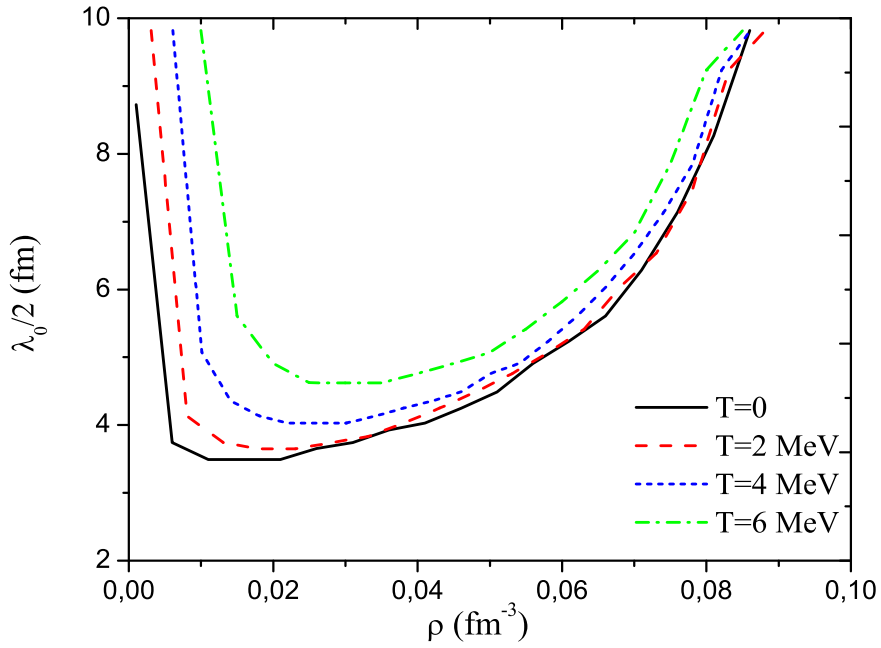

Figure 4.7: The size of the primary clusters in the spinodal region at temperatures $T = 0, 2, 4$ and $6\ MeV$.

4.4 Spectral Intensity of the Density Correlation Functions

In section 3.3, we define the correlation functions $\tilde{\sigma}_{\alpha\alpha}(\vec{k}, t)$ for baryon, scalar and vector densities to calculate the early growth of the baryon density fluctuations in nuclear matter. Figs. 4.8 and 4.9 represent the spectral intensity of the baryon density correlation function (the variance for the unstable modes) as a function of wave number at temperature $T = 1\ MeV$ for two density values $\rho_B = 0.2\ \rho_0$ and $\rho_B = 0.4\ \rho_0$, respectively, using five different initial time values ($t = 0,\ t = 20fm/c,\ t = 30fm/c,\ t = 40fm/c$ and $t = 50fm/c$). We observe from the figure that the largest growth occurs at the wave numbers of the dominant unstable modes which can be seen from Fig. 4.2 and 4.3. The curve shows a more and more peaked-like function around the dominant unstable modes with increasing time. For instance, at time $t = 50fm/c$, the spectral intensity of the most unstable modes of $k = 0.9fm^{-1}$ grows about twenty times for density $\rho_B = 0.2\ \rho_0$ at temperature $T = 1\ MeV$.

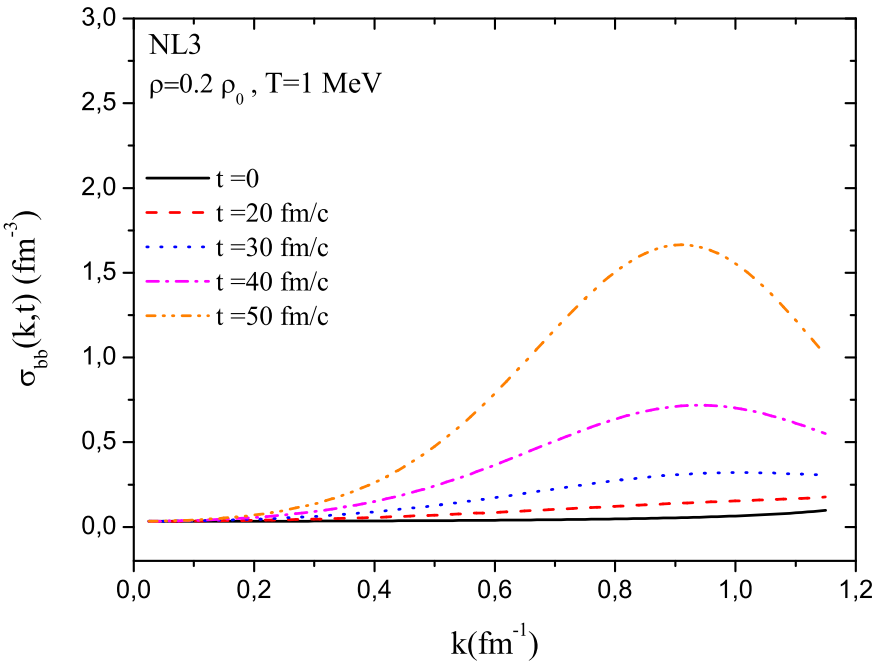

Figure 4.8: : Spectral intensity of baryon density correlation function as a function of wave number at $T = 1\ MeV$ and density $\rho_B = 0.2\ \rho_0$.

In Fig. 4.9, the largest growth of the spectral intensity of the correlation function occurs at the wave number $k = 0.7 fm^{-1}$. The curves are terminated at the wave numbers $k \approx 0.9 fm^{-1} - 1.1 fm^{-1}$ since we only consider the collective modes in our calculations, and non-collective modes which are effective for short wavelengths (higher wave numbers) are not taken into account. As a consequence, the expression of the spectral intensity of the correlation functions is a good approximation for the long wavelengths below the critical value of the wave numbers. The non-collective modes do not change in time and we therefore observe the growth of the collective modes in time in our calculations.

Figs. 4.10 and 4.11 are drawn at $T = 5\ MeV$ for spectral intensity of baryon density correlation function and include the similar information in Figs. 4.8 and 4.9. Again, the largest growth is seen at the range of wave numbers of the unstable dominant modes. The largest growth occurs at $k \approx 0.8 fm^{-1}$ for the density $\rho_B = 0.2\ \rho_0$ and at $k \approx 0.7 fm^{-1}$ for the density $\rho_B = 0.4\ \rho_0$.

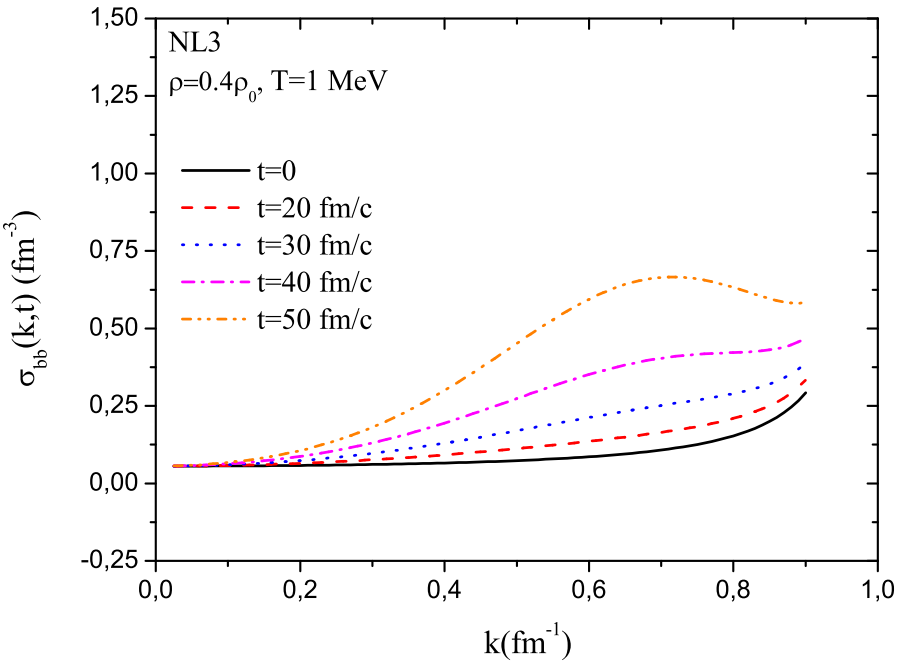

Figure 4.9: : Spectral intensity of baryon density correlation function as a function of wave number at $T = 1\ MeV$ and density $\rho_B = 0.4\ \rho_0$.

Figs. 4.12 and 4.13 at temperature $T = 1\ MeV$ and Figs. 4.14 and 4.15 at temperature $T = 5\ MeV$ demonstrate the spectral intensity of the scalar density correlation function as a function of wave number for two density values, $\rho_B = 0.2\ \rho_0$ and $\rho_B = 0.4\ \rho_0$. The largest growth occurs at $k \approx 0.8 fm^{-1}$ for the baryon density $\rho_B = 0.2\ \rho_0$ and at $k \approx 0.7 fm^{-1}$ for the baryon density $\rho_B = 0.4\ \rho_0$ at $T = 5\ MeV$, and $k \approx 0.9 fm^{-1}$ for the density $\rho_B = 0.2\ \rho_0$ and at $k \approx 0.7 fm^{-1}$ for the density $\rho_B = 0.4\ \rho_0$ at $T = 1\ MeV$. The scalar density case exhibits the similar trend with the baryon density case. The curves are terminated at suitable k values not to include non-collective effects.

For the spectral intensity of the current density correlation function, the curves are given in Figs. 4.16, 4.17, 4.18 and 4.19 at temperatures $T = 1\ MeV$ and $T = 5\ MeV$ for baryon densities $\rho_B = 0.2\ \rho_0$ and $\rho_B = 0.4\ \rho_0$. The peak-like form of the curves around the range of the most unstable modes is observed with the increasing time. In the case of $T = 1\ MeV$, spectral intensity grows about 50 times larger for $\rho_B = 0.2\ \rho_0$ and 10 times larger for $\rho_B = 0.4\ \rho_0$ during

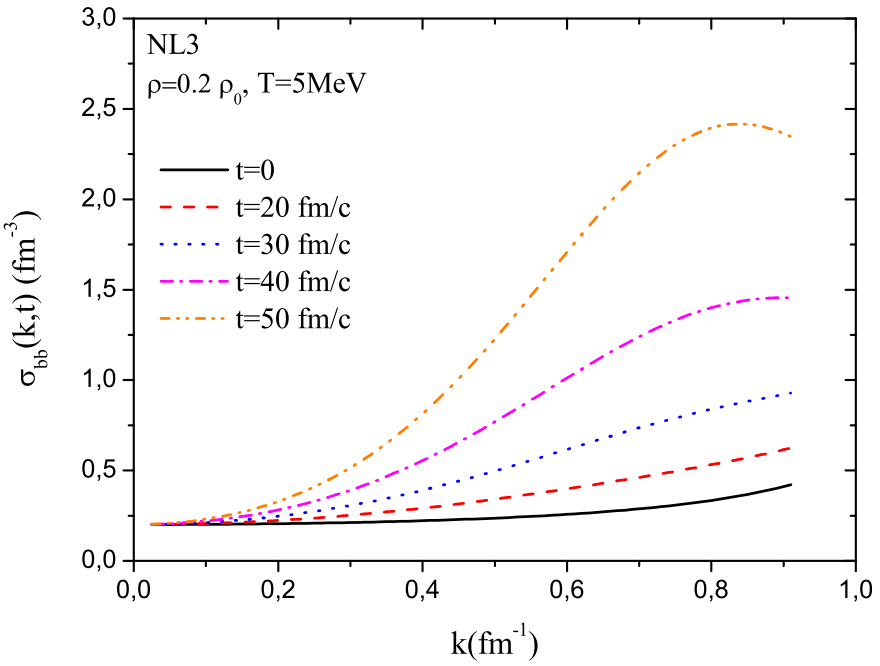

Figure 4.10: : Spectral intensity of baryon density correlation function as a function of wave number at $T = 5\ MeV$ and density $\rho_B = 0.2\ \rho_0$.

the time interval $t = 50 fm/c$. At temperature $T = 5\ MeV$, similar values are observed.

Since the non-collective modes are not included into calculations, the spectral curves of current density are terminated at cut-off wave numbers $k = 1.15 fm^{-1}$ for $T = 1\ MeV$ and $\rho_B = 0.2\ \rho_0$, $k = 0.9 fm^{-1}$ for $T = 1\ MeV$ and $\rho_B = 0.4\ \rho_0$ also $T = 5\ MeV$ and $\rho_B = 0.2\ \rho_0$, and $k = 0.8 fm/c$ for $T = 5\ MeV$ and $\rho_B = 0.4\ \rho_0$.

4.5 Early Growth of Density Correlation Functions

Equal time density correlation functions for baryon, scalar and current density fluctuations as a function of distance between two points in the space are given in Eq.(3.68). These provides valuable information about the unstable behavior of the nuclear dynamics in the spinodal region. Figs. 4.20 and 4.21 show the baryon

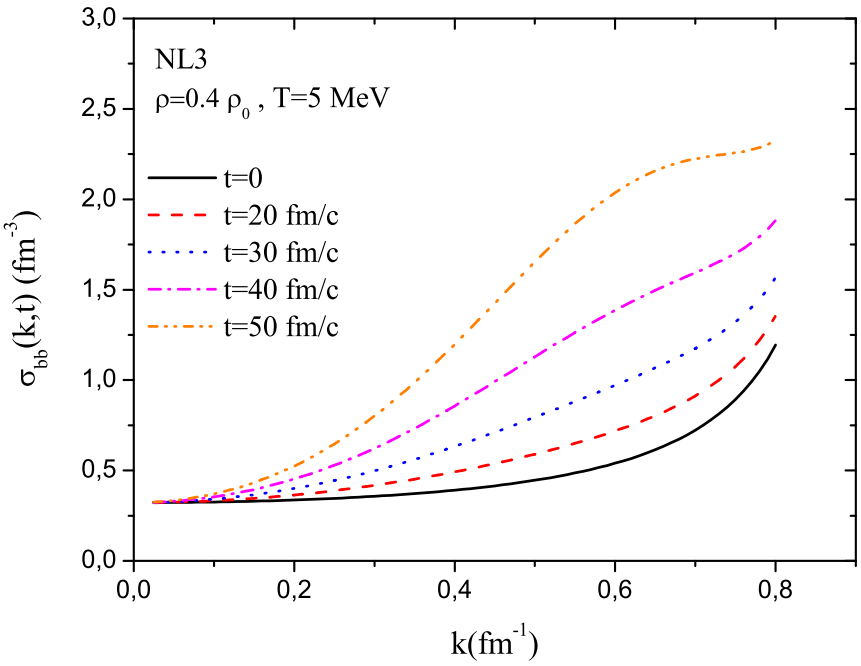

Figure 4.11: : Spectral intensity of baryon density correlation function as a function of wave number at $T = 5\ MeV$ and density $\rho_B = 0.4\ \rho_0$.

density correlation function $\sigma_{BB}(x,t)$ as a function of distance between two space locations at temperature $T = 1\ MeV$ for two initial baryon densities $\rho_B = 0.2\ \rho_0$ and $\rho_B = 0.4\ \rho_0$ and at different times. The width of the correlation function at half maximum named as the correlation length of baryon density fluctuations characterizes the size of the initial condensation region [36]. Correlation length in the linear approximation provides an estimation about the size of condensing fragments formed during the initial phase of spinodal decomposition. From Figs. 4.20 and 4.21, the correlation length reads about 2.5 fm at both densities $\rho_B = 0.2\ \rho_0$ and $\rho_B = 0.4\ \rho_0$ that corresponds to a condensation region including approximately A=12 nucleons. At temperature $T = 1\ MeV$, the evolution of baryon density correlation function in time is faster at lower densities than at higher densities. For example, $\sigma_{BB}(x = 0, t = 50fm/c) \approx 0.032fm^{-6}$ at baryon density $\rho_B = 0.2\ \rho_0$ and $\sigma_{BB}(x = 0, t = 50fm/c) \approx 0.007fm^{-6}$ at $\rho_B = 0.4\ \rho_0$ that is five times larger at $\rho_B = 0.2\ \rho_0$ than the value at $\rho_B = 0.4\ \rho_0$.

In the Figs. 4.22 and 4.23 the same discussion is given for another temperature

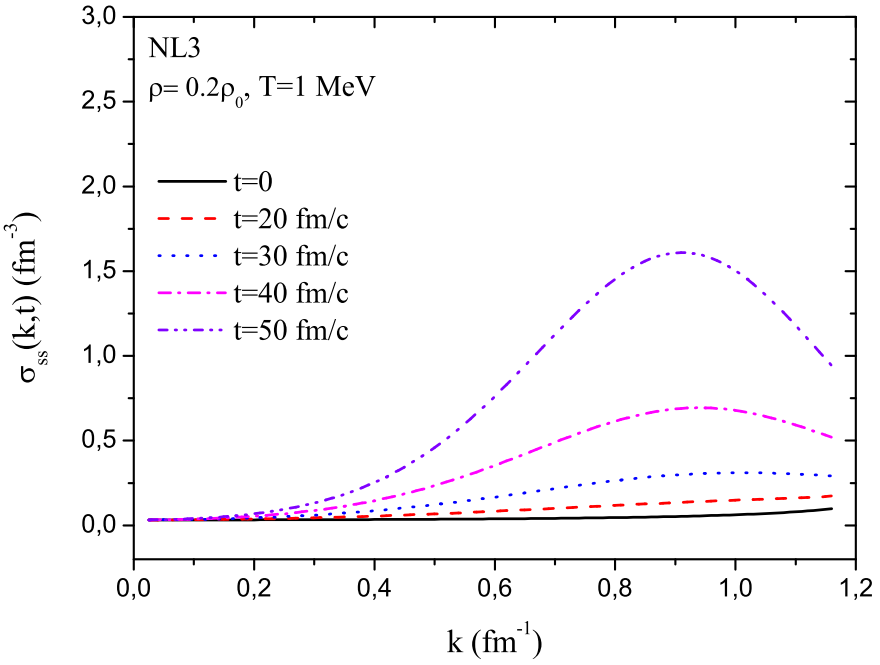

Figure 4.12: : Spectral intensity of scalar density correlation function as a function of wave number at $T = 1\ MeV$ and density $\rho_B = 0.2\ \rho_0$.

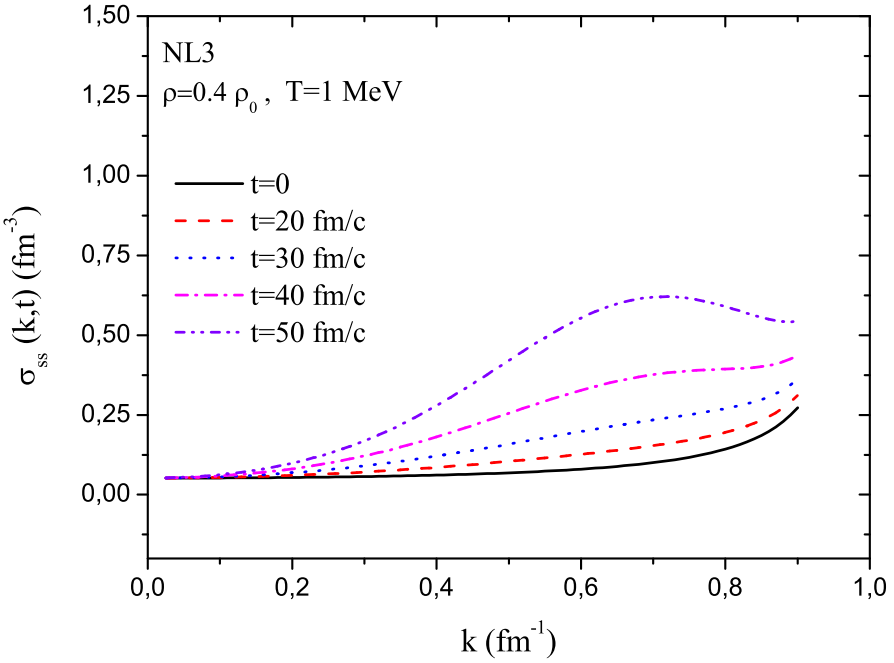

Figure 4.13: : Spectral intensity of scalar density correlation function as a function of wave number at $T = 1\ MeV$ and density $\rho_B = 0.4\ \rho_0$.

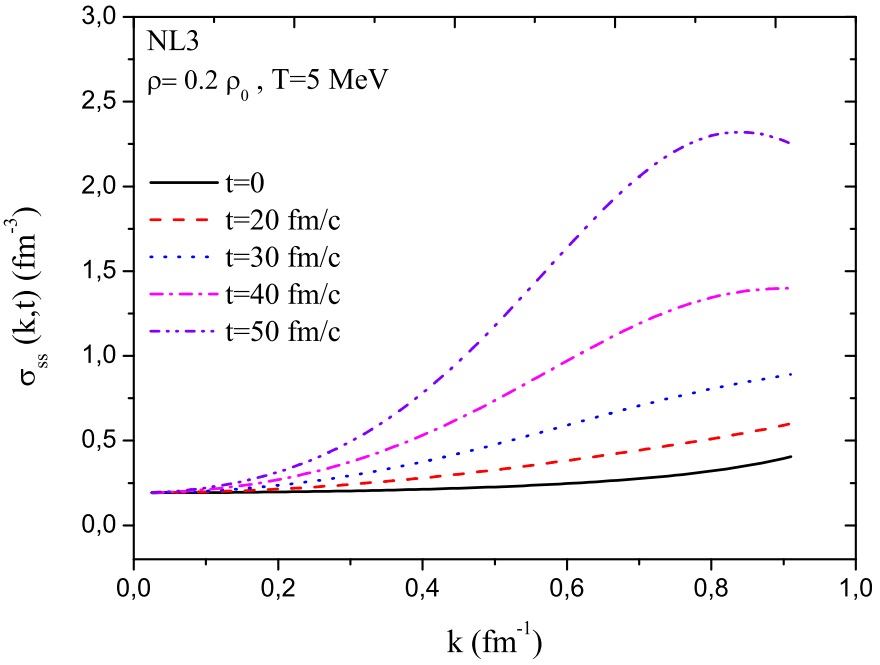

Figure 4.14: : Spectral intensity of scalar density correlation function as a function of wave number at $T = 5\ MeV$ and density $\rho_B = 0.2\ \rho_0$.

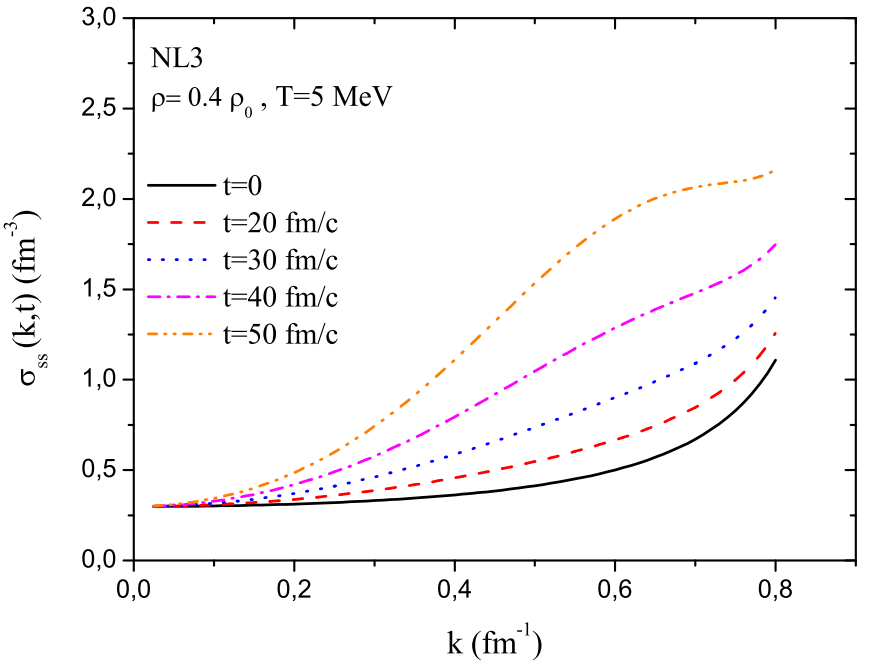

Figure 4.15: : Spectral intensity of scalar density correlation function as a function of wave number at $T = 5\ MeV$ and density $\rho_B = 0.4\ \rho_0$.

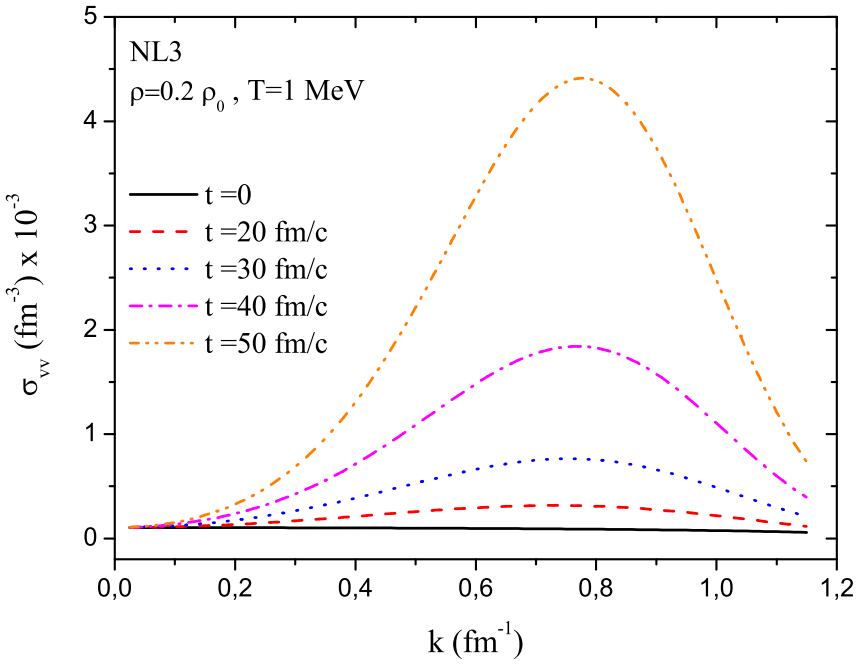

Figure 4.16: : Spectral intensity of current density correlation function as a function of wave number at $T = 1\ MeV$ and density $\rho_B = 0.2\ \rho_0$.

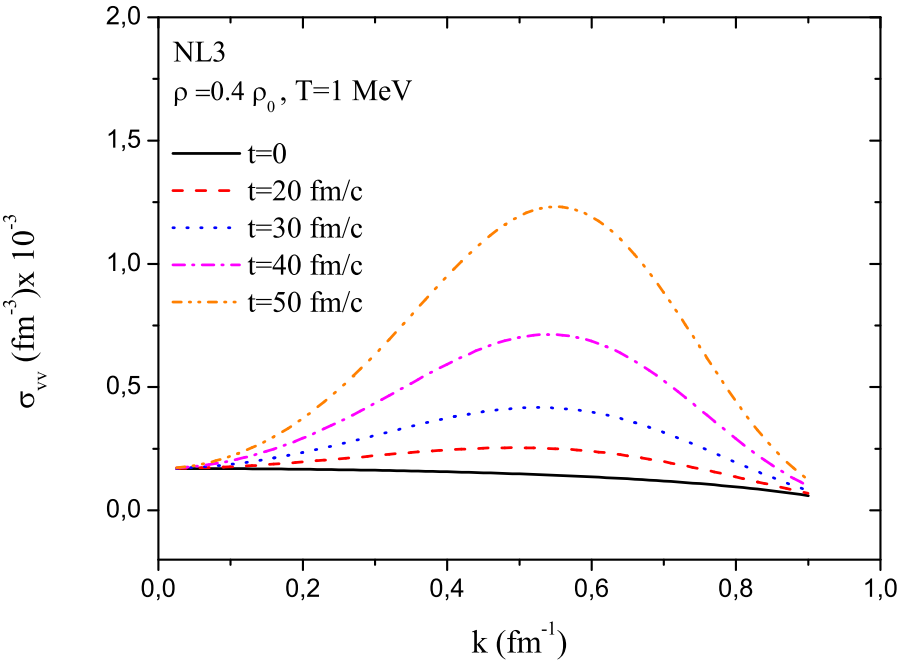

Figure 4.17: : Spectral intensity of current density correlation function as a function of wave number at $T = 1\ MeV$ and density $\rho_B = 0.4\ \rho_0$.

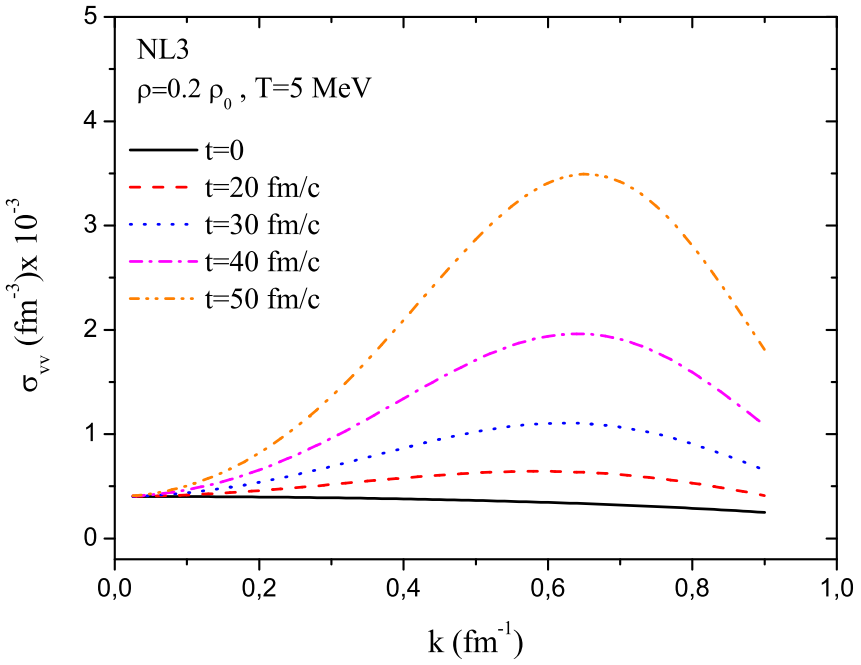

Figure 4.18: : Spectral intensity of current density correlation function as a function of wave number at $T = 5\ MeV$ and density $\rho_B = 0.2\ \rho_0$.

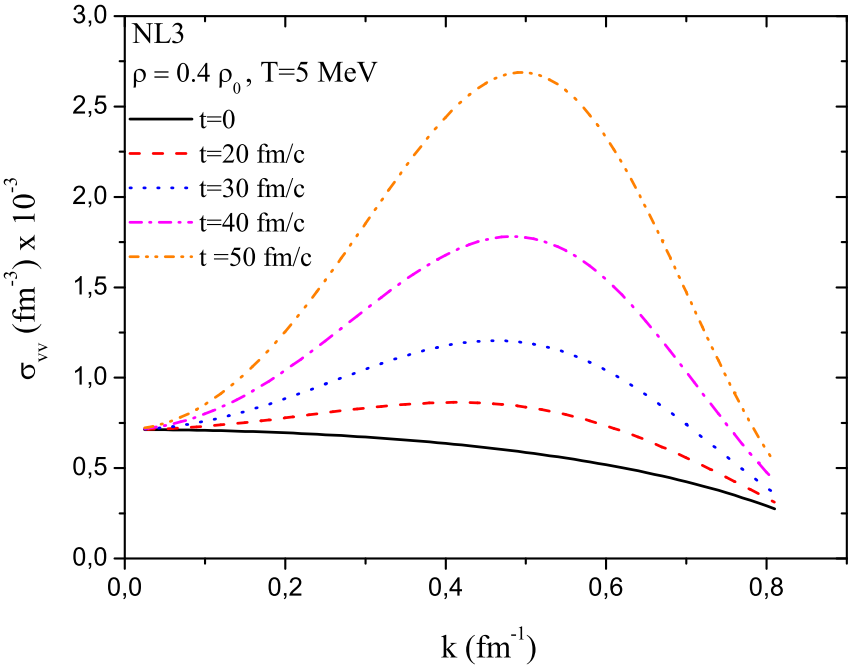

Figure 4.19: : Spectral intensity of current density correlation function as a function of wave number at $T = 5\ MeV$ and density $\rho_B = 0.4\ \rho_0$.

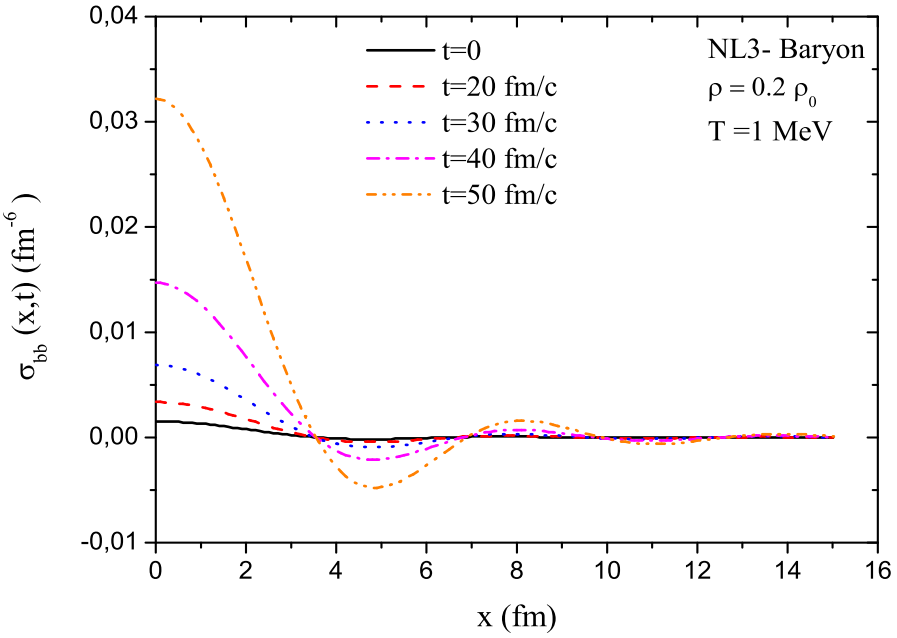

Figure 4.20: : Baryon density correlation function $\sigma_{BB}(x,t)$ as a function of distance $x = |\vec{r} - \vec{r}'|$ between two space points at temperature $T = 1\ MeV$ and density $\rho_B = 0.2\ \rho_0$.

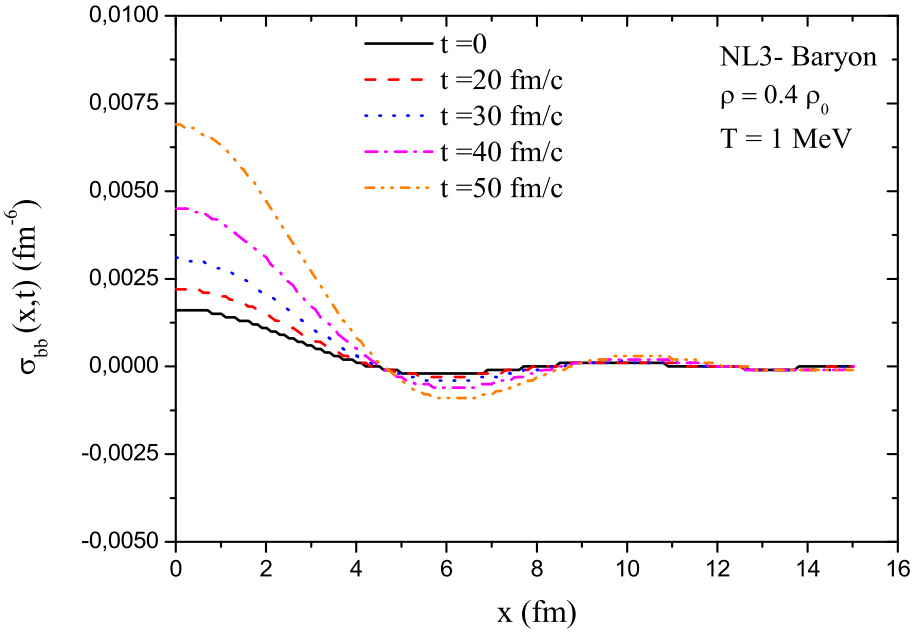

Figure 4.21: : Baryon density correlation function $\sigma_{BB}(x,t)$ as a function of distance $x = |\vec{r} - \vec{r}'|$ between two space points at temperature $T = 1\ MeV$ and density $\rho_B = 0.4\ \rho_0$.

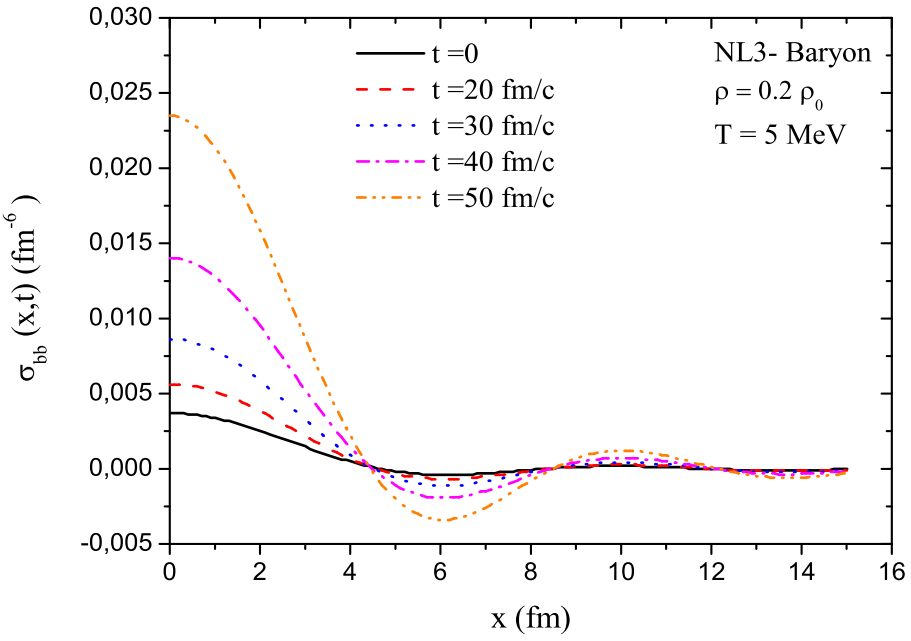

Figure 4.22: : Baryon density correlation function $\sigma_{BB}(x,t)$ as a function of distance $x = |\vec{r} - \vec{r}'|$ between two space points at temperature $T = 5\ MeV$ and density $\rho_B = 0.2\ \rho_0$.

$T = 5\ MeV$. The correlation length is now extracted about $3.0fm$ for both baryon densities $\rho_B = 0.2\ \rho_0$ and $\rho_B = 0.4\ \rho_0$ that corresponds to a condensation region including about A=16 nucleons. In this case, we reads $\sigma_{BB}(x = 0, t = 50fm/c) \approx 0.024fm^{-6}$ at baryon density $\rho_B = 0.2\ \rho_0$ and $\sigma_{BB}(x = 0, t = 50fm/c) \approx 0.017fm^{-6}$ at $\rho_B = 0.4\ \rho_0$. The growth rate is about 1.4 that is smaller compared with the value in the low temperature case.

In both temperature cases, we read the baryon density correlation at $t = 0$ since we are interested only in collective modes. If we include the effects of the non-collective modes, we expect to have no baryon density correlation at $t = 0$.

Figs. 4.24 and 4.25 show the scalar density correlation function $\sigma_{ss}(x,t)$ as a function of distance between two space points at temperature $T = 1\ MeV$ and at different times for initial baryon densities $\rho_B = 0.2\ \rho_0$ and $\rho_B = 0.4\ \rho_0$. For $T = 5\ MeV$ the scalar density correlation function as a function of distance between two space points is shown in Figs. 4.26 and 4.27. The scalar correlation

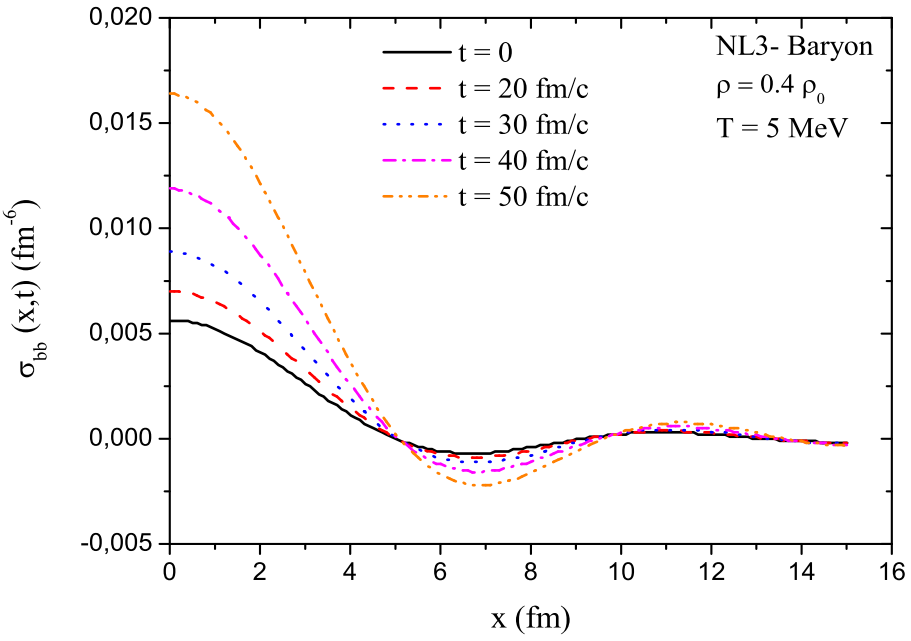

Figure 4.23: : Baryon density correlation function $\sigma_{BB}(x,t)$ as a function of distance $x = |\vec{r} - \vec{r}'|$ between two space points at temperature $T = 5\ MeV$ and density $\rho_B = 0.4\ \rho_0$.

function $\sigma_{ss}(x,t)$ carries the same information as the baryon density correlation function $\sigma_{BB}(x,t)$. We also find the correlation length between $2.5fm$ and $3fm$. Such a condensation region contains approximately A=12-16 nucleons.

Alternatively we can determine the minimal cluster sizes as radius of the object from Fig. 4.7 about $2.0-2.5fm$ for temperature $T = 0-6\ MeV$ corresponding to the most unstable modes around $\rho_B \approx 0.3\ \rho_0$. The values obtained in both ways are comparable with each other. In the correlation calculations, we read directly radius of the initial clusters, therefore results are more physical.

Figs. 4.28, 4.29 and Figs. 4.30, 4.31 demonstrate the current density correlation function $\sigma_{\rm vv}(x,t)$ as a function of distance between two space points under similar conditions as baryon and scalar densities. When scaling the graph, the current density correlation function is multiplied by a factor of 1000 due to the factor ε^*/M^* in the definition of the current density.

The variances of the local velocity fluctuations of the initial condensing frag-

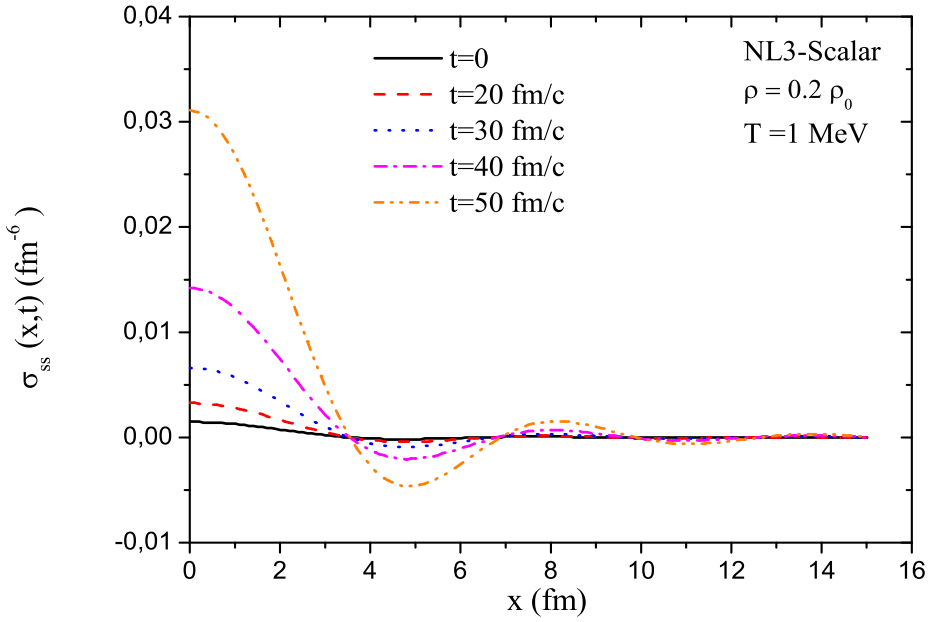

Figure 4.24: : Scalar density correlation function $\sigma_{ss}(x,t)$ as a function of distance $x = |\vec{r} - \vec{r}'|$ between two space points at temperature $T = 1\ MeV$ and density $\rho_B = 0.2\ \rho_0$.

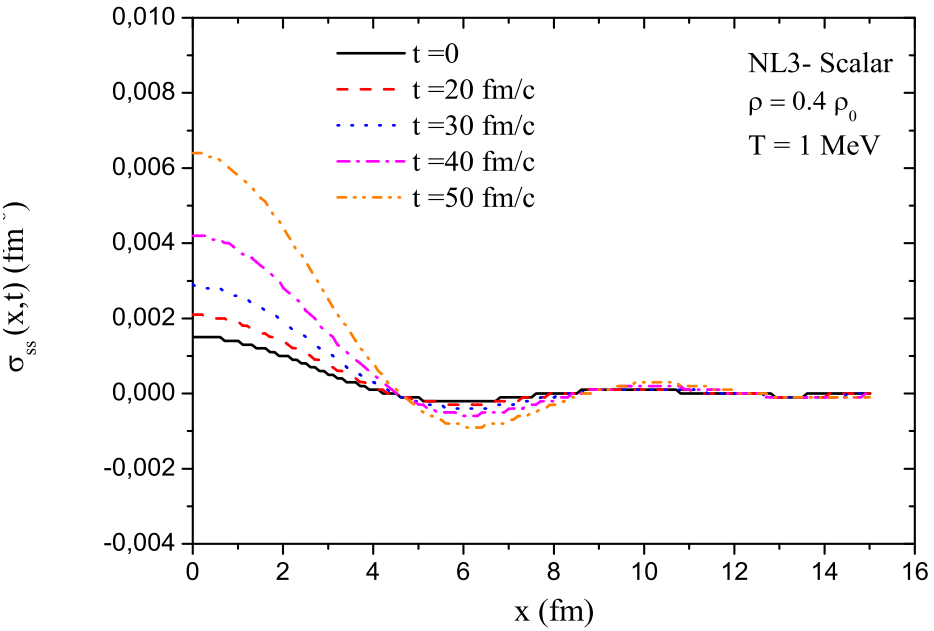

Figure 4.25: : Scalar density correlation function $\sigma_{ss}(x,t)$ as a function of distance $x = |\vec{r} - \vec{r}'|$ between two space points at temperature $T = 1\ MeV$ and density $\rho_B = 0.4\ \rho_0$.

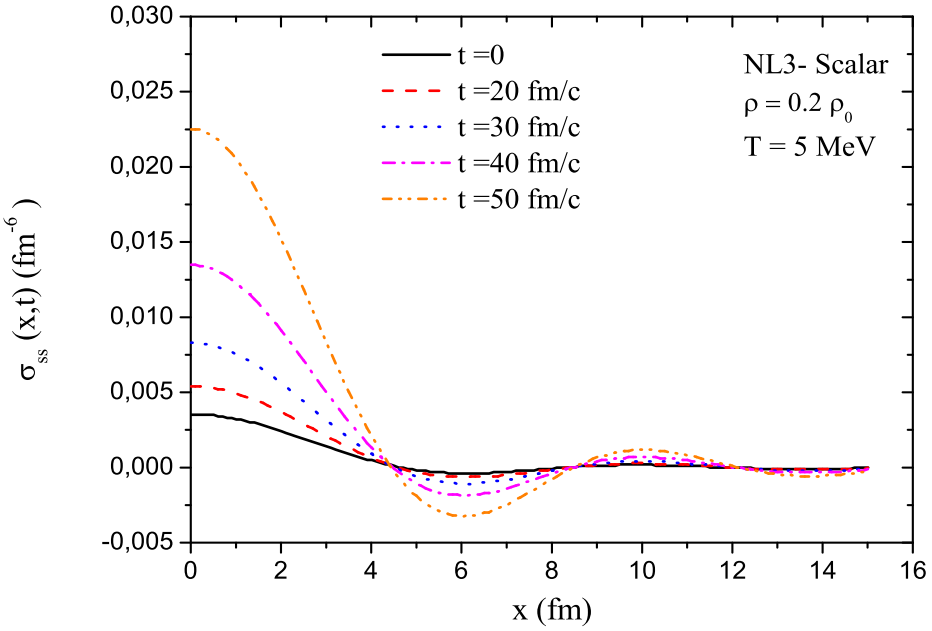

Figure 4.26: : Scalar density correlation function $\sigma_{ss}(x,t)$ as a function of distance $x = |\vec{r} - \vec{r}'|$ between two space points at temperature $T = 5\ MeV$ and density $\rho_B = 0.2\ \rho_0$.

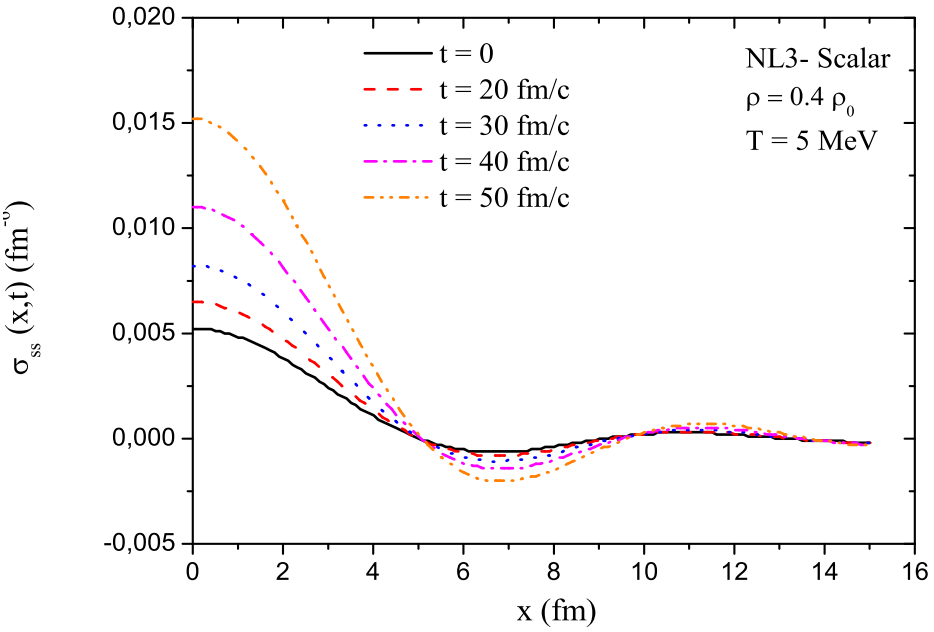

Figure 4.27: : Scalar density correlation function $\sigma_{ss}(x,t)$ as a function of distance $x = |\vec{r} - \vec{r}'|$ between two space points at temperature $T = 5\ MeV$ and density $\rho_B = 0.4\ \rho_0$.

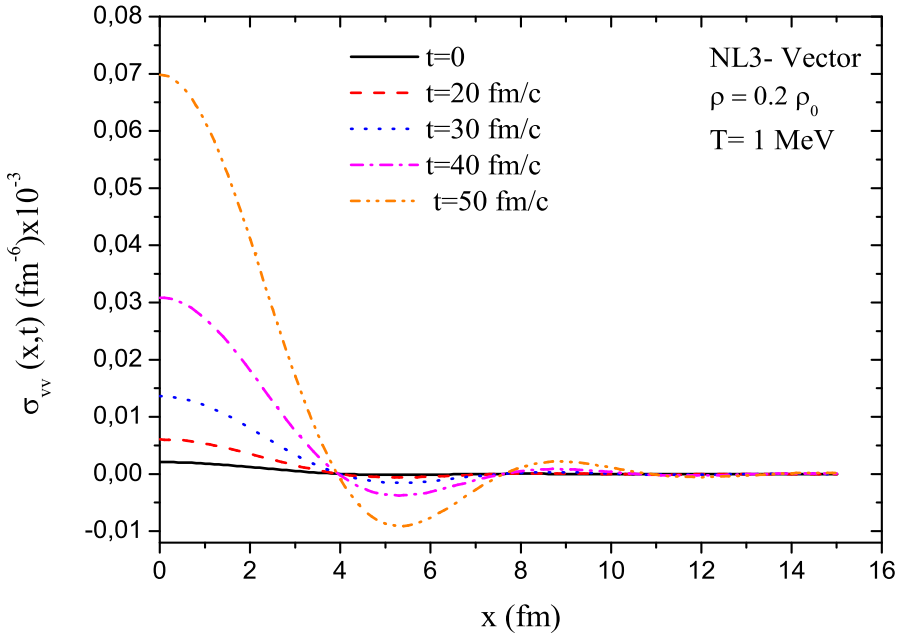

Figure 4.28: : Current density correlation function $\sigma_{\rm vv}(x,t)$ as a function of distance $x = |\vec{r} - \vec{r}'|$ between two space points at temperature $T = 1\ MeV$ and density $\rho_B = 0.2\ \rho_0$.

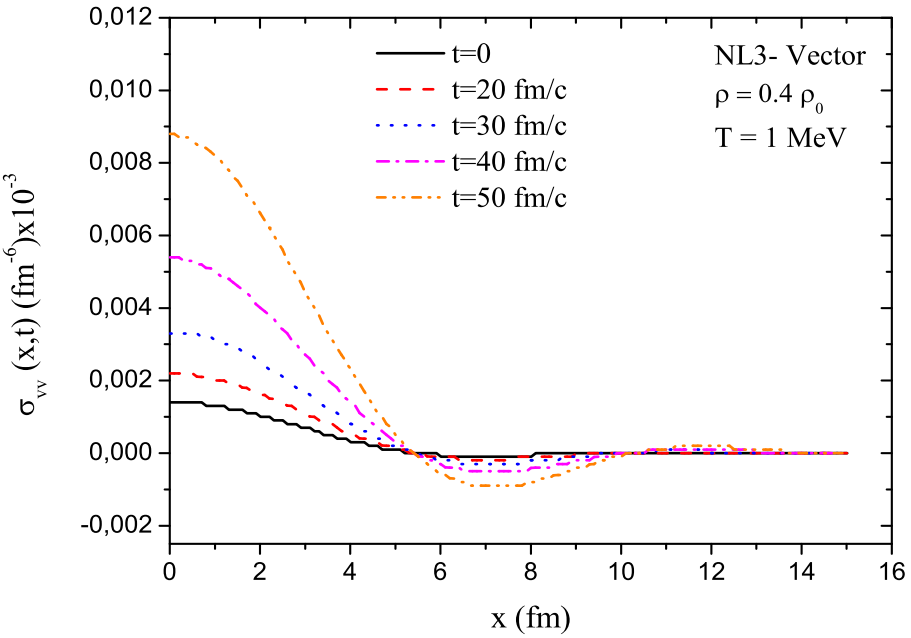

Figure 4.29: : Current density correlation function $\sigma_{\rm vv}(x,t)$ as a function of distance $x = |\vec{r} - \vec{r}'|$ between two space points at temperature $T = 1\ MeV$ and density $\rho_B = 0.4\ \rho_0$.

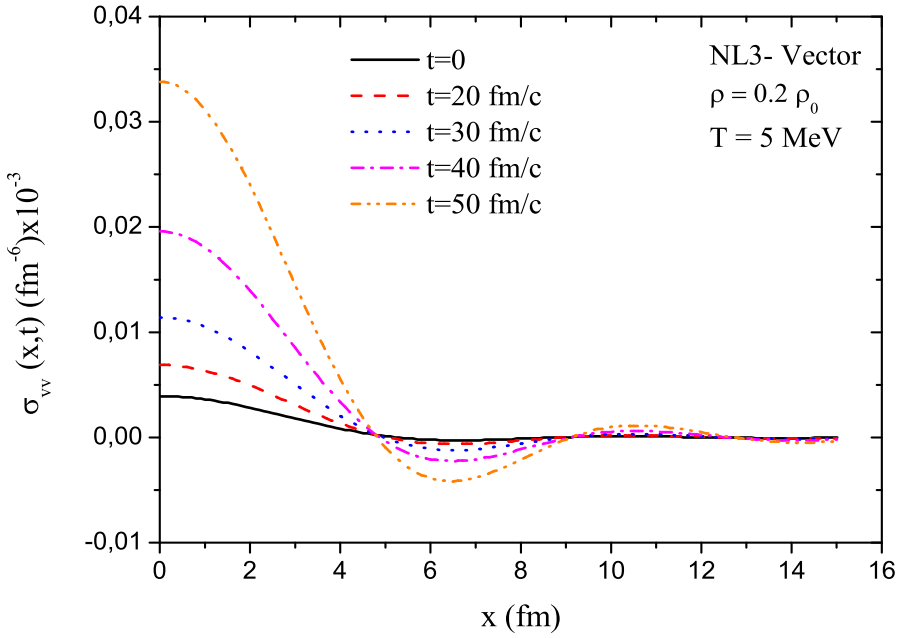

Figure 4.30: : Current density correlation function $\sigma_{\rm vv}(x,t)$ as a function of distance $x = |\vec{r} - \vec{r}'|$ between two space points at temperature $T = 5\ MeV$ and density $\rho_B = 0.2\ \rho_0$.

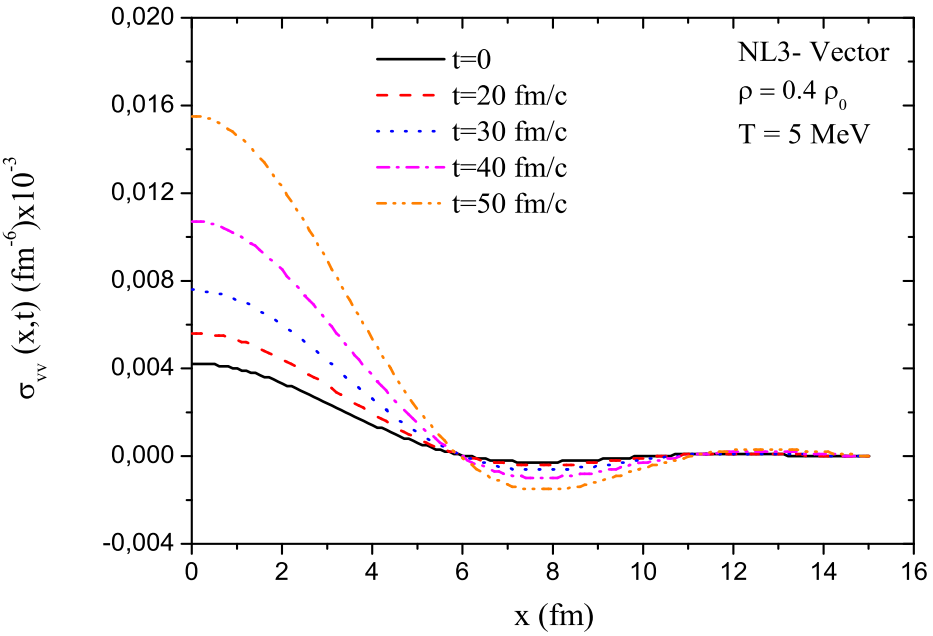

Figure 4.31: : Current density correlation function $\sigma_{\rm vv}(x,t)$ as a function of distance $x = |\vec{r} - \vec{r}'|$ between two space points at temperature $T = 5\ MeV$ and density $\rho_B = 0.4\ \rho_0$.

ments can be estimated from the current density correlation function [36]. The local velocity fluctuations $\delta\vec{u}(\vec{r},t)$ are related to the current density fluctuations according to

$$\delta\vec{\rho}_{\rm v}(\vec{r},t) \approx \delta\vec{u}(\vec{r},t)\rho_B \ . \tag{4.1}$$

By using the relation in Eq. (4.1), the equal time correlation function of the local velocity fluctuations are found as,

$$\overline{\delta\vec{u}(\vec{r},t)\cdot\delta\vec{u}(\vec{r}',t)} = \frac{1}{\rho_b^2}\sigma_{\rm vv}(|\vec{r}-\vec{r}'|,t). \tag{4.2}$$

The variance of the local velocity fluctuations can be determined by taking $x = |\vec{r}-\vec{r}'| = 0$. During the initial phase of spinodal decomposition, the root-mean-square value $u_{rms} = (c/\rho_b)\sqrt{\sigma_{\rm vv}(0,t)}$ provides an approximation for the average speed of condensing fragments [36]. We calculate the evolution of u_{rms} in time based on Figs. 4.28, 4.29 and Figs. 4.30, 4.31 that are given in Table 4.1.

In the case of temperature $T = 1\ MeV$, for the homogenous initial state with baryon density $\rho_B = 0.4\ \rho_0$, the rms value starts from an initial value of $u_{rms} = 0.02c$ and increases up to $u_{rms} = 0.05c$ during $50fm/c$, where c is the speed of light. Moreover, for a lower value of initial baryon density $\rho_B = 0.2\ \rho_0$, the rms value starts from an initial value of $u_{rms} = 0.05c$ and increases up to $u_{rms} = 0.3c$ during the time $t = 50fm/c$. Hovewer, at temperature $T = 5\ MeV$ with baryon density $\rho_B = 0.4\ \rho_0$ the rms value is changing from an initial value of $u_{rms} = 0.03c$ up to $u_{rms} = 0.06c$ and at baryon density of $\rho_B = 0.2\ \rho_0$, from an initial value of $u_{rms} = 0.07c$ and increases up to $u_{rms} = 0.2c$ in $50fm/c$. As a result, we find that the average speed of condensing fragments during the initial phase of spinodal decomposition grows faster at lower densities and low temperature.

Table 4.1: The average speed of initial fragments of spinodal decomposition at T=1 MeV and T=5 MeV .

NL3	T=1 MeV			T=5 MeV		
	t (fm/c)	$\sigma_{\rm vv}(0,t)(fm^{-6})$	u_{rms}	t (fm/c)	$\sigma_{\rm vv}(0,t)(fm^{-6})$	u_{rms}
	0	0.002×10^{-3}	$0.05c$	0	0.004×10^{-3}	$0.07c$
	20	0.006×10^{-3}	$0.08c$	20	0.007×10^{-3}	$0.088c$
$\rho_b=0.2\rho_0$	30	0.014×10^{-3}	$0.13c$	30	0.012×10^{-3}	$0.10c$
	40	0.03×10^{-3}	$0.18c$	40	0.02×10^{-3}	$0.15c$
	50	0.07×10^{-3}	$0.28c$	50	0.034×10^{-3}	$0.20c$
	t (fm/c)	$\sigma_{\rm vv}(0,t)(fm^{-6})$	u_{rms}	t (fm/c)	$\sigma_{\rm vv}(0,t)(fm^{-6})$	u_{rms}
	0	0.0014×10^{-3}	$0.02c$	0	0.004×10^{-3}	$0.03c$
	20	0.0022×10^{-3}	$0.025c$	20	0.0055×10^{-3}	$0.04c$
$\rho_b=0.4\rho_0$	30	0.0032×10^{-3}	$0.03c$	30	0.008×10^{-3}	$0.045c$
	40	0.0054×10^{-3}	$0.04c$	40	0.011×10^{-3}	$0.055c$
	50	0.009×10^{-3}	$0.05c$	50	0.016×10^{-3}	$0.06c$

CHAPTER 5

CONCLUSION

In this thesis, we employ a stochastic mean-field approach by including the nonlinear coupling terms of the scalar meson with NL3 parameter set to investigate the spinodal instabilities in nuclear matter. The stochastic mean-field theory includes the one-body dissipation and the related fluctuation mechanism in accordance with the fluctuation-dissipation relation, and it provides a powerful tool to describe the dynamics of density fluctuations in low energy nuclear reactions.

In the first part of the thesis, the nuclear matter equation of states at zero and finite temperatures are studied with the nonlinear Walecka model in the semiclassical approach. We carry out the relativistic calculations with NL3 parameter set. The effective mass of nuclear matter is found as a function of density for standard Walecka model and the NL3 set and the results are compared. And also, the energy per nucleon values are investigated for different temperatures. Moreover, the spinodal density region and phase transition are determined from pressure-baryon density variances. As a result, the spinodal instability region is observed under the critical temperature $T_c \approx 14\ MeV$ and the critical density $1/3\ \rho_0$. We also give the description of stochastic mean-field approach in this part and lastly the derivation of the relativistic Vlasov equation is performed.

In the second part of the thesis, we investigate the early growth of density fluctuations for symmetric nuclear matter by assuming small fluctuations of the mean-field around its equilibrium value.

We determine the growth rates of unstable collective modes at two different initial densities $\rho_B = 0.2\ \rho_0$ and $\rho_B = 0.4\ \rho_0$ and at different temperatures. We also calculate early behaviors of the density correlation functions in spinodal region that provide valuable information about the size of the fragmentation patterns and the average speed of condensing fragments.

The behavior of the most unstable modes represents a parabola-like curves by depending on initial baryon density and temperature. The system exhibits most unstable behavior in longer wave lengths at higher baryon densities $\rho_B = 0.4\ \rho_0$, while most unstable behavior occurs in shorter wavelengths at lower baryon densities $\rho_B = 0.2\ \rho_0$. The growth rates of the unstable modes calculated in non-relativistic approach with an effective Skyrme force [34] and in the non-linear Walecka model at $T = 5\ MeV$ are obtained to be comparable and the initial growth of the density fluctuations is found approximately the same in both models. The maximum of the growth rates of the most unstable modes as a function of the ratio ρ_B/ρ_0 in both relativistic NL3 and non-relativistic approaches at $T = 5\ MeV$ is obtained to occur around the initial baryon densities $\rho_B \approx 0.3\ \rho_0$.

Boundary of spinodal region in baryon density-temperature plane of the unstable mode gives a critical points around $\rho_c \approx 0.3\ \rho_0$ at a critical temperature $T_c \approx 12\ MeV$. Below this critical point, the system has a liquid-gas phase, however, at and above this point it has only gas phase.

By applying one-sided Fourier transform to the relativistic Vlasov equation, we obtain the initial fluctuations and derive density correlation functions from these initial fluctuations. We thus obtain their early evolution and reach valuable information about condensation.

The size of initial condensation regions is obtained firstly from the half wavelength of the fastest amplified modes. Secondly, we obtain it from the width of the baryon and scalar density correlation functions. These two results are in agreement and they approximately correspond to an initial condensation region

including 12-16 nucleons.

We use the semi-classical framework in our calculations, we neglect the quantum statistical effects on the density correlation functions, which are expected to become important at lower temperatures and also at lower densities. On the other hand, the investigation of spinodal dynamics in charge asymmetric nuclear matter by including the charged vector meson ρ becomes important for the analysis of the quantities as a function of isospin dependence of nuclear matter equation of state at low densities which is important for astrophysical systems (neutron star, etc.) and multi-fragmentation reactions in neutron rich nuclear systems.

The stochastic relativistic mean-field approach is a useful tool for the description of dynamics of density fluctuations in the spinodal region. This approach is also suitable to evaluate the early development of spinodal dynamics of hot nuclear matter produced in heavy-ion collisions.

REFERENCES

[1] B. D. Serot, J. D. Walecka, "Advances in Nuclear Physics Vol.16", Plenium Press, New York, 1997; J. D. Walecka, Ann. Phys. **83** (1974) 491.

[2] B. D. Serot, J. D. Walecka, Int. J. Mod. Phys. **E6** (1997) 515.

[3] H. Jaqaman, A.Z. Mekjian, and L.Zamick, Phys. Rev. **C 27** (1983) 2782.

[4] S.Das Gupta, A.Z. Mekjian, and M.B. Tsang, "Advances in Nuclear Physics Vol.26", Kluwer Academic Publishers, New York, 2002.

[5] A. Lopez, Revista Mexicana de Fisica **38** (1992) 95.

[6] P. Ring, Prog. Part. Nucl. Phys. **37** (1996) 193.

[7] D. Vretenar, H. Berghammer, P. Ring, Nucl. Phys. **A 581** (1995) 679.

[8] D. Vretenar, A. V. Afanasjev, G. A. Lalazissis and P. Ring, Phys. Rep. **409** (2005) 101.

[9] C. M. Ko, Qi Li, R. Wang, Phys. Rev. Lett. **59** (1987) 1084.

[10] G. A. Lalazissis, et al.,Phys. Lett. **B 671** (2009) 36.

[11] G. A. Lalazissis, J. Konig and P. Ring, Phys. Rev. **C 55** (1997) 540.

[12] Ph. Chomaz, M. Colonna and J. Randrup, Phys. Rep. **389** (2004) 263.

[13] G.F. Bertsch and P.J. Siemens, Phys. Lett. **B 126** (1983) 9.

[14] P. Ring and P. Schuck, "The Nuclear Many-Body Problem", Springer, New York, 1980.

[15] W. Cassing, U. Mosel, Prog. Part. Nucl. Phys. **25** (1990) 1.

[16] K. Washiyama, S. Ayik and D. Lacroix, Phys. Rev. **C 80** (2009) 031602(R).

[17] S. Ayik, Ph. Chomaz, M. Colonna and J. Randrup, Z. Phys. **A**(1996) 407.

[18] B.Yilmaz, S. Ayik, D. Lacroix and K. Washiyama,Phys. Rev. **C 83** (2011) 064615.

[19] S. Ayik, K. Washiyama and D. Lacroix, Phys. Rev. **C 79** (2009) 054606.

[20] S. Ayik, Phys. Lett. **B 658** (2008) 174.

[21] R. Balian and M. Veneroni, Phys. Lett. **B 104** (1982) 121.

[22] J. D. Frankland, et al., Nucl. Phys. **A 689** (2001) 940.

[23] J. Colin, et al., Phys. Rev. **C 67** (2003) 064603.

[24] B. Borderie, et al., Phys. Rev. Lett. **86** (2001) 3252.

[25] Nuray Er, "Nuclear Spinodal Instabilities in Stochastic Mean-Field Approaches", PhD Thesis, METU, 2009.

[26] S. Ayik, O. Yilmaz, N. Er, A. Gokalp, and P. Ring, Phys. Rev. **C 80** (2009) 034613.

[27] S. Ayik, N. Er, O. Yilmaz and A. Gokalp, Nucl. Phys. **A 812** (2008) 44.

[28] R. Machleidt, "In Relativistic Dynamics and Quark Nuclear Physics", edited by M. B. Johnson and A. Picklesimer, John Wiley & Sons, 1986.

[29] J. Boguta and A. R. Bodmer, Nuc. Phys.**A 292** (1977) 413.

[30] J. P. Diener, "Relativistic Mean-Field Theory Applied to the Study of Neutron Star Properties", MS thesis, Stellenbosch University, 2008.

[31] J.D. Walecka, "Theoretical Nuclear and Subnuclear Physics", Imperial College Press, 2004.

[32] C. B. Das, S. Das Gupta, and A. Z. Mekjian, Phys. Rev. **C 67** (2003) 064607.

[33] G. Sauer, H. Chandra, and U. Mosel, Nucl. Phys. **A 264** (1976) 221.

[34] J. Randrup, and E. de Lima Medeiros, Nucl. Phys. **A 529** (1991) 115.

[35] P. Bozek, Phys. Lett. **B 383** (1996) 121.

[36] S. Ayik, O. Yilmaz, F. Acar, B. Danisman, N. Er and A. Gokalp, Nucl. Phys. **A 859** (2011) 73.

[37] E. M. Lifshitz and P. L. Pitaevskii, "Physical Kinetics", Pergamon, 1981.

[38] G. Huo, L. Bo, M. Di Toro, Phys. Rev. **C 62** (2000) 035203.

APPENDIX A

DERIVATION OF SCALAR AND BARYON DENSITIES

To evaluate the expectation values of $\langle\overline{\psi}\gamma^0 i\hbar\partial_0\psi\rangle$ and $\langle\overline{\psi}\gamma^i i\hbar\partial_i\psi\rangle$, it is needed to find an explicit form of Dirac field ψ. If we use $\psi(x)$ in Dirac equation $\left[\gamma^\mu i\hbar\partial_\mu - g_v\gamma^0 V_0 - (Mc^2 - g_s\phi_0)\right]\psi = 0$, we then find

$$\left[\gamma^0 i\hbar\partial_0 + \vec{\gamma}\cdot i\hbar\vec{\nabla} - g_{\rm v}\gamma^0 V_0 - (Mc^2 - g_s\phi_0)\right] u(\vec{p},s)e^{-i\varepsilon(\vec{p})t/\hbar + i\vec{p}\cdot\vec{x}/\hbar} = 0$$
$$\left[\gamma^0 i\left(-i\varepsilon(\vec{p})\right) + \vec{\gamma}\cdot i(i\vec{p}) - g_{\rm v}\gamma^0 V_0 - (Mc^2 - g_s\phi_0)\right] u(\vec{p},s) = 0\ . \quad \text{(A.1)}$$

If we multiply both sides by $\gamma^0 \equiv \beta$ and using the followings $u(\vec{p},s) = \begin{pmatrix} \phi \\ \chi \end{pmatrix}$, $\beta = \gamma^0 = \begin{pmatrix} 1 & 0 \\ 0 & -1 \end{pmatrix}$ and $\vec{\alpha} = \gamma^0\vec{\gamma} = \begin{pmatrix} 0 & \vec{\sigma} \\ \vec{\sigma} & 0 \end{pmatrix}$ we then find

$$\left[\varepsilon(\vec{p}) - \vec{\alpha}\cdot c\vec{p} - g_{\rm v}V_0 - \beta M^* c^2\right] u(\vec{p},s) = 0\ , \quad \text{(A.2)}$$

where $M^*c^2 = Mc^2 - g_s\phi_0$ is the reduced baryon mass. Dirac Hamiltonian can be found from the Eq. (A.2) as

$$\begin{aligned} \varepsilon(\vec{p})u(\vec{p},s) &= \left(\vec{\alpha}\cdot c\vec{p} + g_{\rm v}V_0 + \beta M^* c^2\right) u(\vec{p},s) \\ H_D &= \vec{\alpha}\cdot c\vec{p} + g_{\rm v}V_0 + \beta M^* c^2\ . \end{aligned} \quad \text{(A.3)}$$

By using the Eq. (2.18) and the step function which is given by

$$\Theta\left(\mu - e(\vec{p})\right) = \begin{cases} 1 & if \quad |\vec{k}| \leq k_f \\ 0 & if \quad |\vec{k}| > k_f \end{cases} , \tag{A.4}$$

we can calculate the expectation value of the Dirac Hamiltonian as follows

$$\begin{aligned} \langle \overline{\psi} H_D \psi \rangle &\equiv \sum_s \int \frac{d^3p}{(2\pi\hbar)^3} \left(\psi^\dagger H_D \psi\right)_{\vec{p},s} \Theta\left(\mu - e(\vec{p})\right) \\ &= \sum_s \int \frac{d^3p}{(2\pi\hbar)^3} e(\vec{p}) \Theta\left(\mu - e(\vec{p})\right) \\ &= \sum_s \int \frac{d^3p}{(2\pi\hbar)^3} \left[g_{\rm v} V_0 + \sqrt{(c\vec{p})^2 + (M^*c^2)^2}\right] \Theta\left(\mu - e(\vec{p})\right) \\ &= g_{\rm v} V_0 \sum_s \int_0^{p_F} \frac{d^3p}{(2\pi\hbar)^3} + \sum_s \int_0^{p_F} \frac{d^3p}{(2\pi\hbar)^3} \sqrt{(c\vec{p})^2 + (M^*c^2)^2} \\ &= g_{\rm v} V_0 \frac{\gamma}{(2\pi\hbar)^3} \int_0^{p_f} d^3p + \frac{\gamma}{(2\pi\hbar)^3} \int_0^{p_f} d^3p \sqrt{(c\vec{p})^2 + (M^*c^2)^2} \ . \end{aligned} \tag{A.5}$$

In order to derive the expectation value of $\langle \overline{\psi} \gamma^i i\hbar\partial_i \psi \rangle$, we calculate firstly its single particle eigenvalue. $\langle \overline{\psi} \gamma^i i\hbar\partial_i \psi \rangle = \langle \psi^\dagger \left(-i\vec{\alpha} \cdot \vec{\nabla}\right) \psi \rangle$ in natural units.

$$\begin{aligned} \left(\overline{\psi}\vec{\gamma} \cdot c\vec{p}\psi\right)_{\vec{p},s} &= \left(\overline{\psi}\vec{\gamma}\psi\right)_{\vec{p},s} \cdot c\vec{p} = \left(\psi^\dagger \vec{\alpha}\psi\right)_{\vec{p},s} \cdot c\vec{p} \\ &= \left(\overline{\psi}\vec{\nabla}_p H_D \psi\right)_{\vec{p},s} \cdot c\vec{p} \\ &= \left[\vec{\nabla}_p \varepsilon(\vec{p})\right] \cdot c\vec{p} = \left[\vec{\nabla}_p \left(g_{\rm v} V_0 + \sqrt{(\vec{p}c)^2 + (M^*c^2)^2}\right)\right] \cdot c\vec{p} \\ &= \frac{c\vec{p} \cdot c\vec{p}}{\sqrt{(c\vec{p})^2 + (M^*c^2)^2}} \ . \end{aligned} \tag{A.6}$$

Now, the expectation value becomes

$$\begin{aligned} \langle \psi^\dagger \left(-i\vec{\alpha} \cdot \vec{\nabla}\right) \psi \rangle &= \sum_s \int \frac{d^3p}{(2\pi\hbar)^3} \left(\overline{\psi}\vec{\gamma} \cdot c\vec{p}\psi\right)_{\vec{p},s} \Theta\left(\mu - e(\vec{p})\right) \\ &= \sum_s \int \frac{d^3p}{(2\pi\hbar)^3} \frac{c\vec{p} \cdot c\vec{p}}{\sqrt{(c\vec{p})^2 + (M^*c^2)^2}} \Theta\left(\mu - e(\vec{p})\right) \\ &= \frac{\gamma}{(2\pi\hbar)^3} \int_0^{p_f} d^3p \frac{\left(c\vec{p}\right)^2}{\sqrt{(c\vec{p})^2 + (M^*c^2)^2}} \ . \end{aligned} \tag{A.7}$$

Finally, to find the expectation value of the scalar density, we should consider

the derivative of the Dirac Hamiltonian with respect to baryon mass, which is $\frac{\partial H_D}{\partial M} = \gamma^0$. From this expression the single particle expectation value becomes

$$\begin{aligned}
\left(\overline{\psi}\psi\right)_{\vec{p},s} &= \left(\psi^\dagger\gamma^0\psi\right)_{\vec{p},s} \equiv \left(\psi^\dagger\frac{\partial H_D}{\partial M}\psi\right)_{\vec{p},s} \\
\left(\overline{\psi}\psi\right)_{\vec{p},s} &= \frac{\partial}{\partial M}\varepsilon(\vec{p}) = \frac{M^*c^2}{\sqrt{(c\vec{p})^2+(M^*c^2)^2}} \ .
\end{aligned} \tag{A.8}$$

By using the general expression, the expectation value can be found as

$$\begin{aligned}
\langle\overline{\psi}\psi\rangle &= \sum_s \int \frac{d^3p}{(2\pi\hbar)^3}\left(\overline{\psi}\psi\right)_{\vec{p},s}\Theta\left(\mu - e(\vec{p})\right) \\
&= \sum_s \int \frac{d^3p}{(2\pi\hbar)^3}\frac{M^*c^2}{\sqrt{(c\vec{p})^2+(M^*c^2)^2}}\Theta\left(\mu - e(\vec{p})\right) \\
&= \frac{\gamma}{(2\pi\hbar)^3}\int_0^{p_f} d^3p\frac{M^*c^2}{\sqrt{p^2c^2+(M^*c^2)^2}} \ ,
\end{aligned} \tag{A.9}$$

and similarly for baryon density we find

$$\langle\overline{\psi}\gamma^0\psi\rangle = \langle\psi^\dagger\psi\rangle = \sum_s \int \frac{d^3p}{(2\pi\hbar)^3}\Theta\left(\mu - e(\vec{p})\right) = \frac{\gamma}{(2\pi\hbar)^3}\int_0^{p_f} d^3p. \tag{A.10}$$

By using the results of expectation values the scalar and the baryon densities become

$$\rho_s^0 = \frac{\gamma}{(2\pi\hbar)^3}\int_0^{p_f} d^3p\frac{M^*c^2}{\sqrt{p^2c^2+(M^*c^2)^2}} \tag{A.11}$$

$$\rho_B^0 = \frac{\gamma}{(2\pi\hbar)^3}\int_0^{p_f} d^3p = \frac{\gamma}{6\pi^2}k_F^3 \tag{A.12}$$

APPENDIX B

DERIVATION OF BARYON CORRELATION

The spectral intensity of baryon density function is defined by

$$\begin{aligned}\tilde{\sigma}_{BB}(\vec{k},t)(2\pi)^3\delta(\vec{k}-\vec{k}') &= \overline{\delta\tilde{\rho}_B(\vec{k},t)\left(\delta\tilde{\rho}_B(\vec{k}',t)\right)^*} \\ &= \overline{\delta\rho_B^+(\vec{k})\left(\delta\rho_B^+(\vec{k}')\right)^*}e^{2\Gamma_k t}+\overline{\delta\rho_B^-(\vec{k})\left(\delta\rho_B^-(\vec{k}')\right)^*}e^{-2\Gamma_k t} \\ &\quad +\overline{\delta\rho_B^+(\vec{k})\left(\delta\rho_B^-(\vec{k}')\right)^*}+\overline{\delta\rho_B^-(\vec{k})\left(\delta\rho_B^+(\vec{k}')\right)^*}, \quad \text{(B.1)}\end{aligned}$$

with the initial amplitude of baryon density fluctuation

$$\delta\tilde{\rho}_B^{\mp}(\vec{k}) = -\left[\frac{D_1^b\tilde{S}_B(\vec{k},\omega)+D_2^b\tilde{S}_{\rm s}(\vec{k},\omega)+D_3^b\tilde{S}_{\rm v}(\vec{k},\omega)}{\partial\varepsilon(\vec{k},\omega)/\partial\omega}\right]_{\omega=\mp i\Gamma_k}. \quad \text{(B.2)}$$

The correlation of the growing pole is written as follows,

$$\begin{aligned}&\left[\left(\delta\rho_B(\vec{k})\right)^+\right]\left[\left(\delta\rho_B(\vec{k})\right)^+\right]^* \\ &=\left[\frac{S_B^+D_1+S_s^+D_2+S_v^+iD_3'}{iN}\right]\left[\frac{S_B^+D_1+S_s^+D_2+S_v^+iD_3'}{iN}\right]^* \quad \text{(B.3)}\end{aligned}$$

where $\left(\frac{\partial\varepsilon(k,\omega)}{\partial\omega}\right)_{\omega=+i\Gamma}=iN$ and $\left(\frac{\partial\varepsilon(k,\omega)}{\partial\omega}\right)_{\omega=-i\Gamma}=-iN$.

$$\overline{\delta\rho_B^+(\vec{k})\left(\delta\rho_B^+(\vec{k'})\right)^*}|N|^2 =$$
$$\overline{S_B^+(k)S_B^+(k')^*}|D_1|^2 + \overline{S_s^+(k)S_s^+(k')^*}|D_2|^2 + \overline{S_v^+(k)S_v^+(k')^*}|D_3'|^2$$
$$+\overline{S_B^+(k)S_s^+(k')^*}D_1D_2 - i\overline{S_B^+(k)S_v^+(k')^*}D_1D_3 + \overline{S_s^+(k)S_B^+(k')^*}D_2D_1$$
$$-i\overline{S_s^+(k)S_v^+(k')^*}D_2D_3' + i\overline{S_v^+(k)S_B^+(k')^*}D_3'D_1 + i\overline{S_v^+(k)S_s^+(k')^*}D_3'D_2. \tag{B.4}$$

In this expression $D_1,\ D_2$ are real but D_3 is imaginary and we use D_3' to represent the real part of it. In addition, we use $S_B,\ S_s,\ S_v$ instead of $\tilde{S}_B,\ \tilde{S}_s,\ \tilde{S}_v$ in the following calculations. The correlation of decaying pole is

$$\overline{\delta\rho_B^-(\vec{k})\left(\delta\rho_B^-(\vec{k'})\right)^*}|N|^2 =$$
$$\overline{S_B^-(k)S_B^-(k')^*}|D_1|^2 + \overline{S_s^-(k)S_s^-(k')^*}|D_2|^2 + \overline{S_v^-(k)S_v^-(k')^*}|D_3'|^2$$
$$+\overline{S_B^-(k)S_s^-(k')^*}D_1D_2 + i\overline{S_B^-(k)S_v^-(k')^*}D_1D_3' + \overline{S_s^-(k)S_B^-(k')^*}D_2D_1$$
$$+i\overline{S_s^-(k)S_v^-(k')^*}D_2D_3' - i\overline{S_v^-(k)S_B^-(k')^*}D_3'D_1 - i\overline{S_v^-(k)S_s^-(k')^*}D_3'D_2\ , \tag{B.5}$$

and for the mixed terms

$$\overline{\delta\rho_B^+(\vec{k})\left(\delta\rho_B^-(\vec{k'})\right)^*}\left(-|N|^2\right) =$$
$$\overline{S_B^+(k)S_B^-(k')^*}|D_1|^2 + \overline{S_B^+(k)S_s^-(k')^*}D_1D_2 + i\overline{S_B^+(k)S_v^-(k')^*}D_1D_3'$$
$$+\overline{S_s^+(k)S_B^-(k')^*}D_2D_1 + \overline{S_s^+(k)S_s^-(k')^*}|D_2|^2 + i\overline{S_s^+(k)S_v^-(k')^*}D_2D_3'$$
$$+i\overline{S_v^+(k)S_B^-(k')^*}D_3'D_1 + i\overline{S_v^+(k)S_s^-(k')^*}D_3'D_2 - \overline{S_v^+(k)S_v^-(k')^*}|D_3'|^2\ , \tag{B.6}$$

$$\overline{\delta\rho_B^-(\vec{k})\left(\delta\rho_B^+(\vec{k'})\right)^*}\left(-|N|^2\right) =$$
$$\overline{S_B^-(k)S_B^+(k')^*}|D_1|^2 + \overline{S_B^-(k)S_s^+(k')^*}D_1D_2 - i\overline{S_B^-(k)S_v^+(k')^*}D_1D_3'$$
$$+\overline{S_s^-(k)S_B^+(k')^*}D_2D_1 + \overline{S_s^-(k)S_s^+(k')^*}|D_2|^2 - i\overline{S_s^-(k)S_v^+(k')^*}D_2D_3'$$
$$-i\overline{S_v^-(k)S_B^+(k')^*}D_3'D_1 - i\overline{S_v^-(k)S_s^+(k')^*}D_3'D_2 - \overline{S_v^-(k)S_v^+(k')^*}|D_3'|^2\ , \tag{B.7}$$

The source terms are

$$\begin{pmatrix} \tilde{S}_{\rm v}^{\pm}(\vec{k},\omega) \\ \tilde{S}_{\rm s}^{\pm}(\vec{k},\omega) \\ \tilde{S}_{B}^{\pm}(\vec{k},\omega) \end{pmatrix} = \gamma \int \frac{d^3p}{(2\pi\hbar)^3} \begin{pmatrix} c\vec{p}\cdot\vec{k}/\varepsilon_0^* \\ M_0^* c^2/\varepsilon_0^* \\ 1 \end{pmatrix} \frac{\delta\tilde{f}(\vec{k},\vec{p},0)}{\pm i\Gamma - \vec{\rm v}_0\cdot\vec{k}} \ . \tag{B.8}$$

By using the stochastic mean-field approach, the correlation of the first source term is

$$\begin{aligned} \overline{S_B^+(k)S_B^+(k')^*} &= \gamma^2 \int \frac{d^3p'}{(2\pi\hbar)^3}\frac{d^3p}{(2\pi\hbar)^3} \frac{\overline{\delta f(\vec{k},\vec{p},0)\delta f^*(\vec{k'},\vec{p'},0)}}{(i\Gamma - \vec{\rm v}_0\cdot\vec{k})(i\Gamma - \vec{\rm v}_0\cdot\vec{k'})^*} \\ &= \gamma^2(2\pi)^3\delta(\vec{k}-\vec{k'}) \int \frac{d^3p}{(2\pi\hbar)^3} \frac{f(\vec{p})[1-f(\vec{p})]}{\Gamma^2 + (\vec{v}_0\cdot\vec{k})^2} \ . \end{aligned} \tag{B.9}$$

By the similar way, the other terms are

$$\overline{S_s^+(k)S_s^+(k')^*} = \gamma^2(2\pi)^3\delta(\vec{k}-\vec{k'}) \int \frac{d^3p}{(2\pi\hbar)^3} \left(\frac{M_0^* c^2}{\varepsilon_0^*}\right)^2 \frac{f(\vec{p})[1-f(\vec{p})]}{\Gamma^2 + (\vec{v}_0\cdot\vec{k})^2} \ , \tag{B.10}$$

$$\overline{S_v^+(k)S_v^+(k')^*} = \gamma^2(2\pi)^3\delta(\vec{k}-\vec{k'}) \int \frac{d^3p}{(2\pi\hbar)^3} \left(\frac{cp\cos\theta}{\varepsilon_0^*}\right)^2 \frac{f(\vec{p})[1-f(\vec{p})]}{\Gamma^2 + (\vec{v}_0\cdot\vec{k})^2} \ , \tag{B.11}$$

and from the other terms

$$\overline{S_B^+(k)S_s^+(k')^*} = \gamma^2(2\pi)^3\delta(\vec{k}-\vec{k'}) \int \frac{d^3p}{(2\pi\hbar)^3} \left(\frac{M_0^* c^2}{\varepsilon_0^*}\right) \frac{f(\vec{p})[1-f(\vec{p})]}{\Gamma^2 + (\vec{v}_0\cdot\vec{k})^2} \ , \tag{B.12}$$

$$\begin{aligned} \overline{S_B^+(k)S_v^+(k')^*} &= \overline{S_v^+(k)S_B^+(k')^*} = 0 \\ \overline{S_s^+(k)S_v^+(k')^*} &= \overline{S_v^+(k)S_s^+(k')^*} = 0 \ . \end{aligned} \tag{B.13}$$

If we define the following integrals,

$$K_{11}^{++} = \gamma^2 \int \frac{d^3p}{(2\pi\hbar)^3} \frac{f(\vec{p})[1-f_(\vec{p})]}{\Gamma^2 + (\vec{v}_0\cdot\vec{k})^2} \ , \tag{B.14}$$

$$K_{22}^{++} = \gamma^2 \int \frac{d^3p}{(2\pi\hbar)^3} \left(\frac{M_0^* c^2}{\varepsilon_0^*}\right)^2 \frac{f(\vec{p})[1-f(\vec{p})]}{\Gamma^2 + (\vec{v}_0 \cdot \vec{k})^2} \ , \tag{B.15}$$

$$K_{33}^{++} = \gamma^2 \int \frac{d^3p}{(2\pi\hbar)^3} \left(\frac{cp\ x}{\varepsilon_0^*}\right)^2 \frac{f(\vec{p})[1-f(\vec{p})]}{\Gamma^2 + (\vec{v}_0 \cdot \vec{k})^2} \ , \tag{B.16}$$

$$K_{12}^{++} = \gamma^2 \int \frac{d^3p}{(2\pi\hbar)^3} \frac{M_0^* c^2}{\varepsilon_0^*} \frac{f(\vec{p})[1-f(\vec{p})]}{\Gamma^2 + (\vec{v}_0 \cdot \vec{k})^2} \ . \tag{B.17}$$

The correlation of the source terms can be expressed as

$$\begin{aligned}
\overline{S_B^+(k) S_B^+(k')^*} &= (2\pi)^3 \delta(\vec{k} - \vec{k}') K_{11}^+, \\
\overline{S_s^+(k) S_s^+(k')^*} &= (2\pi)^3 \delta(\vec{k} - \vec{k}') K_{22}^+, \\
\overline{S_v^+(k) S_v^+(k')^*} &= (2\pi)^3 \delta(\vec{k} - \vec{k}') K_{33}^+, \\
\overline{S_B^+(k) S_s^+(k')^*} &= (2\pi)^3 \delta(\vec{k} - \vec{k}') K_{12}^+.
\end{aligned} \tag{B.18}$$

Consequently, we obtain the correlation for the growing mode as

$$\begin{aligned}
&\left[\overline{\left(\delta\rho_B(\vec{k})\right)^+}\right] \left[\overline{\left(\delta\rho_B(\vec{k})\right)^+}\right]^* = \\
&(2\pi)^3 \delta^3(\vec{k} - \vec{k}') \left[\frac{|D_1^B|^2 K_{11}^{++} + |D_2^B|^2 K_{22}^{++} + |D_3^B|^2 K_{33}^{++} + 2 D_1^B D_2^B K_{12}^{++}}{\left|\left(\frac{\partial\varepsilon(k,\omega)}{\partial\omega}\right)_{\omega = i\Gamma}\right|^2}\right].
\end{aligned} \tag{B.19}$$

By following the same steps, we obtain the correlation for decaying poles

$$\overline{S_B^-(k) S_B^-(k')^*} = \gamma^2 (2\pi)^3 \delta(\vec{k} - \vec{k}') \int \frac{d^3p}{(2\pi\hbar)^3} \frac{f(\vec{p})[1-f(\vec{p})]}{\Gamma^2 + (\vec{v}_0 \cdot \vec{k})^2}, \tag{B.20}$$

$$\overline{S_s^-(k) S_s^-(k')^*} = \gamma^2 (2\pi)^3 \delta(\vec{k} - \vec{k}') \int \frac{d^3p}{(2\pi\hbar)^3} \left(\frac{M_0^* c^2}{\varepsilon_0^*}\right)^2 \frac{f(\vec{p})[1-f(\vec{p})]}{\Gamma^2 + (\vec{v}_0 \cdot \vec{k})^2}, \tag{B.21}$$

$$\overline{S_v^-(k)S_v^-(k')^*} = \gamma^2(2\pi)^3\delta(\vec{k}-\vec{k}')\int\frac{d^3p}{(2\pi\hbar)^3}\left(\frac{cp\cos\theta}{\varepsilon_0^*}\right)^2\frac{f(\vec{p})[1-f(\vec{p})]}{\Gamma^2+(\vec{v}_0\cdot\vec{k})^2}, \quad \text{(B.22)}$$

$$\begin{aligned}\overline{S_B^-(k)S_s^-(k')^*} &= \overline{S_s^-(k)S_B^-(k')^*} \\ &= \gamma^2(2\pi)^3\delta(\vec{k}-\vec{k}')\int\frac{d^3p}{(2\pi\hbar)^3}\left(\frac{M_0^*c^2}{\varepsilon_0^*}\right)\frac{f(\vec{p})[1-f(\vec{p})]}{\Gamma^2+(\vec{v}_0\cdot\vec{k})^2},\end{aligned} \quad \text{(B.23)}$$

and

$$\begin{aligned}\overline{S_B^-(k)S_v^-(k')^*} &= \overline{S_v^-(k)S_B^-(k')^*} = 0 \\ \overline{S_s^-(k)S_v^-(k')^*} &= \overline{S_v^-(k)S_s^-(k')^*} = 0.\end{aligned} \quad \text{(B.24)}$$

The expression for the decaying pole is same as that of the growing pole:

$$\begin{aligned}&\left[\overline{\left(\delta\rho_B(\vec{k})\right)^-}\right]\left[\overline{\left(\delta\rho_B(\vec{k})\right)^-}\right]^* = \left[\overline{\left(\delta\rho_B(\vec{k})\right)^+}\right]\left[\overline{\left(\delta\rho_B(\vec{k})\right)^+}\right]^* \\ &= (2\pi)^3\delta^3(\vec{k}-\vec{k}')\left[\frac{|D_1^B|^2K_{11}^{++}+|D_2^B|^2K_{22}^{++}+|D_3^B|^2K_{33}^{++}+2D_1^BD_2^BK_{12}^{++}}{\left|\left(\frac{\partial\varepsilon(k,\omega)}{\partial\omega}\right)_{\omega=i\Gamma}\right|^2}\right].\end{aligned} \quad \text{(B.25)}$$

For the mixed terms

$$\begin{aligned}&\overline{S_B^+(k)S_B^-(k')^*} = \\ &\gamma^2(2\pi)^3\delta(\vec{k}-\vec{k}')\int\frac{d^3p}{(2\pi\hbar)^3}\frac{-\Gamma^2+(\vec{v}_0\cdot\vec{k})^2}{\left[\Gamma^2+(\vec{v}_0\cdot\vec{k})^2\right]^2}f(\vec{p})[1-f(\vec{p})],\end{aligned} \quad \text{(B.26)}$$

$$\begin{aligned}&\overline{S_s^+(k)S_s^-(k')^*} = \\ &\gamma^2(2\pi)^3\delta(\vec{k}-\vec{k}')\int\frac{d^3p}{(2\pi\hbar)^3}\left(\frac{M_0^*c^2}{\varepsilon_0^*}\right)^2\frac{-\Gamma^2+(\vec{v}_0\cdot\vec{k})^2}{\left[\Gamma^2+(\vec{v}_0\cdot\vec{k})^2\right]^2}f(\vec{p})[1-f(\vec{p})],\end{aligned} \quad \text{(B.27)}$$

$$\overline{S_v^+(k)S_v^-(k')^*} =$$
$$\gamma^2(2\pi)^3\delta(\vec{k}-\vec{k}')\int\frac{d^3p}{(2\pi\hbar)^3}\left(\frac{cp\ x}{\varepsilon_0^*}\right)^2\frac{-\Gamma^2+(\vec{v}_0\cdot\vec{k})^2}{[\Gamma^2+(\vec{v}_0\cdot\vec{k})^2]^2}f(\vec{p})[1-f(\vec{p})], \tag{B.28}$$

$$\overline{S_B^+(k)S_s^-(k')^*} =$$
$$\gamma^2(2\pi)^3\delta(\vec{k}-\vec{k}')\int\frac{d^3p}{(2\pi\hbar)^3}\frac{M_0^*c^2}{\varepsilon_0^*}\frac{-\Gamma^2+(\vec{v}_0\cdot\vec{k})^2}{[\Gamma^2+(\vec{v}_0\cdot\vec{k})^2]^2}f(\vec{p})[1-f(\vec{p})]. \tag{B.29}$$

Finally, we obtain the expression

$$\left[\overline{\left(\delta\rho_B(\vec{k})\right)^+}\right]\left[\overline{\left(\delta\rho_B(\vec{k})\right)^-}\right]^* = \left[\overline{\left(\delta\rho_B(\vec{k})\right)^-}\right]\left[\overline{\left(\delta\rho_B(\vec{k})\right)^+}\right]^*$$
$$= (2\pi)^3\delta^3(\vec{k}-\vec{k}')\left[\frac{|D_1^B|^2K_{11}^{+-}+|D_2^B|^2K_{22}^{+-}-|D_3^B|^2K_{33}^{+-}+2D_1^BD_2^BK_{12}^{+-}}{\left[\left(\frac{\partial\varepsilon(k,\omega)}{\partial\omega}\right)_{\omega=i\Gamma}\right]\left[\left(\frac{\partial\varepsilon(k,\omega)}{\partial\omega}\right)_{\omega=-i\Gamma}\right]}\right] \tag{B.30}$$

where the integrals are defined as follows

$$\begin{pmatrix}K_{11}^{+-}\\K_{22}^{+-}\\K_{33}^{+-}\\K_{12}^{+-}\end{pmatrix} = \gamma^2\int\frac{d^3p}{(2\pi\hbar)^3}\begin{pmatrix}1\\\left(\frac{M_0^*c^2}{\varepsilon_0^*}\right)^2\\\left(c\frac{\vec{p}\cdot\hat{k}}{\varepsilon_0^*}\right)^2\\\frac{M_0^*c^2}{\varepsilon_0^*}\end{pmatrix}\frac{-\Gamma^2+(v_0\cdot\vec{k})^2}{\left[\Gamma^2+(v_0\cdot\vec{k})^2\right]^2}f(\vec{p})[1-f(\vec{p}))]. \tag{B.31}$$

Finally, we can write the spectral intensity of the baryon density correlation function by using the above expressions as

$$\begin{aligned}\tilde{\sigma}_{BB}(\vec{k},t) &= \frac{\left[|D_1^b|^2K_{11}^{+}+|D_2^b|^2K_{22}^{+}+|D_3^b|^2K_{33}^{+}+2D_1^bD_2^bK_{12}^{+}\right]}{\left|\left(\frac{\partial\varepsilon(k,\omega)}{\partial\omega}\right)_{\omega=i\Gamma_k}\right|^2}(e^{2\Gamma_kt}+e^{-2\Gamma_kt})\\ &+\frac{2\left[|D_1^b|^2K_{11}^{-}+|D_2^b|^2K_{22}^{-}-|D_3^b|^2K_{33}^{-}+2D_1^bD_2^bK_{12}^{-}\right]}{\left|\left(\frac{\partial\varepsilon(k,\omega)}{\partial\omega}\right)_{\omega=i\Gamma_k}\right|^2}\end{aligned} \tag{B.32}$$

with the integrals

$$\begin{pmatrix} K_{11}^{\mp} \\ K_{22}^{\mp} \\ K_{33}^{\mp} \\ K_{12}^{\mp} \end{pmatrix} = \gamma^2 \int \frac{d^3p}{(2\pi\hbar)^3} \begin{pmatrix} 1 \\ \left(\frac{M_0^* c^2}{\varepsilon_0^*}\right)^2 \\ \left(c\frac{\vec{p}\cdot\hat{k}}{\varepsilon_0^*}\right)^2 \\ \frac{M_0^* c^2}{\varepsilon_0^*} \end{pmatrix} \frac{\Gamma^2 \mp (v_0 \cdot \vec{k})^2}{\left[\Gamma^2 + (v_0 \cdot \vec{k})^2\right]^2} f_0(\vec{p})[1 - f_0(\vec{p})]. \tag{B.33}$$

APPENDIX C

DERIVATIONS OF SCALAR AND VECTOR CORRELATIONS

In Eq. (3.46), we find the initial amplitude of scalar density fluctuations as

$$\delta\rho_{\rm s}^{\mp}(\vec{k}) = -\left[\frac{D_1^s\tilde{S}_B(\vec{k},\omega)+D_2^s\tilde{S}_{\rm s}(\vec{k},\omega)+D_3^s\tilde{S}_{\rm v}(\vec{k},\omega)}{\partial\varepsilon(\vec{k},\omega)/\partial\omega}\right]_{\omega=\mp i\Gamma_k} \tag{C.1}$$

where $D_1^{\rm s}=C_1B_3-B_1C_3$, $D_2^{\rm s}=A_1C_3-C_1A_3$, $D_3^{\rm s}=B_1A_3-A_1B_3$. From the definition of $\tilde{\sigma}_{\alpha\alpha}(\vec{k},t)$, the spectral intensity of the scalar density correlation function is written as

$$\begin{aligned}\tilde{\sigma}_{SS}(\vec{k},t)(2\pi)^3\delta^3(\vec{k}-\vec{k}') &= \overline{\delta\tilde{\rho}_s(\vec{k},t)\left(\delta\tilde{\rho}_s(\vec{k}',t)\right)^*}\\ &= \overline{\delta\rho_s^+(\vec{k})\left(\delta\rho_s^+(\vec{k}')\right)^*}e^{2\Gamma_k t}+\overline{\delta\rho_s^-(\vec{k})\left(\delta\rho_s^-(\vec{k}')\right)^*}e^{-2\Gamma_k t}\\ &\quad+\overline{\delta\rho_s^+(\vec{k})\left(\delta\rho_s^-(\vec{k}')\right)^*}+\overline{\delta\rho_s^-(\vec{k})\left(\delta\rho_s^+(\vec{k}')\right)^*}\end{aligned} \tag{C.2}$$

Scalar and baryon density cases have the same from which is given in Appendix-B. Therefore, the spectral intensity of scalar density correlation function is obtained as

$$\begin{aligned}\tilde{\sigma}_{\rm ss}(\vec{k},t) &= \frac{\left[|D_1^s|^2K_{11}^+ + |D_2^s|^2K_{22}^+ + |D_3^s|^2K_{33}^+ + 2D_1^sD_2^sK_{12}^+\right]}{\left|\left(\frac{\partial\varepsilon(k,\omega)}{\partial\omega}\right)_{\omega=i\Gamma_k}\right|^2}(e^{2\Gamma_k t}+e^{-2\Gamma_k t})\\ &\quad+\frac{2\left[|D_1^s|^2K_{11}^- + |D_2^s|^2K_{22}^- - |D_3^s|^2K_{33}^- + 2D_1^sD_2^sK_{12}^-\right]}{\left|\left(\frac{\partial\varepsilon(k,\omega)}{\partial\omega}\right)_{\omega=i\Gamma_k}\right|^2}.\end{aligned} \tag{C.3}$$

In vector density case, we use the same steps. By using time-dependent vector density fluctuation including growing and decaying poles given by

$$\delta\tilde{\rho}_{\rm v}(\vec{k},t)=\delta\rho_{\rm v}^{+}(\vec{k})e^{+\Gamma_k t}+\delta\rho_{\rm v}^{-}(\vec{k})e^{-\Gamma_k t}. \tag{C.4}$$

The spectral intensity of vector density fluctuation is defined as

$$\begin{aligned}\tilde{\sigma}_{vv}(\vec{k},t)(2\pi)^3\delta^3(\vec{k}-\vec{k}') &= \overline{\delta\tilde{\rho}_v(\vec{k},t)\left(\delta\tilde{\rho}_v(\vec{k}',t)\right)^*}\\ &= \overline{\delta\rho_v^{+}(\vec{k})\left(\delta\rho_v^{+}(\vec{k}')\right)^*}e^{2\Gamma_k t}+\overline{\delta\rho_v^{-}(\vec{k})\left(\delta\rho_v^{-}(\vec{k}')\right)^*}e^{-2\Gamma_k t}\\ &\quad+\overline{\delta\rho_v^{+}(\vec{k})\left(\delta\rho_v^{-}(\vec{k}')\right)^*}+\overline{\delta\rho_v^{-}(\vec{k})\left(\delta\rho_v^{+}(\vec{k}')\right)^*}\end{aligned} \tag{C.5}$$

with the initial amplitudes of vector density fluctuation

$$\delta\rho_{\rm v}^{\mp}(\vec{k})=-\left[\frac{D_1^v\tilde{S}_B(\vec{k},\omega)+D_2^v\tilde{S}_{\rm s}(\vec{k},\omega)+D_3^v\tilde{S}_{\rm v}(\vec{k},\omega)}{\partial\varepsilon(\vec{k},\omega)/\partial\omega}\right]_{\omega=\mp i\Gamma_k} \tag{C.6}$$

where $D_1^{\rm v}\equiv i(B_2C_3-C_2B_3)$, $D_2^{\rm v}\equiv i(C_2A_3-A_2C_3)$, $D_3^{\rm v}\equiv A_2B_3-B_2A_3$.

The correlation of the growing pole is written as follows,

$$\begin{aligned}&\left[\left(\delta\rho_v(\vec{k})\right)^{+}\right]\left[\left(\delta\rho_v(\vec{k})\right)^{+}\right]^*=\\ &\left[\frac{S_B^+D_1^v+S_s^+D_2^v+S_v^+iD_3^v}{iN}\right]\left[\frac{S_B^+D_1^v+S_s^+D_2^v+S_v^+iD_3^v}{iN}\right]^*\end{aligned} \tag{C.7}$$

where $\left(\frac{\partial\varepsilon(k,\omega)}{\partial\omega}\right)_{\omega=+i\Gamma}=iN$ and $\left(\frac{\partial\varepsilon(k,\omega)}{\partial\omega}\right)_{\omega=-i\Gamma}=-iN$.

$$\begin{aligned}&\overline{\delta\rho_v^{+}(\vec{k})\left(\delta\rho_v^{+}(\vec{k}')\right)^*}|N|^2=\\ &\overline{S_B^+(k)S_B^+(k')^*}|D_1'|^2+\overline{S_s^+(k)S_s^+(k')^*}|D_2'|^2+\overline{S_v^+(k)S_v^+(k')^*}|D_3|^2\\ &+\overline{S_B^+(k)S_s^+(k')^*}D_1'D_2'+i\overline{S_B^+(k)S_v^+(k')^*}D_1'D_3+\overline{S_s^+(k)S_B^+(k')^*}D_2'D_1'\\ &+i\overline{S_s^+(k)S_v^+(k')^*}D_2'D_3+i\overline{S_v^+(k)S_B^+(k')^*}D_3(-iD_1')+i\overline{S_v^+(k)S_s^+(k')^*}D_3(-iD_2').\end{aligned} \tag{C.8}$$

The correlation functions for the decaying poles are as follows

$$\left[\left(\delta\rho_v(\vec{k})\right)^-\right]\left[\left(\delta\rho_v(\vec{k})\right)^-\right]^* = \left[\frac{S_B^-(-iD_1')+S_s^-(-iD_2\prime)+S_v^-D_3}{-iN}\right]\left[\frac{S_B^-(-iD_1')+S_s^-(-iD_2\prime)+S_v^-iD_3}{-iN}\right]^*, \tag{C.9}$$

$$\begin{aligned}&\overline{\delta\rho_v^-(\vec{k})\left(\delta\rho_v^-(\vec{k'})\right)^*}|N|^2 = \\ &\overline{S_B^-(k)S_B^-(k')^*}|D_1'|^2+\overline{S_s^-(k)S_s^-(k')^*}|D_2'|^2+\overline{S_v^-(k)S_v^-(k')^*}|D_3|^2 \\ &+\overline{S_B^-(k)S_s^-(k')^*}D_1'D_2'-i\overline{S_B^-(k)S_v^-(k')^*}D_1'D_3+\overline{S_s^-(k)S_B^-(k')^*}D_2'D_1' \\ &-i\overline{S_s^-(k)S_v^-(k')^*}D_2'D_3-i\overline{S_v^-(k)S_B^-(k')^*}D_3D_1'-i\overline{S_v^-(k)S_s^-(k')^*}D_3D_2'.\end{aligned} \tag{C.10}$$

And also, the correlation of the mixed poles are given as

$$\left[\left(\delta\rho_v(\vec{k})\right)^+\right]\left[\left(\delta\rho_v(\vec{k})\right)^-\right]^* = \left[\frac{S_B^+(iD_1')+S_s^+(iD_2')+S_v^+D_3}{iN}\right]\left[\frac{S_B^-(-iD_1')+S_s^-(-iD_2')+S_v^-D_3}{-iN}\right]^*, \tag{C.11}$$

$$\begin{aligned}&\overline{\delta\rho_v^+(\vec{k})\left(\delta\rho_v^-(\vec{k'})\right)^*}\left(-|N|^2\right) = \\ &-\overline{S_B^+(k)S_B^-(k')^*}|D_1'|^2-\overline{S_B^+(k)S_s^-(k')^*}D_1'D_2'+i\overline{S_B^+(k)S_v^-(k')^*}D_1'D_3 \\ &-\overline{S_s^+(k)S_B^-(k')^*}D_2'D_1'-\overline{S_s^+(k)S_s^-(k')^*}|D_2'|^2+i\overline{S_s^+(k)S_v^-(k')^*}D_2'D_3' \\ &+i\overline{S_v^+(k)S_B^-(k')^*}D_3D_1'+i\overline{S_v^+(k)S_s^-(k')^*}D_3D_2'+\overline{S_v^+(k)S_v^-(k')^*}|D_3|^2.\end{aligned} \tag{C.12}$$

$$\left[\left(\delta\rho_v(\vec{k})\right)^-\right]\left[\left(\delta\rho_v(\vec{k})\right)^+\right]^* = \left[\frac{S_B^-(-iD_1')+S_s^-(-iD_2')+S_v^-D_3}{-iN}\right]\left[\frac{S_B^+(iD_1')+S_s^+(iD_2')+S_v^+D_3}{iN}\right]^*, \tag{C.13}$$

$$\overline{\delta\rho_v^-(\vec{k})\left(\delta\rho_v^+(\vec{k'})\right)^*}\left(-|N|^2\right) =$$
$$-\overline{S_B^-(k)S_B^+(k')^*}|D_1'|^2 - \overline{S_B^-(k)S_s^+(k')^*}D_1'D_2' + i\overline{S_B^-(k)S_v^+(k')^*}D_1'D_3$$
$$-\overline{S_s^-(k)S_B^+(k')^*}D_2'D_1' - \overline{S_s^-(k)S_s^+(k')^*}|D_2'|^2 - i\overline{S_s^-(k)S_v^+(k')^*}D_2'D_3$$
$$-i\overline{S_v^-(k)S_B^+(k')^*}D_3D_1' - i\overline{S_v^-(k)S_s^+(k')^*}D_3D_2' + \overline{S_v^-(k)S_v^+(k')^*}|D_3|^2. \tag{C.14}$$

Finally, we obtain the following relations

$$\left[\overline{\left(\delta\rho_v(\vec{k})\right)^+}\right]\left[\overline{\left(\delta\rho_v(\vec{k})\right)^+}\right]^* = \left[\overline{\left(\delta\rho_v(\vec{k})\right)^-}\right]\left[\overline{\left(\delta\rho_v(\vec{k})\right)^-}\right]^*$$
$$= (2\pi)^3\delta^3(\vec{k}-\vec{k'})\left[\frac{|D_1^v|^2K_{11}^{++} + |D_2^v|^2K_{22}^{++} + |D_3^v|^2K_{33}^{++} + 2D_1^vD_2^vK_{12}^{++}}{\left|\left(\frac{\partial\varepsilon(k,\omega)}{\partial\omega}\right)_{\omega=i\Gamma}\right|^2}\right], \tag{C.15}$$

and

$$\left[\overline{\left(\delta\rho_v(\vec{k})\right)^+}\right]\left[\overline{\left(\delta\rho_v(\vec{k})\right)^-}\right]^* = \left[\overline{\left(\delta\rho_v(\vec{k})\right)^-}\right]\left[\overline{\left(\delta\rho_v(\vec{k})\right)^+}\right]^*$$
$$= (2\pi)^3\delta^3(\vec{k}-\vec{k'})\left[\frac{-|D_1^v|^2K_{11}^{+-} - |D_2^v|^2K_{22}^{+-} + |D_3^v|^2K_{33}^{+-} - 2D_1^BD_2^vK_{12}^{+-}}{\left[\left(\frac{\partial\varepsilon(k,\omega)}{\partial\omega}\right)_{\omega=i\Gamma}\right]\left[\left(\frac{\partial\varepsilon(k,\omega)}{\partial\omega}\right)_{\omega=-i\Gamma}\right]^*}\right]. \tag{C.16}$$

Note that

$$\left[\left(\frac{\partial\varepsilon(k,\omega)}{\partial\omega}\right)_{\omega=i\Gamma}\right]\left[\left(\frac{\partial\varepsilon(k,\omega)}{\partial\omega}\right)_{\omega=-i\Gamma}\right]^* =$$
$$\left[i\frac{\partial\varepsilon(k,\omega)}{\partial\omega}\right]\left[-i\frac{\partial\varepsilon(k,\omega)}{\partial\omega}\right]^* = i^2\left|\frac{\partial\varepsilon(k,\omega)}{\partial\omega}\right|^2. \tag{C.17}$$

From the definitions of $K^{\pm}$ given in Eq. (3.64) and by using the following relations $K_1^{+-}1 \equiv -K_{11}^+$, $K_1^{+-}1 \equiv -K_{11}^+$, $K_1^{+-}1 \equiv -K_{11}^+$, $K_1^{+-}1 \equiv -K_{11}^+$, we find the spectral intensity of vector density correlation function as

$$\tilde{\sigma}_{\rm vv}(\vec{k},t) = \frac{\left[|D_1^{\rm v}|^2 K_{11}^+ + |D_2^{\rm v}|^2 K_{22}^+ + |D_3^{\rm v}|^2 K_{33}^+ + 2D_1^{\rm v} D_2^{\rm v} K_{12}^+\right]}{\left|\left(\frac{\partial\varepsilon(k,\omega)}{\partial\omega}\right)_{\omega=i\Gamma_k}\right|^2}\left(e^{2\Gamma_k t} + e^{-2\Gamma_k t}\right)$$
$$-\frac{2\left[|D_1^{\rm v}|^2 K_{11}^- + |D_2^{\rm v}|^2 K_{22}^- - |D_3^{\rm v}|^2 K_{33}^- + 2D_1^{\rm v} D_2^{\rm v} K_{12}^-\right]}{\left|\left(\frac{\partial\varepsilon(k,\omega)}{\partial\omega}\right)_{\omega=i\Gamma_k}\right|^2} \ . \qquad \text{(C.18)}$$

APPENDIX D

DISPERSION RELATION FOR ZERO TEMPERATURE

At finite temperature, we used Fermi Dirac distribution $f_0(\vec{p}) = \frac{1}{e^{\beta(\varepsilon_0^* - \mu_0^*)}+1}$for the equilibrium phase-space distribution function. At zero temperature, phase-space distribution function is demonstrated by the step function, which is

$$f_0(\vec{p}) = \Theta(\mu_0^* - \varepsilon_0^*) = \begin{cases} 1 \quad if \quad \mu_0^* > \varepsilon_0^* \\ 0 \quad if \quad \mu_0^* < \varepsilon_0^* \end{cases} , \tag{D.1}$$

where the reduced chemical potential is $\mu_0^* = \mu - \left(\frac{g_\mathrm{v}}{\mu_\mathrm{v}^2}\right)\rho_B^0$.

In chapter 3, we obtain three coupled equations, which are Eq. (3.23), Eq. (3.25) and Eq. (3.27), for the baryon, scalar and current density fluctuations by linearization of relativistic Vlasov Equation. In these equations, for the zero temperature case the following expressions are used,

$$\begin{aligned} \vec{\nabla}_p f_0(\vec{p}) &= \vec{\nabla}_p \Theta\left(\mu_0^* - \sqrt{(c\vec{p})^2 + (M_0^* c^2)^2}\right) \\ &= -\frac{c(c\vec{p})}{\sqrt{(c\vec{p})^2 + (M_0^* c^2)^2}} \frac{\mu_0^*}{\sqrt{\mu_0^{*2} - (M_0^* c^2)^2}}\, \delta\left(cp - \sqrt{\mu_0^{*2} - (M_0^* c^2)^2}\right). \end{aligned} \tag{D.2}$$

$\vec{\nabla}_p f_0$ can be rewritten in the following form $\vec{\nabla}_p f_0 = -c\hat{p}\ \delta(cp - cp_1)$ then we obtain $\vec{\nabla}_p f \cdot \vec{k} = -ck\cos\theta\ \delta(cp - cp_1)$, where $cp_1 = \sqrt{\mu_0^{*2} - (M_0^* c^2)^2}$.

For the longitudinal modes, these three coupled equations can be written in

matrix form same with the finite temperature case:

$$\begin{pmatrix} A_1 & A_2 & A_3 \\ B_1 & B_2 & B_3 \\ C_1 & C_2 & C_3 \end{pmatrix} \begin{pmatrix} \delta\tilde{\rho}_{\rm v}(\vec{k},\omega) \\ \delta\tilde{\rho}_{\rm s}(\vec{k},\omega) \\ \delta\tilde{\rho}_B(\vec{k},\omega) \end{pmatrix} = i \begin{pmatrix} \tilde{S}_B(\vec{k},\omega) \\ \tilde{S}_{\rm s}(\vec{k},\omega) \\ \tilde{S}_{\rm v}(\vec{k},\omega) \end{pmatrix} , \tag{D.3}$$

where the components of the coefficient matrix are defined by the following matrix

$$\begin{pmatrix} A_1 & A_2 & A_3 \\ B_1 & B_2 & B_3 \\ C_1 & C_2 & C_3 \end{pmatrix} = \begin{pmatrix} -G_\omega^2\chi_{\rm v}(\vec{k},\omega) & -G_{\rm s}^2\chi_{\rm s}(\vec{k},\omega) & 1+G_\omega^2\chi_B(\vec{k},\omega) \\ -G_\omega^2\tilde{\chi}_{\rm v}(\vec{k},\omega) & 1+G_{\rm s}^2\tilde{\chi}_{\rm s}(\vec{k},\omega) & G_\omega^2\chi_{\rm s}(\vec{k},\omega) \\ 1+G_\omega^2\tilde{\chi}_B(\vec{k},\omega) & -G_{\rm s}^2\chi_{\rm v}(\vec{k},\omega) & G_\omega^2\chi_{\rm v}(\vec{k},\omega) \end{pmatrix} . \tag{D.4}$$

In the above expressions, the terms $\chi_{\rm v}(\vec{k},\omega)$, $\chi_B(\vec{k},\omega)$, $\chi_{\rm s}(\vec{k},\omega)$ and the functions $\tilde{\chi}_{\rm v}(\vec{k},\omega)$, $\tilde{\chi}_B(\vec{k},\omega)$, $\tilde{\chi}_{\rm s}(\vec{k},\omega)$ are different from those in finite temperature case. For zero temperature case, the relativistic Linhard functions are represented by

$$\begin{pmatrix} \chi_{\rm v}(\vec{k},\omega) \\ \chi_{\rm s}(\vec{k},\omega) \\ \chi_B(\vec{k},\omega) \end{pmatrix} = \frac{2\pi\gamma}{(2\pi\hbar c)^3}\frac{(cp_1)^3}{\mu_0^*}k^2 \begin{pmatrix} \frac{1}{k}i\Gamma/c \\ \frac{M_0^*c^2}{\mu_0^*} \\ 1 \end{pmatrix} L_2(p_1) \tag{D.5}$$

and

$$\tilde{\chi}_{\rm s}(\vec{k},\omega) = \frac{2\pi\gamma}{(2\pi\hbar c)^3}\left[2I_4(p_1) - (cp_1)^2\left(\frac{M_0^*c^2}{\mu_0^*}\right)^2\left(\frac{cp_1}{\mu_0^*}\right)k^2L_2(p_1)\right] \tag{D.6}$$

$$\tilde{\chi}_{\rm v}(\vec{k},\omega) = \frac{2\pi\gamma}{(2\pi\hbar c)^3}\left(\frac{M_0^*c^2}{\mu_0^*}\right)(cp_1)^3k(i\Gamma/c)L_2(p_1) \tag{D.7}$$

$$\tilde{\chi}_B(\vec{k},\omega) = \frac{2\pi\gamma}{(2\pi\hbar c)^3}\left[2I_2(p_1) - \frac{2}{3}I_4(p_1) - \left(\frac{(cp_1)^2}{\mu_0^*}\right)^2\left(\frac{cp_1}{\mu_0^*}k\right)kL_4(p_1)\right] \tag{D.8}$$

where the following integrals are defined as

$$I_2 \equiv \int_0^{p_1'} dp' \frac{p'^2}{[p'^2 + (M_0^*c^2)^2]^{1/2}} \tag{D.9}$$

$$I_4 \equiv \int_0^{p_1^{'}} dp^{'} \frac{p'^4}{[p'^2 + (M_0^* c^2)^2]^{3/2}} \tag{D.10}$$

and

$$L_0(p') \equiv \int_{-1}^{1} dx \frac{1}{(\Gamma/c)^2 + \left(k\frac{cp}{\varepsilon_0^*}\right)^2 x^2} = \frac{2}{\alpha'\Gamma'} \arctan\left(\frac{\alpha'}{\Gamma'}\right) \tag{D.11}$$

$$L_2(p') \equiv \int_{-1}^{1} dx \frac{x^2}{(\Gamma/c)^2 + \left(k\frac{cp}{\varepsilon_0^*}\right)^2 x^2} = \frac{2}{\alpha'^2} \left[1 - \frac{\Gamma'}{\alpha'} \arctan\left(\frac{\alpha'}{\Gamma'}\right)\right] \tag{D.12}$$

$$L_4(p') \equiv \int_{-1}^{1} dx \frac{x^4}{(\Gamma/c)^2 + \left(k\frac{cp}{\varepsilon_0^*}\right)^2 x^2} = -\frac{2\Gamma'^2}{\alpha'^4} + \frac{2}{3\alpha'^2} + \frac{2\Gamma'^4}{\alpha'^5} \arctan\left(\frac{\alpha'}{\Gamma'}\right) \tag{D.13}$$

here $\Gamma' \equiv \Gamma/c$, $\alpha\prime = kcp/\varepsilon_0^*$ and $x = \cos\theta$.

By using the above definitions, the coefficients A_i, B_i and C_i for zero temperature are expressed as follows,

$$A_1 = -G_\omega^2 \frac{2\pi\gamma}{(2\pi\hbar c)^3} \frac{(cp_1)^3}{\mu_0^*} k(i\Gamma/c) L_2(p_1), \tag{D.14}$$

$$A_2 = -G_s^2 \frac{2\pi\gamma}{(2\pi\hbar c)^3} \frac{(cp_1)^3}{\mu_0^*} k^2 \frac{M_0^* c^2}{\mu_0^*} L_2(p_1), \tag{D.15}$$

$$A_3 = 1 + G_\omega^2 \frac{2\pi\gamma}{(2\pi\hbar c)^3} \frac{(cp_1)^3}{\mu_0^*} k^2 L_2(p_1), \tag{D.16}$$

$$B_1 = -G_\omega^2 \frac{2\pi\gamma}{(2\pi\hbar c)^3} \left(\frac{M_0^* c^2}{\mu_0^{*2}}\right) (cp_1)^3 k(i\Gamma/c) L_2(p_1), \tag{D.17}$$

$$B_2 = 1 + G_s^2 \frac{2\pi\gamma}{(2\pi\hbar c)^3} \left[2I_4(p_1) - (cp_1)^2 \left(\frac{M_0^* c^2}{\mu_0^*}\right)^2 \left(\frac{cp_1}{\mu_0^*}\right) k^2 L_2(p_1)\right], \tag{D.18}$$

$$B_3 = G_\omega^2 \frac{2\pi\gamma}{(2\pi\hbar c)^3} \frac{(cp_1)^3}{\mu_0^*} k^2 \frac{M_0^* c^2}{\mu_0^*} L_2(p_1), \tag{D.19}$$

$$C_1 = 1 + G_\omega^2 \frac{2\pi\gamma}{(2\pi\hbar c)^3} \left[2I_2(p_1) - \frac{2}{3} I_4(p_1) - \left(\frac{(cp_1)^2}{\mu_0^*} \right)^2 \left(\frac{cp_1}{\mu_0^*} k \right) k L_4(p_1) \right], \tag{D.20}$$

$$C_2 = -G_s^2 \frac{2\pi\gamma}{(2\pi\hbar c)^3} \left(\frac{M_0^* c^2}{\mu_0^{*2}} \right) (cp_1)^3 k (i\Gamma/c) L_2(p_1), \tag{D.21}$$

$$C_3 = G_\omega^2 \frac{2\pi\gamma}{(2\pi\hbar c)^3} \frac{(cp_1)^3}{\mu_0^*} k (i\Gamma/c) L_2(p_1). \tag{D.22}$$

The dispersion relation of the system is obtained when the susceptibility $\varepsilon(\vec{k}, \omega) = 0$. The susceptibility is written same as in the finite temperature case

$$\varepsilon(\vec{k}, \omega) = A_1(B_2C_3 - B_3C_2) - A_2(B_1C_3 - B_3C_1) + A_3(B_1C_2 - B_2C_1). \tag{D.23}$$